Quaternary faulting and soil formation on the County Dump fault, Albuquerque, New Mexico

J. P. McCalpin, S. S. Olig, J. B. J. Harrison, and G. W. Berger

CIRCULAR **212** NEW MEXICO BUREAU OF GEOLOGY AND MINERAL RESOURCES **2006**

A DIVISION OF

NEW MEXICO INSTITUTE OF MINING AND TECHNOLOGY

Quaternary faulting and soil formation on the County Dump fault, Albuquerque, New Mexico

The New Mexico Bureau of Geology and Mineral Resources
A Division of New Mexico Institute of Mining and Technology
801 Leroy Place
Socorro, NM 87801
(505) 835-5145
http://geoinfo.nmt.edu

Project Editor
Jane C. Love

Layout
Nancy Gilson

Cartography
Thomas Kaus
James Tabinski

Editorial Assistance
Nancy Gilson

Library of Congress Cataloging-in-Publication Data

Quaternary faulting and soil formation on the County Dump fault, Albuquerque, New Mexico / by J.P. McCalpin... [et al.].
p. cm. — (Circular ; 212)
Includes bibliographical references.
ISBN 1-883905-18-4
1. Geology, Stratigraphic—Quaternary. 2. Faults (Geology)—New Mexico—Albuquerque. 3. Soil formation—New Mexico—Albuquerque. I. McCalpin, James. II. Circular (New Mexico. Bureau of Geology and Mineral Resources) ; 212.
QE696.Q294 2006
551.8'720978961—dc22

2005037406

Published by authority of the State of New Mexico, NMSA 1953 Sec. 63-1-4
Printed in the United States of America
First Printing

Cover
Oblique aerial view looking northeast toward Albuquerque and the Sandia Mountains. The County Dump fault can be traced through the south-facing escarpment, visible in the lower foreground, on the north side of the old Bernalillo County dump. North of the dump, this east-dipping normal fault skirts the western margin of the Albuquerque volcanic field and continues north, west of Rio Rancho; photo © Adriel Heisey.

Summary

The Albuquerque—Santa Fe urban corridor is one of the fastest growing areas in the western United States. Twenty-seven Quaternary-age (1.8 million years ago to the present) faults have been identified within 40 km of downtown Albuquerque. The faults are associated with the Rio Grande rift and are responsible for 10 earthquakes of MMI (Modified Mercalli Intensity) V or greater since 1849. The largest of these was the MMI VII—VIII earthquake at Cerrillos on May 18, 1918. The County Dump fault is a 35-km-long, north-trending normal fault that is located in an area of suburban development west of the Albuquerque metropolitan area. The fault dips eastward under the city.

To determine how often the County Dump fault ruptures the surface and to more fully understand the fault's paleoseismic history, the authors undertook a study that included: (1) measuring the height of the scarp formed by the fault, (2) opening multiple trenches across the fault, (3) describing stratigraphic and structural features in the trenches and sampling soil horizons exposed, and (4) collecting samples for thermoluminescence dating. The trench data indicate that perhaps as many as 14 earthquakes have ruptured along the County Dump fault in the past one million years. The pattern observed in the trenches suggests that the fault moves at intervals of about 20,000-40,000 years and results in displacements of approximately 1 m or less. The last three ground ruptures have estimated ages of 30,000, 45,000, and 80,000 years ago. If surface rupture spanned the entire 35-km length of the fault, a magnitude 6.9 earthquake would be possible.

Table of Contents

Figures

Tables

Abstract

The County Dump fault is a 35-km-long, north-trending, east-dipping normal fault located on the eastern margin of the Llano de Albuquerque, approximately 12 km west of downtown Albuquerque, New Mexico. The fault has formed a subdued, 24-m-high but 800-m-wide fault scarp across the Llano de Albuquerque by repeated faulting in the past ca. 1 m.y. The County Dump fault juxtaposes sand and gravel of the uppermost (Ceja) member of the Santa Fe Group (Pliocene) against younger mixed colluvial and eolian sediments reworked from the footwall. The fault plane and the colluvium shed from the scarp are exposed in cross section in badlands topography east of the fault, where five buried soils were described and dated by Machette (1978). In this study we excavated a series of six backhoe trenches across the fault trace where it descends the badlands topography, exposing the fault from the surface to a depth of approximately 19 m. The five buried soils of Machette transform into a surface soil and 13 buried soils within 5 m of the fault plane, the lower 11 of which are in fault contact with the upper Santa Fe Group in the fault footwall.

Carbonate-rich soils in the colluvial wedge were dated by six thermoluminescence (TL) age estimates ranging from 4 ka (at the surface) to > 293 ka (8.3 m below the surface). The age of older soils (from 8.3 to 17.3 m below the surface) was estimated based on their weight of secondary calcium carbonate and the trend of increasing carbonate with TL age of ca. 0.26 g $CaCO_3$ per thousand years in the upper 8.3 m. The extrapolated age of the lowest colluvium exposed in our trenches using this method is ca. 800 ka and should approximate the age of burial of the Llano de Albuquerque surface on the hanging wall by the earliest scarp-derived colluvium. This age is reasonably consistent with recent estimates of ca. 1 Ma for the age of the Llano de Albuquerque and suggests that the syntectonic wedge records the entire post-Llano de Albuquerque history of faulting, although the first faulting event may have occurred 100 k.y. or more after abandonment of the Llano de Albuquerque.

The latest three faulting events can be reconstructed from relationships in the highest trench and yielded ages of ca. 30 ka (0.4 m vertical displacement), 40 ± 5 ka (0.35 m vertical displacement), and 85 ± 10 ka (< 3.5 m vertical displacement). Older displacement events are more difficult to characterize because their associated colluvial deposits have no preserved correlatives on the upthrown fault block. However, if we assume that the preservation of colluvial parent materials on the downthrown block results from downfaulting, and that soil formation is interrupted by faulting, we can use soil thickness and soil development time as first approximations of fault displacement and recurrence interval, respectively.

The trench data suggest that perhaps as many as 14 earthquakes occurred on the County Dump fault since the abandonment of the Llano de Albuquerque with vertical displacements averaging 1.2 ± 0.6 m per event. The long-term (post-Llano de Albuquerque abandonment) vertical slip rate on the fault is as high as 0.03 mm/yr if the faulting began ca. 800 ka, but may be as low as 0.016 mm/yr if the Llano de Albuquerque is closer to 1.5 Ma (as suggested by recent workers), and faulting began soon after abandonment. The short-term slip rate over the past 82 k.y. is < 0.052 mm/yr, and may be considerably less if a graben formed along the fault. In the past two earthquake cycles 0.75 m of vertical slip was released since about 40 ka for a slip rate of 0.019 mm/yr. The lower slip rate values cited above (0.016-0.019 mm/yr) are probably more representative of the average slip rate in Quaternary time.

Introduction

The Albuquerque—Santa Fe urban corridor is one of the fastest growing areas in the western United States and contains many late Quaternary normal faults associated with the Rio Grande rift (Chapin and Cather 1994; Machette et al. 1998; Personius et al. 1999). Since 1849 there have been 10 earthquakes of Modified Mercalli Intensity (MMI) V or greater in this area (Table 1). The largest of these events was the May 18, 1918, earthquake (MMI = VII to VIII at Cerrillos, near Santa Fe), where people were thrown off their feet and a break in the earth's surface was noted (Von Hake 1975). These earthquakes, plus the presence of Quaternary fault scarps (Machette 1982; Connell et al. 1995; Connell 1997; Machette et al. 1998; Personius et al. 1999) indicate a potential for larger (M > 6.5) surface-rupturing earthquakes in the area.

Despite the abundance of geologically recent faults, few studies on earthquake hazards were performed in northern New Mexico until 1996. Since that time, several Quaternary faults have been trenched, of which the County Dump was the first (this report). Subsequent trenches have been excavated on the Pajarito fault system (Gardner et al. 2003; McCalpin 2005), Hubbell Springs fault (Personius et al. 2000; Olig et al. in press), the Tijeras fault (Kelson et al. 1999), the Calabacillas fault (McCalpin and Harrison 2000; McCalpin et al. in press), the East Paradise fault (Personius and Mahan 2000), the Sangre de Cristo fault (Kelson et al. 2004), the Sandia fault (McCalpin unpub. data), and the Zia fault (McCalpin and Harrison 2001). Despite these initial studies, there is still a need for paleoseismic studies of other Quaternary faults to determine their typical recurrence times and maximum earthquake magnitude. In addition to their seismic hazard aspects, the Quaternary faults in the Albuquerque Basin can influence ground water flow and are thus important elements in ongoing studies to model ground water movement (Hawley et al. 1995).

Goals of this study

This study describes the recent activity of the County Dump fault[1] west of Albuquerque, New Mexico, and assesses its potential earthquake hazard. The County Dump fault lies 9 km west of Albuquerque (measured from the Rio Grande, Fig. 1 top), in an area of suburban development. Although the County Dump fault is only one of 27 Quaternary faults within 40 km of downtown Albuquerque (Machette et al. 1998; "Regional setting," p. 4), it is one of the closest Quaternary faults to urban Albuquerque and dips east under the city. In addition, the fault is well exposed in the vicinity of the old Bernalillo County landfill, and previous studies have documented evidence for recurrent Quaternary faulting (see "Previous work," following).

[1]The County Dump fault was originally mapped and named by Lambert (1968). Kelley (1977) renamed this structure the Nine Mile fault but included with it an additional down-to-the-west fault south of 1-40. Machette (1982) used the name "Bernalillo County Dump fault" for this structure, but most workers since Kelley (1977) have used either "County Dump fault" (Machette, 1978) or included it within the broader "West Mesa fault zone" (Hawley et al. 1995). The comprehensive USGS compilation of Quaternary faults in New Mexico (Machette et al. 1998) terms it the County Dump fault.

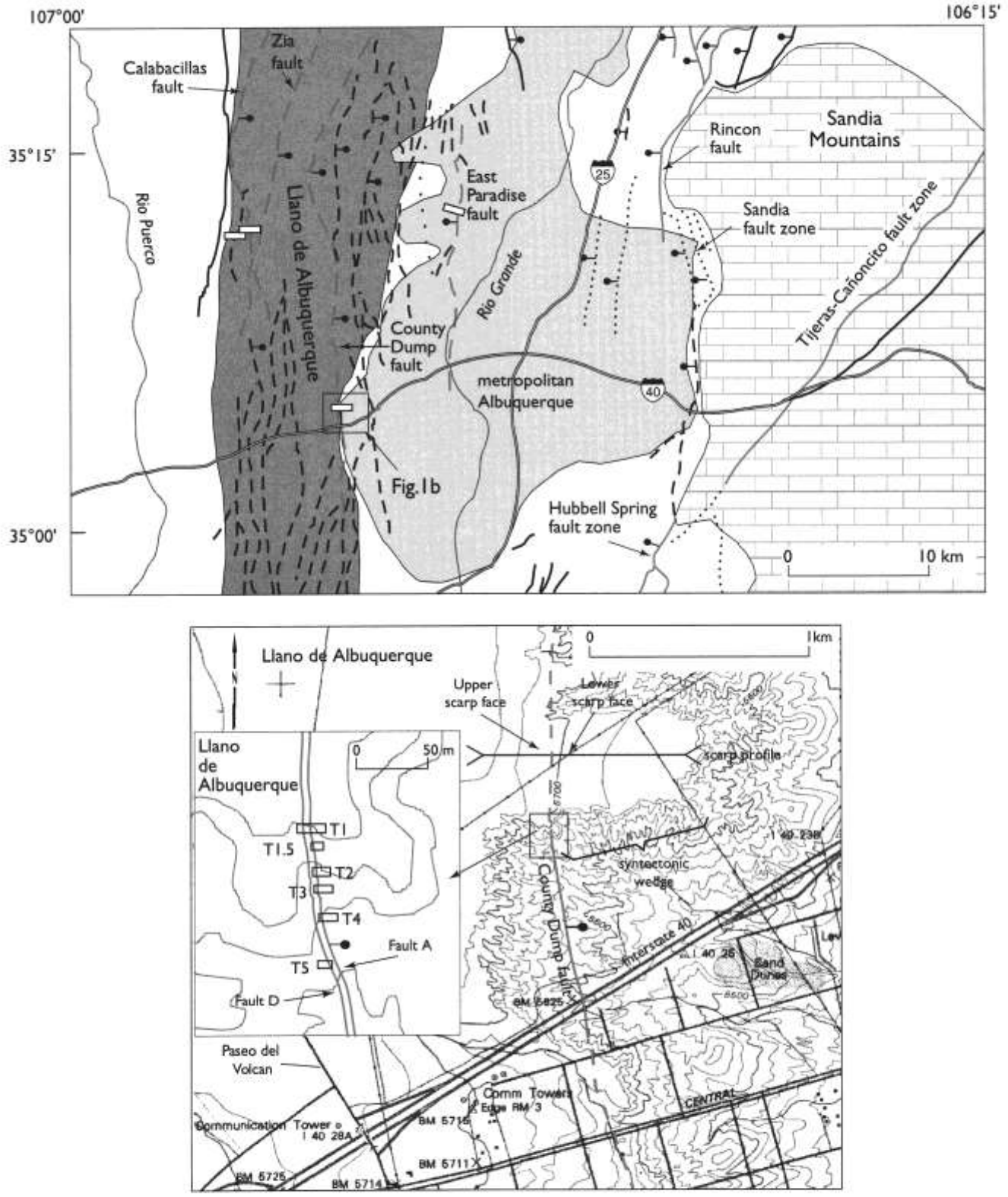

FIGURE 1—Location maps of the County Dump fault. **Top**—Simplified map of faults near Albuquerque, New Mexico. Faults with movement in the Holocene or late Pleistocene are shown by red lines; black faults are Quaternary (undivided). Narrow, steep fault scarps are represented by solid lines; broad, gentle scarps by dashed lines; concealed faults by dotted lines. Paleoseismic trenches are shown by small open rectangles on the (from west to east) Calabacillas, County Dump, and East Paradise faults. Developed areas in metropolitan Albuquerque are shown in light gray, the Llano de Albuquerque is shown in medium gray. **Bottom**—Site map of the County Dump trenches and vicinity. Base map from the La Mesita Negra SE 7.5-min quadrangle. Inset shows the location of the six trenches with respect to faults A and D, which are labeled on the trench logs (Figs. 4, 6, 9, 11, 13).

TABLE 1—Historical earthquakes in the Albuquerque–Santa Fe urban corridor (from Von Hake 1975; Sanford et al. 1991).

Date	Epicentral location	Modified Mercalli Intensity
July 12, 1893	Albuquerque	three Intensity V shocks
May 18, 1918	Santa Fe	VII–VIII
Dec. 30, 1930	Albuquerque	VI
Feb. 4, 1931	Albuquerque	VI
Nov. 6, 1947	Zamora (east of Albuquerque)	VI
Nov. 3, 1954	Albuquerque	V
Nov. 28, 1970	Albuquerque	VI (M_L 3.8)*
Jan. 4, 1971	Albuquerque	VI

*Local (Richter) magnitude.

Previous work

One reason we chose to study the County Dump fault, rather than other area faults, was that previous work documented recurrent Quaternary faulting. Machette (1978) described natural exposures at and east of the fault trace, and estimated that four faulting events had occurred on the fault in the past 500,000 yrs. These events were associated with 2.1 m displacement at ca. 20 ka, 3.0 m at ca. 120 ka, 4.1 m at ca. 310 ka, and > 7.8 m at ca. 400 ka.

At the time of Machette's 1978 study, the science of paleoseismology was in its infancy (McCalpin 1996a). The significance of small scarp-derived colluvial wedges and the relations among earthquake magnitude, surface rupture length, and surface displacement were largely unstudied. However, 20 yrs later we know that: (1) small colluvial wedges are the best indicators of normal fault paleoearthquakes, and (2) displacements from 2.1 m to > 7.8 m are anomalously large for a fault only 25 km long. In fact historic normal fault ruptures 25 km long have been accompanied by average displacements of only 0.55 m and maximum displacements of 1.35 m (Wells and Coppersmith 1994). Thus one impetus of our study was to determine why Machette's estimates of displacement were so large and whether better artificial exposures in the fault zone might reveal small scarp-derived colluvial wedges that resulted from smaller displacement events.

The most significant aspect of Machette's 1978 study was the recognition that recurrent faulting in a semi-arid environment created a colluvial deposit on the downthrown fault block and that soils developed in this deposit represented the time spans between faulting events. This concept has been expanded by subsequent workers (e.g., Birkeland 1984; Machette et al. 1997; McCalpin and Berry 1996), but all workers follow Machette in quantifying soil development indices to estimate time of soil formation and thus recurrence times between faulting events.

Another pioneering aspect of Machette's study was the use of thermoluminescence (TL) dating applied to scarp-derived deposits and calcareous paleosols (May and Machette 1984). We took advantage of 20 yrs of improvements in TL dating to expand on May and Machette's work. This paper is an expanded version of the original final technical report to the U.S. Geological Survey (McCalpin 1997).

Methods

A critical task in any normal fault study is to measure the height of the scarp formed by the fault, in order to assess the total vertical displacement across the fault, and to detect any tilting of the hanging wall and footwall. The simplest method for measuring scarp height is to survey a topographic profile across the scarp. This topographic profile permits us to relate vertical stratigraphic sections and soil profiles measured in the sediments underlying the Llano de Albuquerque to the ground surface, which gives us a relatively complete two-dimensional cross section of the fault zone. Following the example of Machette (1978), we described and sampled all the soil horizons exposed in our trenches to calculate total secondary calcium carbonate, as a measure of soil age, and thus of the age of discrete faulting events.

Topographic profiling—We measured a topographic profile across the County Dump fault scarp by measuring the surface slope along an 800-m-long line oriented east-west, perpendicular to the scarp (see Fig. 3, p. 7). The slope angle was measured over a series of contiguous 50-ft-long (15.25-m-long) slope segments, with segment length measured by a 50-ft steel tape measure laid on the ground surface. The slope angle of each segment was measured from each end by an Abney level and Brunton compass, and the two measurements were averaged. Accuracy of slope measurements is ± 0.5°.

Trenching—The trenches described in this paper were excavated by a Komatsu 220 track-mounted excavator with a 0.9-m-wide bucket but in a different geometry than in most fault trenching investigations. Because the County Dump fault is exposed in a south-facing escarpment below the Llano de Albuquerque surface, we used the excavator to dig a series of trenches, each located on the southern side of an erosional ridge in the badlands below the Llano de Albuquerque (Fig. 1 bottom). The upper part of each trench was composed of one or two vertical south-facing walls, each 1.5-2 m high, separated in a given trench by 1-m-wide horizontal benches. The lower part of each trench was also benched but was below the original ground surface and contained one or more vertical walls that faced each other. The lowest strati-graphic units exposed in one trench overlapped with the highest stratigraphic units exposed in the next trench downslope. Using a series of six overlapping trenches spaced approximately 5-10 m apart along strike, we exposed a vertical thickness of approximately 20 m along the fault trace. The trench walls were cleaned, gridded with a 1-m string grid, and logged manually. Logging followed the objective approach, in which all stratigraphic and structural features were recorded regardless of direct paleoseismic significance (McCalpin 1996b).

After each trench was logged, we surveyed level lines between each trench using an Abney level and a 4.5-m-long telescoping level rod. Level lines were sighted southward from known points on the string control grid of the higher trench and intercepted the extended rod held against the wall of the next lower trench. In this way we established the relative elevation among the trenches and the absolute depth of all trench walls beneath the Llano de Albuquerque surface.

Soils—Soils on the downthrown fault block were defined using a modification of procedures outlined in Soil Survey Staff (1975), Birkeland (1984), and Soil Conservation Service (1994). Soil Survey Staff (1975) uses the initial number in a horizon designation to indicate the presence of soil parent materials of different texture or genesis (e.g., loess overlying glacial till, or floodplain silts overlying fluvial gravels). However, in a typical 1.5-m-deep soil survey pit there might be at most two or three parent materials, which are usually of similar age. In contrast, at the County Dump exposure our trenches exposed a 19-m-thick stacked sequence of 14 soils in a package of eolian and colluvial deposits. The parent materials of these 14 soils are essentially identical in texture and origin (silty sands deposited by direct airfall and reworked by slopewash, except for the fluvial gravels in unit 3) but are of different age, ranging from modern at the surface to > 500 ka at a depth of ca. 19 m below the surface. Therefore, our horizon numbering scheme was modified to reflect that the 14 soils are developed in parent materials of similar origin but of different age, as reflected by their position in the stratigraphic sequence.

Based on the sharp boundaries between soils, we infer that each soil was developed on a single eolian/colluvial deposit that was rapidly deposited near the fault between faulting events. One reason for this conclusion is that we did not observe any of the soils to extend downward and to intermingle or "overprint" the soil and deposit below it. Because we infer that the surface soil and 13 buried soils are each developed on a separate colluvial deposit of distinctly different age, we number each deposit and its accompanying soil sequentially from the ground surface downward. Thus, soil 1 is the surface soil developed on deposit 1 (a Holocene-late Pleistocene blanket of eolian sand), and soil 14 is the oldest soil developed on deposit 14, the oldest colluvium that lies on the Santa Fe Group on the downthrown block. Within each numbered soil we differentiate horizons.

Our second departure from Soil Survey Staff is related to the modifications outlined above, and consists of omitting "b1," "b2," "b3," etc. from the end of each horizon label for the first, second, third, etc. buried soils as measured down from the modern ground surface. Not only would all these "b" numbers make the horizon abbreviations lengthy, but they would be redundant, because the number of the parent material/buried soil sequence is already represented by the initial number in the label, as explained above. Instead, we merely labeled buried soils with a final "b" without a following number. Otherwise, horizon designations follow Soil Survey Staff (1975) and Birkeland (1984). Bk horizons contain secondary carbonate but also contain minor illuviated clay and /or reddening compared to underlying C horizons. Ck horizons typically contain 3-5% total carbonate, although some horizons contain as much as 8% total carbonate. K horizons contain 8-52% total carbonate and display stage III or IV carbonate morphology (Gile et al. 1966). Cn horizons represent unaltered parent material. Grain size analysis of the insoluble fraction was measured by sieve and hydrometer methods, bulk density by the paraffin immersion method, and carbonate content by the Chittick apparatus.

Luminescence dating—The luminescence dating methods measure emitted light (photons) released as a sediment sample is heated to temperatures of ca. 450°C (Forman et al. 1998) or stimulated by photons at <100°C (Aitken 1998). This light represents electrons released from lattice defects, where they were trapped by accumulated radiation damage during sediment burial. The amount of emitted luminescence increases the longer the sediment is buried, which permits the phenomenon to be used as a dating technique. For sediments of a given age, luminescence increases as the radiation dose rate from the sediment increases. Dose rate is a function of uranium (U), thorium (Th), and potassium (K) content.

Dose rates for U and Th were determined by thick-source alpha counting, and K concentrations by atomic absorption spectrophotometry. Water contents were assumed to be one-third of present saturation values. Alpha-efficiency values were determined from a comparison of extrapolated alpha-dose-response curves with beta-dose-response curves. Alpha doses were administrated by sealed-foil 241Am sources. Procedures follow those of Berger (1988).

For luminescence experiments, interior portions of the collected TL samples were removed from the light-tight containers in dim (<< mW/cm^2) amber-colored laboratory illumination. Routine steps were followed to remove carbonate using dilute hydrochloric acid (HCl) and organic matter using 30% hydrogen peroxide (H_20_2) solution, to produce 4-11 micron polymineral grains (Wintle and Huntley 1980).

For the youngest sample (ATD96-21) the conservative recommendation of Berger (1990) for low-energy (550-800 nm wavelengths) laboratory optical bleaching was used for removing the relict thermoluminescence. For all other samples a near-solar bleaching spectrum was used (390-740 nm). For infrared stimulated luminescence (IRSL) experiments, an infrared bleaching spectrum was used (see "Soils and geochronology," p. 15), building on the experience of Huntley and Clague (1996). For all samples, luminescence only near the 410-nm emissions usually from K-feldspars was detected.

The equivalent dose (D_E) values were determined from extrapolations of beta-dose-response curves (Berger et al. 1987). Beta doses were administered by a 125 mCi sealed-foil ^{90}Sr-^{90}Y source. For TL, the partial-bleach (PB; R-beta) and total bleach (TB) procedures (Aitken 1985; Berger 1988) were used to measure DE values, which were then plotted against readout temperature to provide a plateau test (Aitken 1985). For IRSL no internal plateau test exists. The ideal procedure is to employ dual annealing experiments (see next paragraph) after 01lerhead et al. (1994). Agreement of DE plateaus for the different annealing experiments implies that the correct DE has been measured. Here, annealing temperatures for IRSL dating were chosen on the basis of such experiments conducted on other sediments in Glenn Berger's laboratory.

To remove thermally unstable and minimize anomalous-fading luminescence components from the laboratory-irradiated subsamples before signal readout, elevated-temperature storage treatments were employed (cited literature in Berger 1994). Chosen preheating temperatures are listed in "Soils and geochronology," p. 15.

Regional setting

The city of Albuquerque is located in the AlbuquerqueBelen Basin of the Rio Grande rift. The Rio Grande rift is a 1,000-km-long, north-trending complex of elongated structural depressions and adjacent uplifts bounded by Tertiary and Quaternary normal faults. Regional studies by Chapin and Cather (1994), May and Russell (1994), Russell and Snelson (1994a,b), and Hawley et al. (1995) show the Albuquerque Basin is an east-tilted half graben with down-to-thewest master faults on the eastern side and a complexly faulted hinge zone on the western side (Fig. 1 top). The basin is composed of three structural elements. The "north Albuquerque structural bench" is bounded on the east by the older Sandia master fault at the base of the Sandia Mountains and on the west by the younger Rio Grande master fault, which was inferred by Russell and Snelson (1994a,b) to underlie the Holocene floodplain of the Rio Grande. This bench is characterized by relatively thin deposits of early Tertiary age (1 km thick), and mid-to-late Tertiary (Santa Fe Group) age (1.5 km thick). Russell and Snelson's (1994a,b) "north graben block" contains the deepest Tertiary basin fill (> 2 km of Paleogene sediments, 7 km of Neogene Santa Fe Group sediments), which thickens from west to east against the (inferred) Rio Grande master fault. At the western margin of the basin, thin lower Santa Fe Group sediments overlie the Mesozoic section in the "Laguna structural bench."

The western (hinged) side of the Russell and Snelson's (1994a,b) north graben block is underlain by an east-dipping sequence of Tertiary valley fill sediments cut by as many as eight east-dipping normal faults. These north-trending, down-to-the-east normal faults are termed the West Mesa fault zone by Hawley et al. (1995). Individual faults in this zone displace beds of the lower Santa Fe Group as much as 500 m, with displacement decreasing upsection. The County Dump fault is in the eastern part of the Hawley et al.'s (1995) West Mesa fault zone at the latitude of 1-40 and forms the western boundary of a broad graben that contains the Albuquerque volcanic field. This spatial association suggests a possible interplay between faulting and magmatic activity.

Recent mapping (Connell et al. 1998; Maldonado et al. 1999) casts doubt on the existence of the 40-km-long Rio Grande master normal fault as defined by Russell and Snelson (1994a,b). Connell and Wells (1999) suggest that this fault does not exist as a throughgoing, 40-km-long north-south-trending fault and instead was a mis-correlation between two northwest-trending faults that happened to fall on Russell and Snelson's two seismic lines. Connell et al. (1998) show essentially no displacement of the Atrisco member of the Santa Fe Group across the trace of Russell and Snelson's Rio Grande master fault in Albuquerque.

Faults of the West Mesa fault zone are best exposed on the planar surface of the Llano de Albuquerque (Llano de Albuquerque is also called the West Mesa by local residents) that lies parallel to but west of the Rio Grande. The Llano de Albuquerque is an elongate upland surface (5-10 km in east-west dimension, 100 km in north-south dimension) that represents the "abandoned basin-plain constructional surface that defines the end of Santa Fe Group deposition west of the Rio Grande valley" (Maldonando et al. 1999). Because of subsequent incision by the Rio Grande and its tributaries, the Llano de Albuquerque now stands 140-250 m above river level and forms a topographic divide between the Rio Grande and Rio Puerco drainage basins. The Llano de Albuquerque is underlain by sands and gravels originally assigned to the Upper Buff or Ceja Member of the Santa Fe Formation (Bryan and McCann 1937; Kelley 1977), but which are now included in the Arroyo Ojito Formation of the upper Santa Fe Group (Connell et al. 1999). Across most of the Llano de Albuquerque a strong soil (stage IV K horizon) has formed directly beneath the surface on the uppermost beds of the Santa Fe Group. Pazzaglia et al. (1999, p. 109) state that "Many of the broad, flat geomorphic surfaces common to the Albuquerque Basin, such as the Llano de Albuquerque, do not represent a single constructional (depositional) top of the Santa Fe Group, everywhere abandoned more or less isochronously. Rather, such surfaces are complex and polygenetic, owing their origin to a long history of recycled Santa Fe sediments, diachronous abandonment in the face of continued footwall uplift and basin-floor tilting, and later local modifications attributed to fluvial and eolian processes."

The age of the Llano de Albuquerque currently is uncertain. Basalts of the Albuquerque volcanic field (dated at 156 ± 21 ka; Peate et al. 1996) overlie both the Llano de Albuquerque and the uppermost terrace (Tercero Alto) incised into the Llano de Albuquerque by the Rio Grande, indicating the Llano de Albuquerque is considerably older than 156 ka. Machette (1978) and May and Machette (1984) considered the Llano de Albuquerque surface to have been abandoned about 500 ka, based on: (1) correlation of the Llano de Albuquerque with geomorphically equivalent surfaces elsewhere in the Rio Grande valley of New Mexico; (2) the presence of vertebrate fossils and dated volcanic ashes in the deposits that form these surfaces; and (3) dated underlying and overlying basalt flows (Hawley et al. 1976; Hawley 1978; Machette 1978). More recently, Maldonado et al. (1999) report age constraints of from 98-490(?) ka to 3.0 Ma on the southern part of the Llano de Albuquerque in the Isleta Reservation from dated basalt flows. A Pliocene maximum age for abandonment of the Llano de Albuquerque by major rivers is suggested by two lines of evidence: (1) there are 19 m of Santa Fe Group sediments beneath the Llano de Albuquerque surface but above the Cat Mesa basalt flow dated at 3 Ma (Maldonado et al. 1999), and (2) Pliocene faunas dominate the fluvial sediments beneath the Llano de Manzano surface, which are correlated with those beneath the Llano de Albuquerque (Morgan and Lucas 1999). Further evidence comes from age estimates of 0.6-1.6 Ma for the Sunport surface, which is younger than the Llano de Albuquerque, and from the presence of Lava Creek B ash (0.6 Ma) in terraces inset against the Sunport surface. Together these ages argue for a minimum age of much greater than 0.6 Ma, possibly as much as 1.6 Ma, and a maximum age of Pliocene for the Llano de Albuquerque. Connell et al. (2001) estimate that the Rio Grande initiated incision of the llano sometime between 0.7 and 1.2 Ma.

County Dump fault

Geomorphology

The County Dump fault is expressed north of I-40 mainly as a broad, sand-covered, 15-25-m-high east-facing fault scarp that trends north-south across the Llano de Albuquerque (Fig. 1 bottom). Directly north of I-40 the fault ascends through the badlands-type topography of a south-facing escarpment on the north side of the old Bernalillo County dump. This escarpment is eroded into beds of the upper Santa Fe Group west of the fault and into a 15-20-m-thick section of post-Llano de Albuquerque sediments and soils east of the fault (Fig. 2). North of the dump, the fault skirts the western margin of the Albuquerque volcanic field and continues northward as a broad escarpment in upper Santa Fe Group sediments and eroded remnants of the Llano de Albuquerque. South of I-40 the fault is exposed intermittently in upper Santa Fe Group sediments for several kilometers on the flanks of the Llano de Albuquerque, but then it appears to merge with an unnamed down-to-the-west fault that parallels the eastern rim of the Llano de Albuquerque and continues southward to the Isleta Reservation.

We constructed a detailed topographic profile across the fault scarp directly north of the County Dump exposure (Fig. 3). The scarp is 24 m high, 800 m wide, and attains a maximum scarp slope angle of 3.5°. Most features of the fault scarp profile only become apparent under high vertical exaggeration, but they have geomorphic/structural relations similar to those found in smaller, steeper fault scarps. For example, the steepest part of the scarp profile (labeled "scarp face" on Fig. 3) overlies and is centered on the fault plane. The scarp is asymmetrical with the upper (erosional) part of the scarp between the fault and scarp crest being approximately 220 m wide (25% of total scarp width), whereas the lower (depositional) part of the scarp between the fault and scarp toe is approximately 580 m wide (75% of total scarp width). This asymmetry indicates that the volume of post-Llano de Albuquerque deposits on the downthrown block, which fill in the fault-angle depression, is much too large to be accounted for solely by erosion of the scarp crest (we find no evidence for extensive stripping of the Llano de Albuquerque west of the scarp). The ratio of "area eroded" vs "area deposited" scaled from Figure 3 is 1:4. This suggests that about 20% of the post-Llano de Albuquerque deposits on the hanging wall were derived by direct erosion of the scarp crest. The remaining hanging-wall sediments must have been deposited by mechanisms such as slopewash redeposition of eolian sand that fell onto the upper scarp face (and farther west), direct eolian deposition onto the scarp face, and fluvial deposition at the scarp base by streams flowing parallel to the scarp. Connell et al. (1999) suggest that these sediments of mixed origin be called a "syntectonic depositional wedge," reflecting the fact that most of the sediments are not scarp-derived colluvium as is the case on smaller fault scarps (McCalpin 1996a).

The surface of the lower scarp face is mantled by a 30-50-cm-thick blanket of Holocene eolian sand (unit He, Fig. 3), possibly reworked locally by slopewash, which pinches out at the center of the scarp. The sand is unstratified, contains only an incipient A horizon, and has been TL dated at 4 ± 1.4

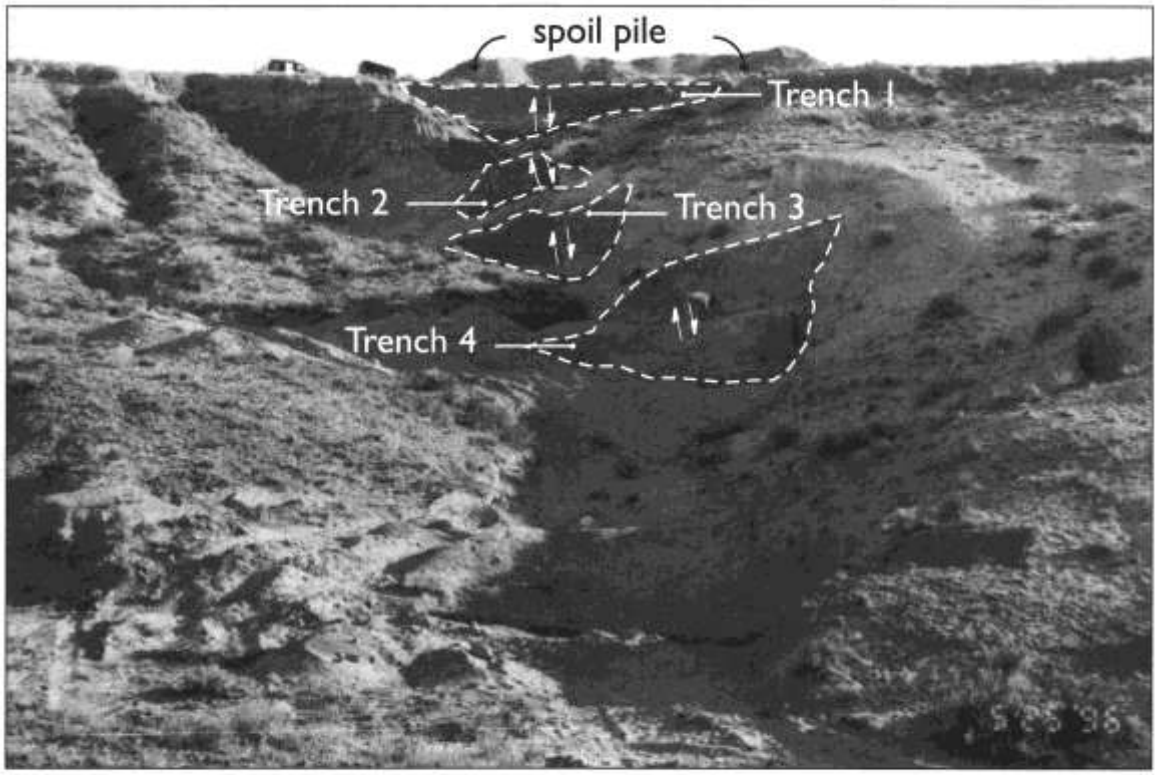

FIGURE 2—Telescopic view of trenches 1–4 at the County Dump trench site, looking north. Visible (upper) parts of each trench are outlined with a dashed line; lower parts of each trench are hidden by erosional ridges and trench spoil. Fault traces are shown by arrows.

ka at a depth of 20-25 cm. This deposit is important, despite its small thickness, because it is the modern analog for older post-Llano de Albuquerque deposits in the syntectonic depositional wedge. The pinchout of the sand layer at mid-scarp can be explained by two depositional mechanisms: (1) the sand was deposited by direct airfall in a wind eddy on the lee side of the scarp, or (2) the sand was partly retransported by slopewash from the upper scarp face. Deflation hollows exist at the toe of the scarp but not on the lower scarp face (Fig. 3), which suggests that westerly winds do not strongly impinge on the lower scarp face; this observation supports mechanism (1) above. Probably both airfall and slopewash mechanisms have contributed to deposition of the Holocene sand blanket. The pinchout of the Holocene sand on the upper scarp face underscores the fact that the upper (western) half of the scarp is a site of erosion, whereas the lower (eastern) half of the scarp is a site of deposition.

Soil stratigraphy of the syntectonic depositional wedge

The geomorphic processes described previously also affect soil formation on the Llano de Albuquerque. Where the County Dump fault scarp steepens the near-horizontal surface of the Llano de Albuquerque, soils developed in erosional areas (e.g., upper half of the County Dump fault scarp) evolve differently than soils forming in depositional areas (e.g., the syntectonic wedge). First, the soil on the upper scarp face and scarp crest undergoes stripping after faulting events, as the sharp topographic nickpoint in the scarp profile produced by surface rupture migrates upslope. On the County Dump scarp, the soil developed on the scarp face is composed of a very hard K horizon overlain by a thin A, AB, or Bk horizon. During periodic erosion episodes, the thinner horizons are stripped down to the top of the K horizon, and the top of the K horizon itself may undergo some limited dissolution due to exposure to meteoric water. In this manner, the soil on the erosional upper scarp face is repeatedly exposed and partially stripped, forming a complex, thinned, but very old, relict soil. In contrast soils on the lower scarp face (downslope from the fault) experience an opposite history. As normal faulting proceeds on the County Dump fault, the hanging wall drops down and tilts slightly back toward the fault, forming a fault-angle depression. Soils and sediments of the syntectonic depositional wedge are severed at the fault and dropped down to the east, which physically disconnects them from the stripped relict soil on the upper scarp face. The downdropped soils are subsequently buried by the erosion products stripped from the upper scarp face (a minor component) and by eolian, reworked eolian, and fluvial sediments (the major component) such as the Holocene sand blanket. If the post-faulting sediments are thick enough, they bury the faulted soil too deeply to be affected by subsequent soil formation, and thus the buried soil retains its soil properties from before the time of faulting. The 19-m-thick syntectonic wedge deposits can thus be visualized as a series of eolian, colluvial, and fluvial deposits (and the soils developed on them) that have descended on a tectonic "elevator" by repeated faulting over the past ca. 1 m.y.

Like Machette (1978), we measured six soil profiles between the fault and the toe of the scarp (Fig. 3). We correlate the soils and parent materials between profiles to construct the subsurface geology of the post-Llano de Albuquerque syntectonic depositional wedge. Beneath the Holocene eolian sand is an older, ca. 1-m-thick eolian sand with a relatively weak (stage II) Bk /Ck1 /Ck2 soil profile (our soil 1, Machette's [1978] soil U). This unit maintains a roughly uniform thickness beneath the lower scarp face, but the upper soil horizon changes from a Ck to Bk beneath the deflation hollows at the toe of the scarp. This slight increase of red color is probably due to increased infiltration of precipitation in the deflation hollows.

Unit 2 (included in Machette's soil U) also covers the fault

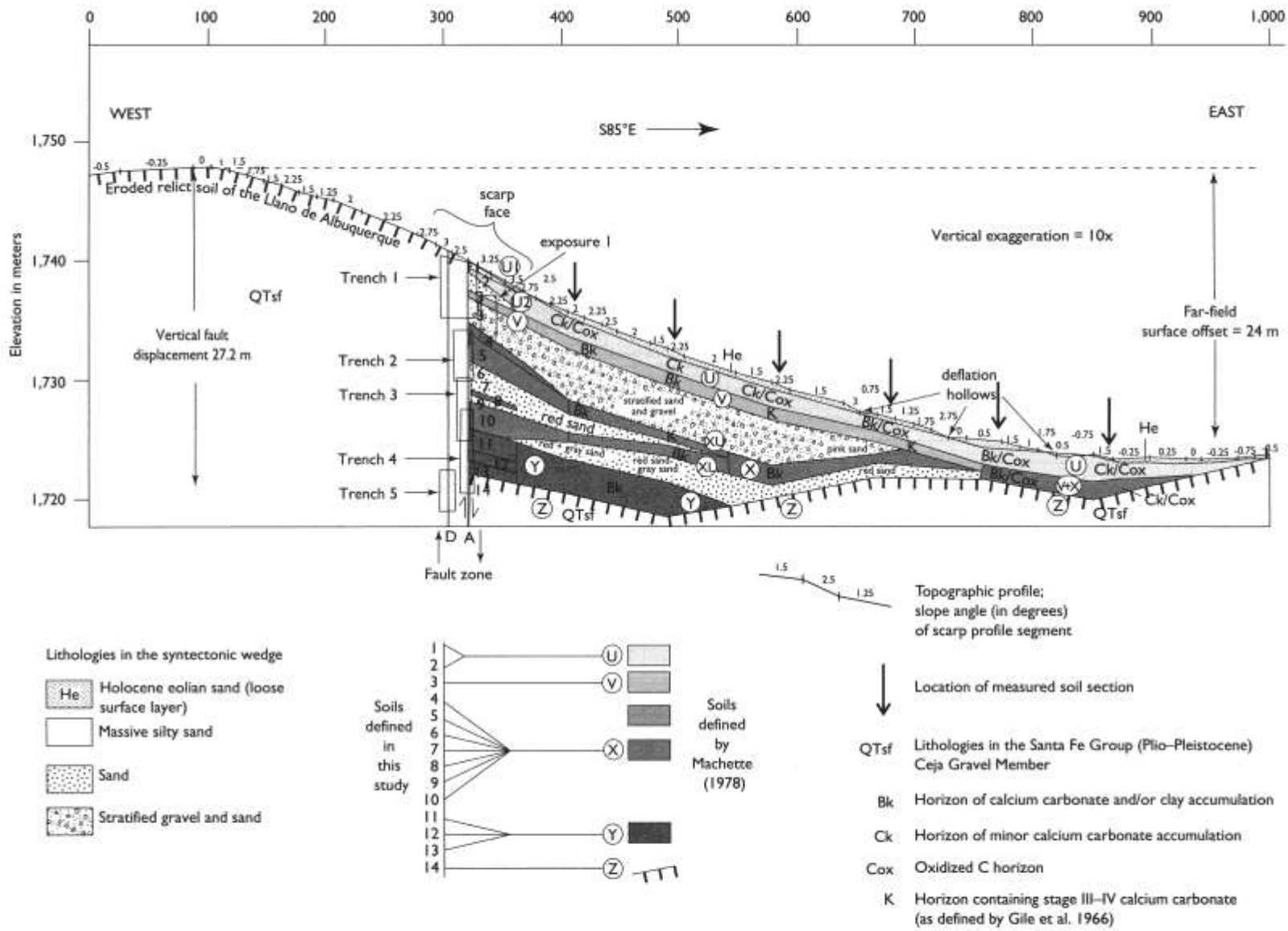

FIGURE 3—Scarp profile and stratigraphy of the syntectonic depositional wedge. Soil stratigraphy of the wedge is based on six measured sections (located below arrows just above ground surface), and generally conforms to the soil stratigraphy of Machette (1978) except adjacent to the fault zone, where 14 soils are distinguished. Soil horizons away from fault are based on measured sections; for more detailed breakdowns, see Machette (1978). Horizons near fault are described on the individual logs for trenches 1–5. Vertical contacts between soils, and pinchouts between measured soil sections, are schematic. Actual lateral transitions between soils and horizons are gradational.

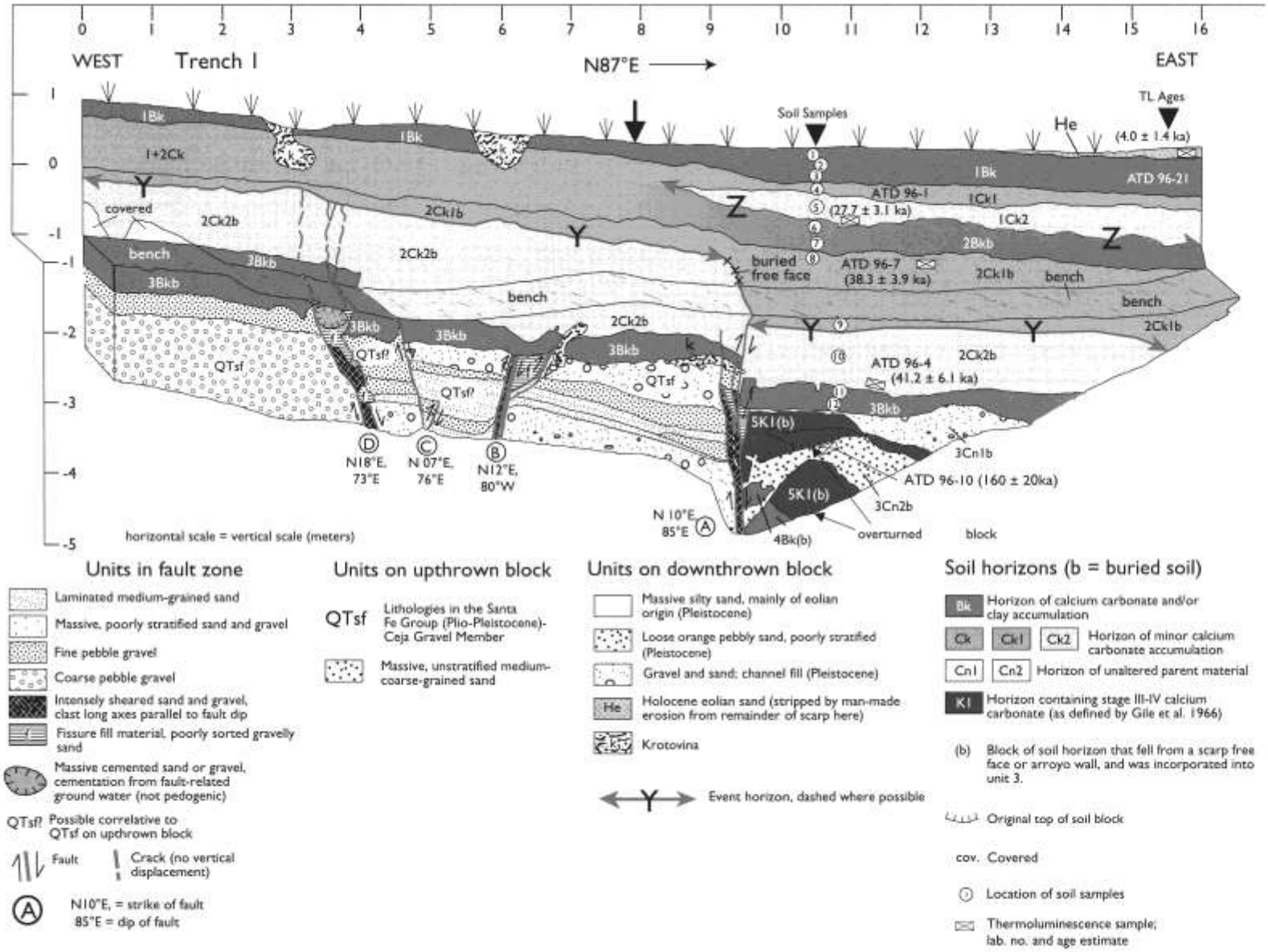

FIGURE 4—Log of trench 1, north wall. This log and those for trenches 2, 3, and 4 are shown in pseudo perspective. In this type of view, vertical walls are correctly scaled and contain no vanishing point, and the bench was made visible by merely shifting the lower wall down and to the right with respect to the upper wall. This view is not a true orthographic drawing, but it does show the 3-dimensional attitudes of faults better than the more normal 2-dimensional cross section, in which a bench can only be rendered as a line. Types of soil horizons are shown by shading (darker tones represent stronger soil development), whereas deposit textures are shown by patterns.

trace and resembles unit 1 in thickness and degree of soil development. As in unit 1, the maximum horizon development in unit 2 increases from a Bk on the scarp face to a K horizon near the scarp toe. At the fault plane unit 2 abruptly thickens, suggesting that it buries a fault scarp.

Unit 3 is a lens of stratified, medium-coarse sand and small pebble gravel as much as 4 m thick that underlies most of the lower scarp. The lenticular shape of unit 3 suggests the sediment was deposited by a stream channel that flowed parallel (southward?) to the scarp. The upper 0.3-0.5 m of unit 3 is a finer-grained clayey sand soil horizon that ranges from a Bk closer to the fault to a K horizon farther east (our soil 3, Machette's soil V). Approximately 400 m east of the fault, the sand and gravel lens of unit 3 pinches out, and the soil 3K horizon merges with the soil that underlies unit 3.

Beneath unit 3 are our units 4-7 (upper part of Machette's soil X) developed on eolian sand. This red sand deposit thins eastward and pinches out approximately 200 m east of the fault, east of which our soils 4-10 merge to form a single soil (Machette's soil X). This very strongly developed soil (stage IV carbonate morphology) continues east until unit 3 pinches out, east of which it merges with our soil 3 (Machette's soil V).

The red sand that lies between soils XU and XL (upper and lower parts of Machette's soil X; Fig 3) thins away from the fault and thus has the shape of a scarp-derived colluvial wedge. In contrast, soil 10 and the underlying red and gray sand reach their combined maximum thickness approximately 200 m east of the fault, and may be a remnant of a sand layer that once blanketed the entire scarp.

Machette's soil Y (our soils 11-13) also thins eastward, pinching out approximately 200 m east of the fault. The lowest soil exposed in our trenches (our soil 14) is inferred to be directly above the Santa Fe Group and its relict soil (Machette's soil Z), because its top is the same elevation as the top of soil Z in badlands exposures several tens of meters east of our trenches.

The cross section (Fig. 3) also shows how the top of the Santa Fe Group (Ceja Member of the Arroyo Ojito Formation) dips gently west beneath the syntectonic wedge, in contrast to its regional gentle eastward dip. This geometry suggests that the downthrown block has been tilted slightly toward the fault and explains how 19.5 m of colluvium has accumulated at the base of a scarp with a height of only 24 m (colluvium thickness = 81% of scarp height, compared to the usual value of 50%; see McCalpin [1996a]).

Trench descriptions

In the following sections we describe the stratigraphy and structure exposed in each trench, beginning with the uppermost trench (trench 1)

Trench 1

Trench 1 was excavated across the fault trace directly beneath the surface of the Llano de Albuquerque and was 16 m long and as much as 5 m deep (Fig. 4). Because of the style of excavation, trench 1 is a half-trench composed only of a benched north wall.

Stratigraphy—In the upper 2.5 m of the trench wall, three stratigraphic units and their associated soils are exposed along the entire trench. In the lower 1.5-2 m of the trench wall, different stratigraphic units are present west of the fault zone, versus in the fault zone, and east of the fault zone. The upper, continuous stratigraphic section is composed of soil 1 (the surface soil) developed on parent material 1, a massive silty eolian sand. Although the upper horizon of this soil (1Bk) underlies the ground surface along most of the trench wall, it is about twice as thick on the downthrown (east) side of the eastern fault (fault A in Fig. 4). On the downthrown side of fault A horizon 1Bk is overlain (east of the 13 m horizontal mark on the log, or **13mH) by an** eastward-thickening wedge of Holocene eolian sand.

Beneath soil 1 (1Bk/ 1Ck1 / 1Ck2) is soil 2 (2Bkb/2Ck1b / 2Ck2b), developed on unit 2. Unit 2 is a massive medium sand with no visible sedimentary structures. East of fault A unit 2 is separated from unit 1 by a wedge of eolian sand (horizon 1Ck2) that pinches out above fault A. West of this pinchout, soil 1 is superimposed on the upper part of soil 2 (horizon 1+2Ck), whereas beneath the sand wedge soil 2 has a Bk horizon (2Bkb). Horizon 2Bkb decreases in redness (hue, chroma) to the west and is transitional to horizon 1+2Ck. The lower two soil horizons in unit 2 (2Ck1b, 2Ck2b) exist on both sides of fault A, but horizon 2Ck1b is about twice as thick on the eastern (downthrown) side of the fault.

Unit 3 is composed of a 30-cm-thick silty sand (horizon 3Bkb) that overlies channel gravels (horizon 3Cn1b) and orange sands (horizon 3Cn2b) that exist only on the downthrown side of fault A. The gravelly alluvium of unit 3 thickens eastward (Fig. 3). Within 2 m of fault A unit 3 contains two large blocks of well-indurated soil K horizons (stage III to IV carbonate morphology). The degree of induration and carbonate content are greatest at the bottom of these blocks suggesting they are upside-down, and probably fell from a fault free face along fault A. The blocks could also have fallen from a channel sidewall eroded during the deposition of unit 3.

West of fault A, horizon 3Bkb overlies gravels of the Ceja Member of the Santa Fe Group (QTsf). This formation has a different character west of fault D (west of the fault zone), as opposed to between faults D and A (i.e., in the fault zone). The beds west of the fault zone (QTsf in Fig. 4) are moderately dense, medium-coarse sand and pea gravel that can be traced for many meters westward into the upthrown fault block. In contrast, the beds in the fault zone (QTsf? in Fig. 4) are more friable, thinner bedded, more variable in grain size, and do not correlate with beds west of fault D. Unit QTsf? may be considerably younger than unit QTsf on the footwall, and may represent sediments deposited in small streams flowing in a depression along the fault zone.

Structure—Trench 1 exposes a 6-m-wide fault zone composed of four major faults. On the east fault A strikes N10°E and dips 85°E. It places soils 2-3 of the syntectonic wedge sequence against beds of QTsf? in the fault zone (Fig. 5). The fault is composed of a 10-25-cm-wide zone of sheared sand and gravel, where clast long axes are parallel to fault dip. Intermingled with the rotated clasts are softer pockets of randomly oriented clasts that are interpreted as fissure fills. Fault A displaces horizon 3Bkb approximately 75 cm down to the east. Fault A displaces soil horizons as high as 2Ck2b, whereas higher horizons 2Ck1b and 2Bkb are tilted as much as 20° over the projection of the fault. This 20° dip is much steeper than any part of the present scarp profile (maximum slope of 3.5°) or of any other soils in the syntectonic wedge. The restriction of steep dip to directly above fault A suggests that horizons 2Ck1b and 2Bkb are either depositionally draped over a buried fault scarp or monoclinally warped.

The distinction between warping and draping is critical for defining the age and style of youngest deformation on the County Dump fault. If the 20° dip merely reflects depositional draping over a fault scarp, it is curious that nowhere else in the other trench exposures, in natural exposures, or even on the margins of deflation blowouts, do we observe sand beds that dip more steeply than 3-4°. Due to the constant winds at this site redistributing loose sand at the surface, it is difficult to conceive how a 20° slope in loose sand could be maintained long enough, even locally, to permit the development of a Bk horizon, which presumably took sev-

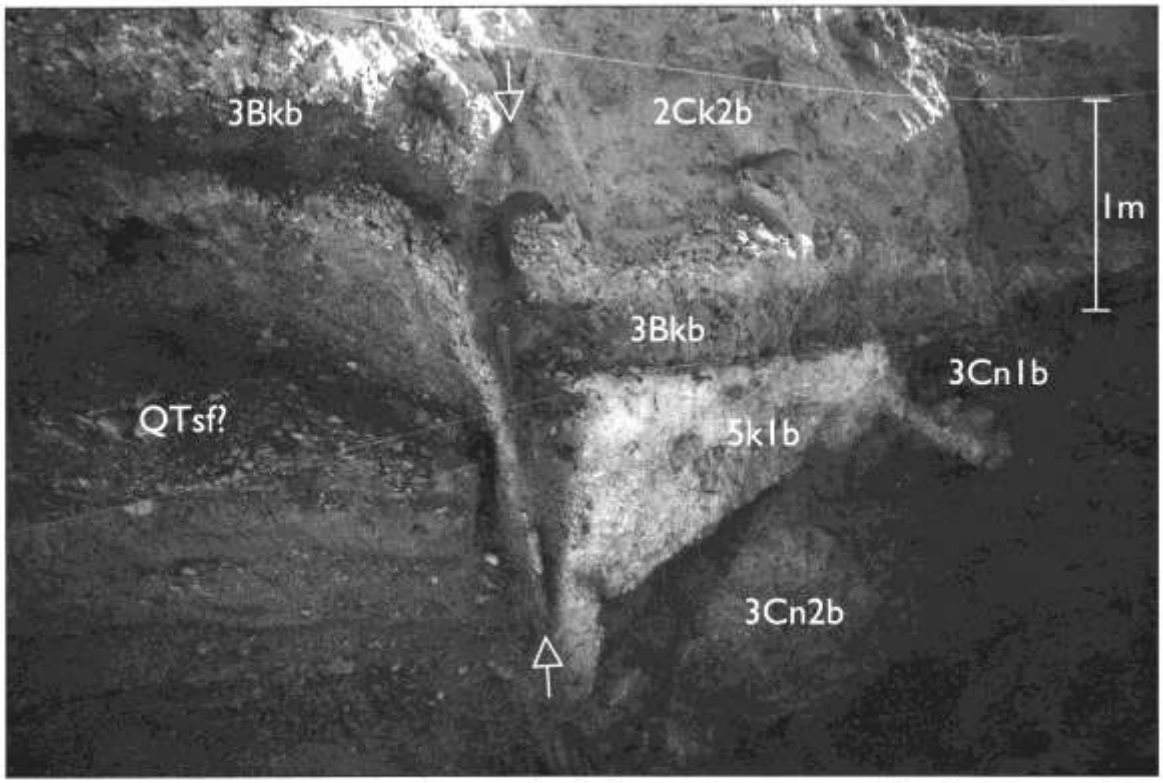

FIGURE 5—Photograph of fault A in trench 1, centered on fault zone A (between arrows). Note the 0.75 m vertical displacement of horizon 3Bkb, and the downward drag of that horizon on the footwall. Horizontal stringlines are 1 m apart.

eral to many thousand years. However, if steep dip was produced after the Bk horizon had developed on unit 2, the indurated Bk horizon could easily maintain a 20° dip without further sloughing. Therefore, our preferred interpretation is that horizon 2Bkb was monoclinally warped from its original dip of from approximately 3-4° to 20° by the most recent displacement event, which had insufficient vertical displacement to cleanly displace unit 2. Instead, the decimeter-scale displacement was absorbed by intergranular rotation in the friable lower part of unit 2, and the overlying more rigid horizon 2Bkb warped downward.

The fault zone is bounded on the west by fault D, which strikes N18°E and dips 73°E. Fault D also contains a 15-20cm-wide zone of sheared gravel with interspersed fissure fills. Fissure fills are distinguished from tectonically sheared gravel by their random clast orientations and softer consistence (McCalpin 1996a, table 3-5). Fractures overlying fault D cut horizon 2Ck2b and are truncated at its top, thus the fractures related to fault D cut to the same stratigraphic level as fault A. Fault D displaces the base of horizon 3Bk by approximately 20 cm but does not displace the top of that horizon.

Within the fault zone, fault C strikes N07°E, dips 76°E, and fault B strikes N12°E, dips 80°W. The westerly dip of fault B gives the appearance of a reverse fault, but the large fissure fill between its branches shows that the fault is dominantly an extensional feature. Similar dip reversals near the top of normal faults are described in other trenches, and are ascribed to refraction due to decrease in the near surface confining stress (Mercier et al. 1983). Both faults B and C displace the QTsf? section, but in general individual gravel and sand beds do not correlate across the faults, so it is difficult to measure vertical displacement. The non-correlation of beds may result from a horizontal component of displacement, which cannot be measured from our trench walls.

Trench 1.5 and exposure 1

Trench 1.5 was excavated by hand after trenches 1-5 were excavated and logged. This trench was excavated because, due to the rugged badlands topography, we could not position the excavator to expose correlative strata between the bottom of trench 1 and the top of trench 2. Trench 1.5 was only approximately 2 m deep and exposed a soil section similar to that at the bottom of trench 1 (Fig. 6). The only fault exposed is the continuation of fault A exposed in trench 1. In trench 1.5 this fault likewise abuts the Ceja Member (QTsf) against parent material 3. As in trench 1, unit 3 contains large blocks of the K horizon of soil 5 (5Klb), lying upside-down. The base of trench 1.5 exposes a second block of soil K horizon that may be in situ, based on comparison to the better exposed sections of soils 4 and 5 exposed in trench 2. However, if these two soil horizons (4Bkb, 5Klb) are in situ, then unit 3 is anomalously thin here. Our preferred interpretation is that even the basal block of soils is out of place, but happened to land in a rightside-up orientation when it fell from a fault (or arroyo) free face.

In order to completely expose the in situ stratigraphic section of units 3 and 4, which lie below trench 1 but above trench 2, we used shovels to clear off a steep natural slope approximately 5 m east of the fault zone (exposure 1, see Fig. 1 bottom). This section (Fig. 7) exposes six soil horizons within unit 3, and two soil horizons in unit 4, over a vertical span of 3.2 m. We infer that these same eight horizons also continue west to the fault plane.

Unit 3 exposed in exposure 1 is mainly composed of a 60-cm-thick cap of silty sand (as in trench 1), underlain by medium to coarse sand with only a trace of small pebble gravel; thus the gravelly fluvial channel deposits exposed in trench 1 grade eastward into finer fluvial sands. More importantly, unit 3 in exposure 1 does not contain detrital blocks of soil 5, as existed next to the fault in both trenches 1 and 1.5. The absence of soil 5 blocks indicates that scarp-

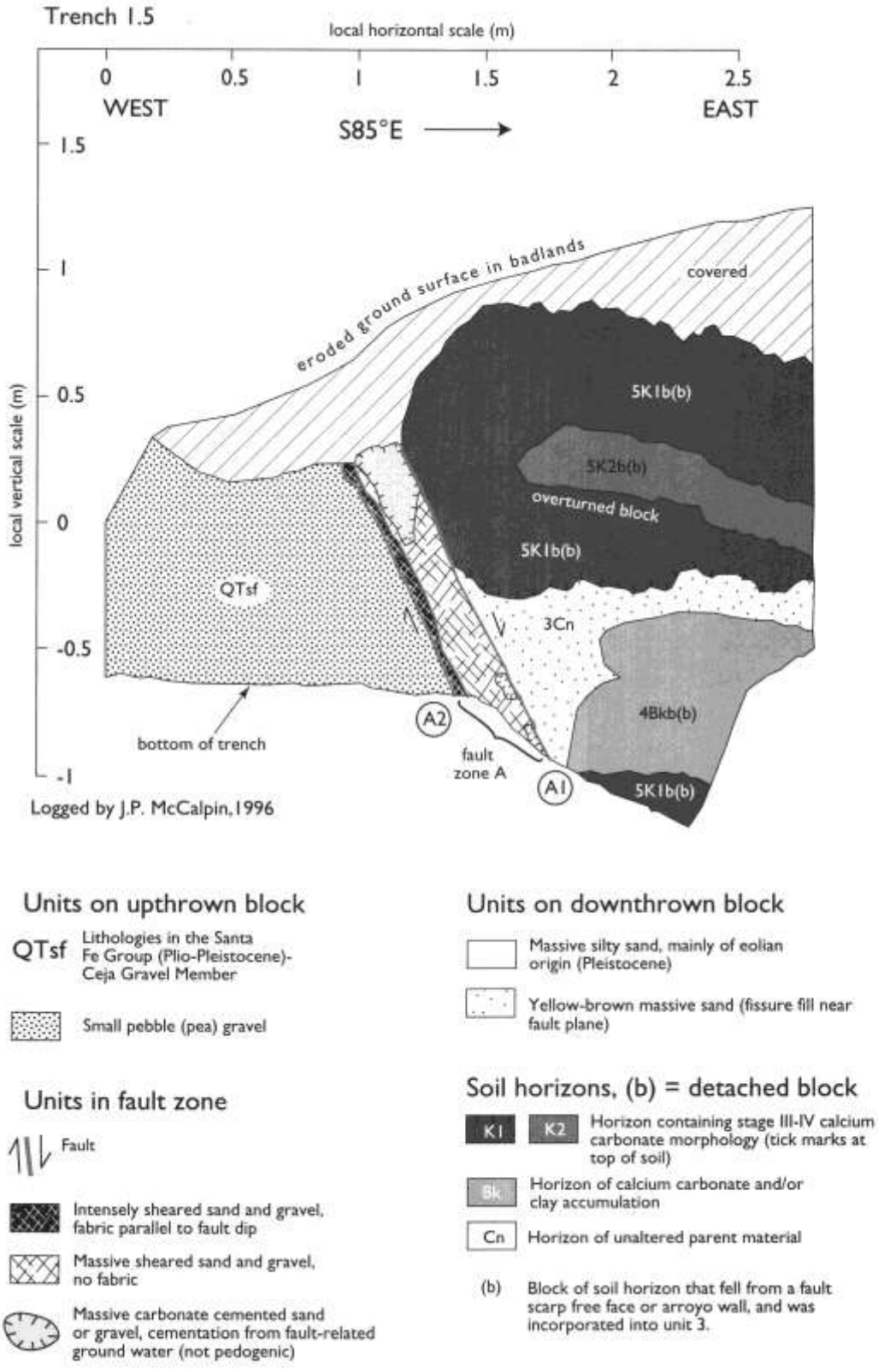

FIGURE 6—Log of trench 1.5, north wall. This trench exposes similar overturned blocks of soil 5 as exposed in the bottom of trench 1.

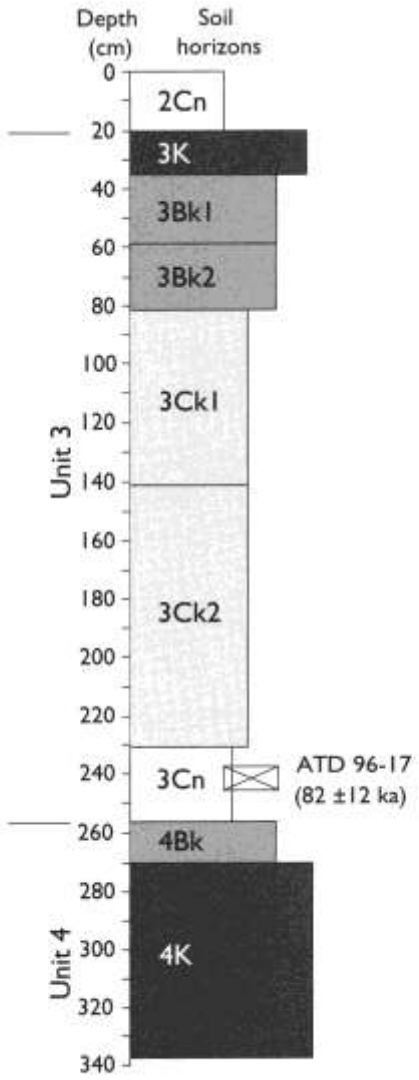

FIGURE 7—Soil stratigraphic section of exposure 1, located 5 m northeast of trench 2 in undisturbed erosional topography. Shading increases with stronger soil development, and width of box increases with increasing induration. The parent material for unit 3 here is mainly sand, in contrast to the gravels exposed in trench 1.

derived colluviation from fault free faces did not extend 5 m east of trench 1.5, and thus was limited to a narrow zone adjacent to the fault.

The soil horizons in the silty upper 60 cm of unit 3 (3K/3Bk1/3Bk2) are slightly better developed and twice as thick as the corresponding horizon in the silty upper 30 cm of unit 3 (3Bkb) exposed in trench 1. Likewise, the underlying 1.7 m of sandy alluvium in exposure 1 contains slightly more carbonate (horizons 3Ck1/3Ck2) than the gravelly alluvium in trench 1 (horizons 3Cn1b, 3Cn2b). This increase in soil carbonate, and thus soil structure, probably stems from the slower infiltration rate of sands compared to the gravels in trench 1.

The lowest 80 cm of exposure 1 is formed by unit 4, a massive medium sand containing a 10-cm-thick 4Bk horizon overlying a > 70-cm-thick 4K horizon. When traced westward to trench 2, the 4K horizon decreases in carbonate content and is classified as a 4Bkb horizon at the top of trench 2.

Trench 2

Trench 2 was a 7.5-m-wide, 4.3-m-deep half-trench (Fig. 8) with a free-standing, 3-m-high upper wall and a 1.5-m-deep incised trench with lower wall. The two wall sections were separated by a 0.8-m-wide bench.

Stratigraphy—Trench 2 exposes the Ceja Member (QTsf) on the upthrown block and in the 0.8-m-wide fault zone, and on the downthrown block trench 2 exposes (in descending order) the base of unit 4, units 5-7, and the upper part of unit 8 (Fig. 9). All five units are composed of massive fine- to coarse-grained sand containing rare, isolated small pebbles. Interestingly, the grain size and bedding in these units do not vary from the eastern end of the trench wall to the fault zone. That is, even immediately adjacent to the fault, none of the units contain any exotic blocks of soils, stone lines, or even an increase in gravel that might have resulted from scarp-derived colluviation. Because the footwall is mainly composed of Ceja Member gravel, any free face created by faulting should have shed abundant Ceja gravel onto the syntectonic wedge. Yet, faulted units 4-8 lack any trace of gravel shed from the footwall and maintain their massive, sandy texture right up to the fault zone. A clean fault truncation is what one might expect if these poorly stratified sands had originally extended farther west onto the footwall at one time, as units 1 and 2 do in trench **1.** In subsequent faulting, a small free face would expose only the sand blanket that lay on the scarp (such as the Holocene sand blanket) and might not be high enough to expose the underlying Ceja gravels. This same lack of scarp-derived gravel is observed for all subjacent units (8-14) and implies that the deposits preserved in the syntectonic wedge may be merely the preserved parts of sand blankets that once mantled the scarp face and hanging wall, just as the surface Holocene sand blanket does today. This sedimentological interpretation has important tectonic implications and is discussed further in "Soils and geochronology," p. 15.

Unit 5 comprises nearly the entire upper trench wall and contains the thickest and strongest soil profile in the syntectonic wedge. The 5K1b and 5K2b horizons contain stage III to IV carbonate morphology and total 1.5 m in thickness. In contrast, the lower trench wall exposes three thinner soils (6, 7, and 8) that average approximately 0.6-1.3 m thick. Soil 6 has a sharp upper contact but very irregular lower contact, as if the lower half of the 6Bkb horizon was extensively burrowed by animals. Thus, much of soil horizon 6Ckb has probably been reworked by burrowing. Soils 7 and 8 have a horizon structure (K/Ck1 /Ck2) very similar to soil 6.

Structure—Trench 2 contains two zones of deformation. The main 1-m-wide fault zone is a continuation of fault A in trenches 1 and 1.5 and abuts colluvium and soils on the downthrown block against slivers and blocks of the Ceja Member (QTsf). The eastern boundary of this fault zone is a 10-15-cm-wide zone (fault Al) of intensely sheared sand and gravel. On the lower trench wall a zone of carbonate-cemented sand and gravel parallels fault Al on the downthrown block; this carbonate cementation cuts across soils and probably resulted from ground water traveling along fault Al. The fault zone is composed of deformed and undeformed blocks of relatively soft QTsf sand and gravel (Fig. 8). The undeformed blocks cannot be correlated with discrete beds west of the fault zone. Some of the finer-grained blocks of sand are internally deformed, but most loose gravel blocks still retain discernible stratification. It is unclear how the intensely sheared zone of fault Al formed against such soft beds on the footwall. F. Maldonado (pers. comm. 1996) suggested that the shearing occurred when harder sand beds were juxtaposed against the colluvial section. The western boundary of the fault zone (fault A2) contains small areas of sheared sand and gravel but is generally a narrow fault plane or an anastomosing network of faults.

The upthrown fault block is composed of sand and gravel beds of the Ceja Member, which dip gently east (toward the

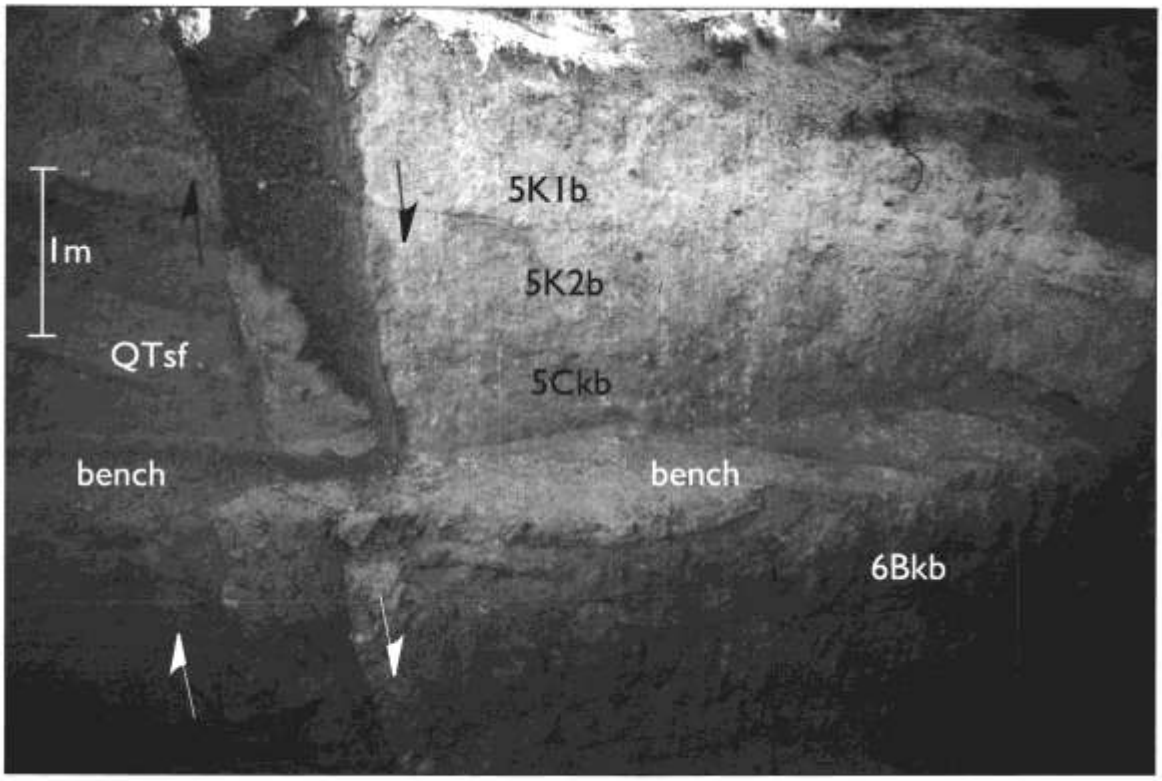

FIGURE 8—Photograph of trench 2, north wall. Fault zone A is shown by arrows. The upper trench wall is entirely composed of soil 5 on the hanging wall, and Ceja Member sand and gravel on the footwall. The lower trench wall is only partly visible.

fault) and are displaced by a series of west-dipping normal faults. These normal faults have small down-to-the-west displacements (10-40 cm), and most either merge with or are truncated by fault A2. The displacement on individual faults tends to decrease upward, but this is probably evidence of upward die out rather than of discrete interstrata faulting events. The 10-15° dip of beds here is considerably greater than the regional dip of the Ceja Member and may indicate local clockwise rotation of fault blocks near the fault. Such rotation is consistent with east-west extension and subsequent "domino-style" rotation of blocks in the upthrown block.

Trench 3

Trench 3 was 7 m long, as much as 5 m deep, and consisted (like trench 2) of a free-standing upper wall and an entrenched lower wall (Fig. 10). The intervening 1-m-wide bench sloped approximately 30 cm to the south, and this 30-cm interval thus appears as a blank (unmapped) interval on the trench log (Fig. 11). The top of the trench was approximately 9.5 m below the Llano de Albuquerque surface and the bottom approximately 15.5 m below.

Stratigraphy—The stratigraphy of trench 3 is similar to that of trench 2, i.e., massive sandy deposits and stacked soils east of the fault zone, blocks of Ceja Member in the fault zone, and east-dipping beds of Ceja Member west of the fault zone. Intrafault blocks of the Ceja Member are composed of sand and gravel layers that generally do correlate with Ceja beds west of the fault zone. Beds on the footwall range from medium- to coarse-grained sand to fine pebble gravel.

On the downthrown block, seven units (6 through 12) are exposed. Some of the units show more lenticularity than others. For example, unit 8 thins toward the fault zone, and horizon 8Bkb pinches out. The overlying horizon (7Cnb) thickens toward the fault, although some of this apparent thickening could be due to burrowing of horizon 8Kb (note the isolated pieces of 8Kb surrounded by 7Cnb). However, some soils also pinch out southward on the eastern (end) wall of the trench. This 3-dimensional lenticularity of some units suggests they were not deposited as uniform-thickness layers on the scarp face, but rather as lenses 0-1 m thick and 2-4 m in lateral extent. However, the modern bluff-edge exposures of the Holocene eolian sand show it is a relatively uniform thickness blanket, so there is no modern analog for lens-shaped deposition on the scarp face. If the component units that compose the syntectonic wedge do thicken and thin along strike, such that in places they pinch out, then the total number of buried soils in the wedge would vary along strike. This variance would then change our estimates of the number of faulting events. Along-strike pinchouts of scarp-derived colluvial wedges have not been previously described in the paleoseismic literature, and pinchouts are not expected where per-event displacements are »1 m and thick colluvial wedges form from gravity and debris processes acting on high free faces (e.g., the Wasatch fault; Machette et al. 1992). However, units 4-14 are generally less than 1 m thick, and their textures suggest that most of the syntectonic wedge sediments are not scarp derived, so their original geometry is unknown. We cannot confirm that most of the wedge units are lenticular along strike because our trench exposures are almost all oriented perpendicular to fault strike.

Structure—The main fault zone in trench 3 widens downward from 0.3 m at the top to 1.3 m wide at the bottom of the trench with an attendant increase in the number and complexity of internal fault strands and blocks. As in trench 2, fault A splits into strands Al, A2, and A3. The eastern mar-

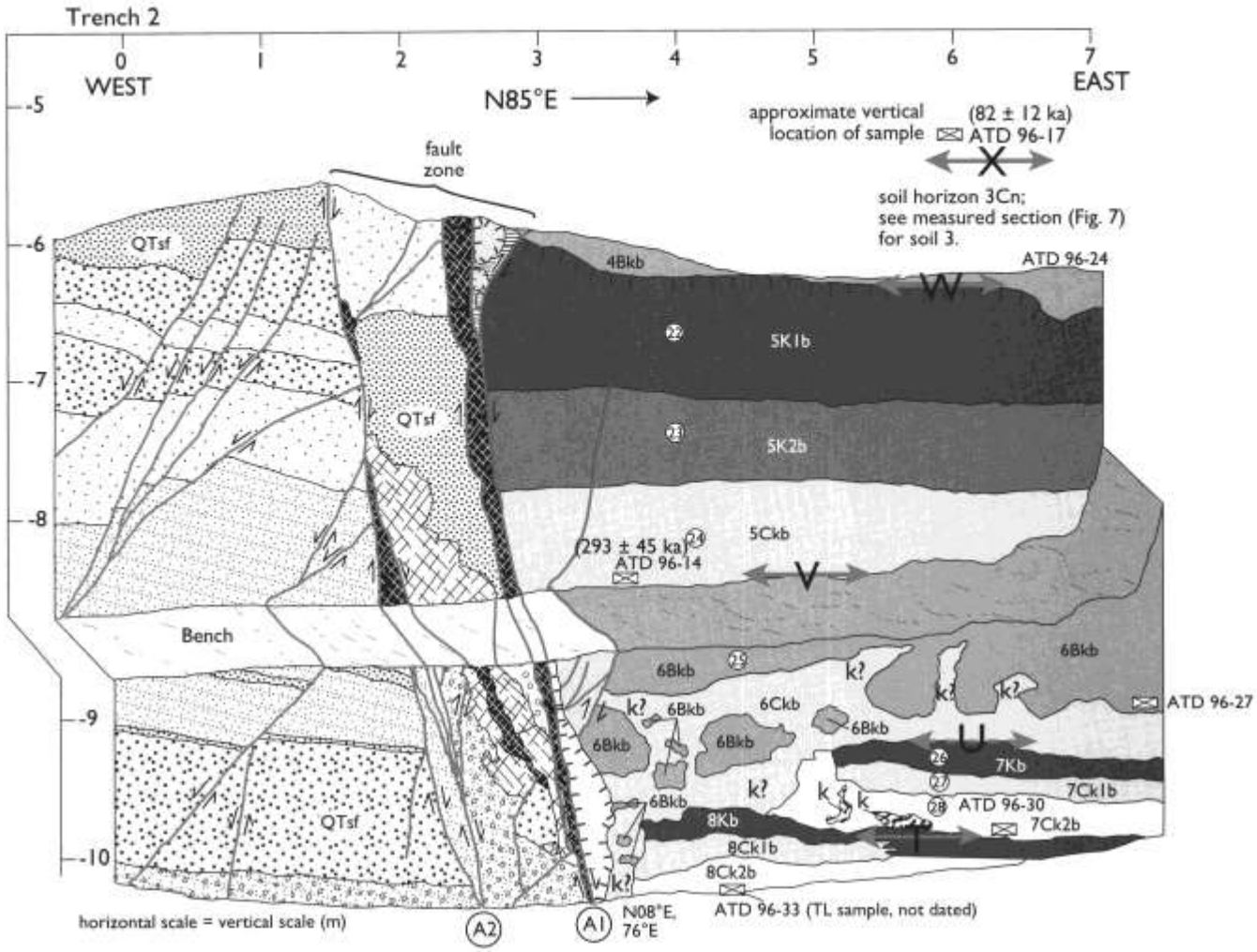

FIGURE 9—Log of trench 2, north wall. At upper right, an arrow shows the stratigraphic position of the TL sample from unit 3 in exposure 1 (82 ± 12 ka). The TL age estimate of 293 ± 45 ka from the base of horizon 5Ckb is a minimum age estimate. The vertical scale at left shows depth below the surface of the Llano de Albuquerque.

gin of the zone (fault Al) is a 10-15-cm-wide zone of intensely sheared sand, bounded on the eastern side by a 10-25-cm-thick zone of anomalous carbonate cementation, possibly caused by infiltration along the fault. Parallel to and west of fault Al is a zone of anastomosing faults that bound slivers of sheared and partially cemented sand and gravel. These interfault slivers appear to be previously intact blocks of various beds of the Ceja Member that have been squeezed and elongated within the fault zone. The western part of the fault zone (between faults A2 and A3) contains relatively intact beds of the Ceja Member that appear to correlate with beds 0.2-0.7 m higher west of the fault zone. If this correlation of beds is correct, then there has been < 1 m of cumulative vertical displacement on fault A3. This inference could also be made in trench 2 and implies that most of the 17-24 m of vertical displacement on this fault has occurred on the eastern strand (fault Al) of the eastern fault zone.

Two types of smaller-displacement faults also occur in trench 3. The first type includes west-dipping, down-to-the-west normal faults within the upthrown block. These faults have displacements of less than 25 cm and may be accommodating east-west extension via a rotating domino style of deformation. A second type of faulting appears on the downthrown block, a type that was sparsely present in trench 2 but becomes more abundant with increasing depth. This fault type is composed of west-dipping reverse faults that splay off fault Al and climb up and east through the wedge deposits. Most of these faults have very small displacement with faults closest to fault Al having displacements as much as 10-15 cm. These reverse faults probably result from some localized irregularity on the Al fault plane or from volume accommodation in the hanging wall.

Trench 4

Trench 4 was the deepest of our six excavations, composed of four vertical walls with three intervening benches (Fig. 12). Only the lowest wall is part of an incised trench. The trench exposed strata from 11.5 m to 19.5 m below the surface of the Llano de Albuquerque (Fig. 13). Although this trench was nearly parallel to trench 3, it was not perpendicular to the strike of the fault, indicating that fault strike had changed to a more northwesterly direction from trench 3 to trench 4.

Stratigraphy—Trench 4 exposes units 6 through 14 on the downthrown block, the latter soil being the lowest unit that we exposed in the syntectonic wedge (Fig. 14). Most units maintain approximately uniform thickness across the 2-6 m length of the trench wall, but some units (e.g., soil 12) pinch out away from the fault. Blocks of the Ceja Member between faults Al and A2 in general do not correlate with strata in the upthrown block and may represent strata from higher stratigraphic levels in the upthrown block. Ceja Member strata on the upthrown block range from silty sand to sandy gravel and dip uniformly east at 10-12°.

Structure—The main fault zone in trench 4 is approximately 1 m wide (Fig. 13) and contains internal elements comparable to those in trenches 2 and 3. The most strongly developed shear structure is the eastern margin fault (Al), although portions of the western margin fault (A2) have shear fabric. Blocks of Ceja Member strata in the fault zone have eastward dips as steep or steeper than strata in the upthrown block, indicating some degree of down-to-the-east rotation in the fault zone. Secondary normal faults in the upthrown block are not as abundant as in trenches 2 and 3.

The upper wall of trench 4 is strongly fractured by west-dipping fractures and faults east of the main fault zone. Some of these faults display reverse-fault displacements of as much as 30 cm in the syntectonic wedge. Displacement decreases upsection, sometimes in abrupt steps rather than as slow upward die out. The fault-soil relations of units 8-11 near the main fault (dashed box on Fig. 13) form the basis for a retrodeformation sequence described in "Interpretation, Origin of sediments and soils in the syntectonic depositional wedge," p. 28.

Trench 4 is unique among the trenches because of the relatively steep easterly dips shown by soils in the syntectonic wedge. The apparent dip of soils on the trench walls ranges from a high of 23° at the top, to ca. 10° at mid-trench, and < 5° at the bottom of the trench. A southerly component of dip is indicated from the depth below the Llano de Albuquerque surface of certain units, compared with that of their correlatives in trench 3. For example, units 10-12 are 1.5-2 m lower in trench 4 than their correlatives in trench 3 (which is 10 m to the north), indicating a southerly dip component of 7.5-10°. This southerly dip component is perpendicular to our trench walls and explains why the depth of units in trench 4 below the Llano de Albuquerque (as much as 19.5 m, Fig. 14) is larger than the cumulative measured stratigraphic thickness (17.3 m) for those same soils.

Trench 5

Trench 5 was the lowest trench (in elevation) in our series of six trenches. It was excavated across the flat floor of an arroyo along strike of fault zone A and up the eastern arroyo bank (Fig. 15). This trench was 9.5 m long, as much as 2 m deep, and exposed stratigraphy from 19 m to 21.5 m below the surface of the Llano de Albuquerque.

Stratigraphy—Trench 5 exposes the Ceja Member and Holocene alluvium but not the syntectonic wedge, which evidently lies east of the trench. The Ceja Member is composed of weakly indurated beds of silty sand to large pebble gravel that dip 3-5° east. Incised into these deposits beneath the arroyo floor are two subunits of Holocene alluvium. The older unit (Hal2) is a poorly stratified sand and gravel that is channeled into the top of unit QTsf. Unit Hall is a massive medium-coarse sand to pea gravel that forms smaller channels and lenses. Although unit Hall is weakly channeled into the top of unit Hal2, there is no soil preserved at their contact, and they are probably similar in age.

Structure—Two areas of deformation are exposed in trench 5. Near the eastern end of the trench are two structures, a 10-cm-wide shear and an east-dipping fault, both of which die out upward in Ceja gravels. These small faults are probably related to fault zone A, which is inferred to lie several meters east of the trench. The western deformation zone in trench 5 consists of several east-dipping shears and faults in a zone approximately 0.6 m wide. This zone has symmetry opposite to fault A as exposed in trenches 2-4, in that the most intensive shearing is on the western side of the zone, whereas interfault blocks of the Ceja Member lie to the east. This fault zone is truncated by unit Hal2, indicating that movement is pre-Holocene. We consider that this fault is probably correlative with fault D in trench 1, which formed the western boundary of the fault zone. Apparently the strike of the County Dump fault is more northwest-southeast south of trench 4 than north of it. Thus, trench 5 only intersects the western part of the zone of normal faulting and does not extend eastward far enough to expose fault A.

Soils and geochronology

The physical and soil stratigraphy exposed in our six trenches provides a framework from which to interpret tectonic and depositional events (as described in "County Dump fault, Geomorphology," p. 5) but without additional data on soil formation and geochronology we have no age control on such events. To provide chronological control on our trench units, we measured quantitative soil horizon parameters throughout the syntectonic wedge and corre-

Text continued on p. *24*.

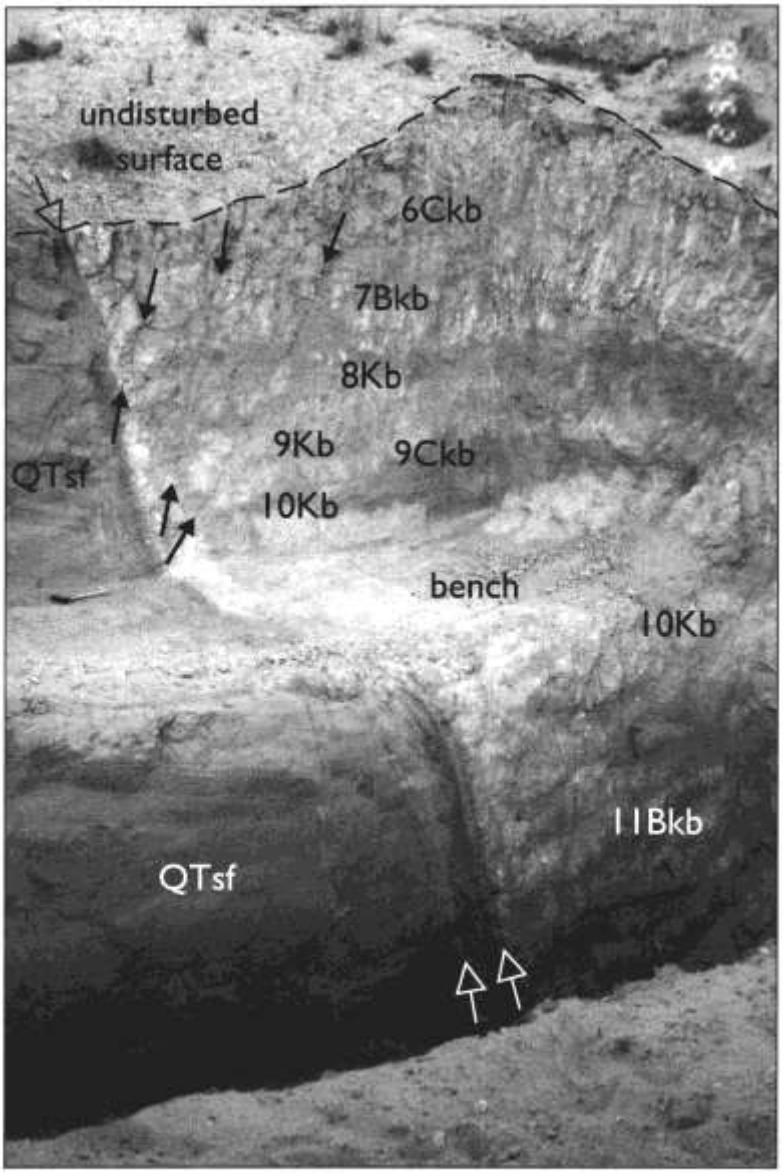

FIGURE 10—Photograph of trench 3, north wall. Fault zone A broadens from 25 cm wide (upper open arrow) at the top of the trench to 1.3 m wide at the bottom of the trench (two open arrows). Arrows with solid heads show west-dipping fractures and small reverse faults.

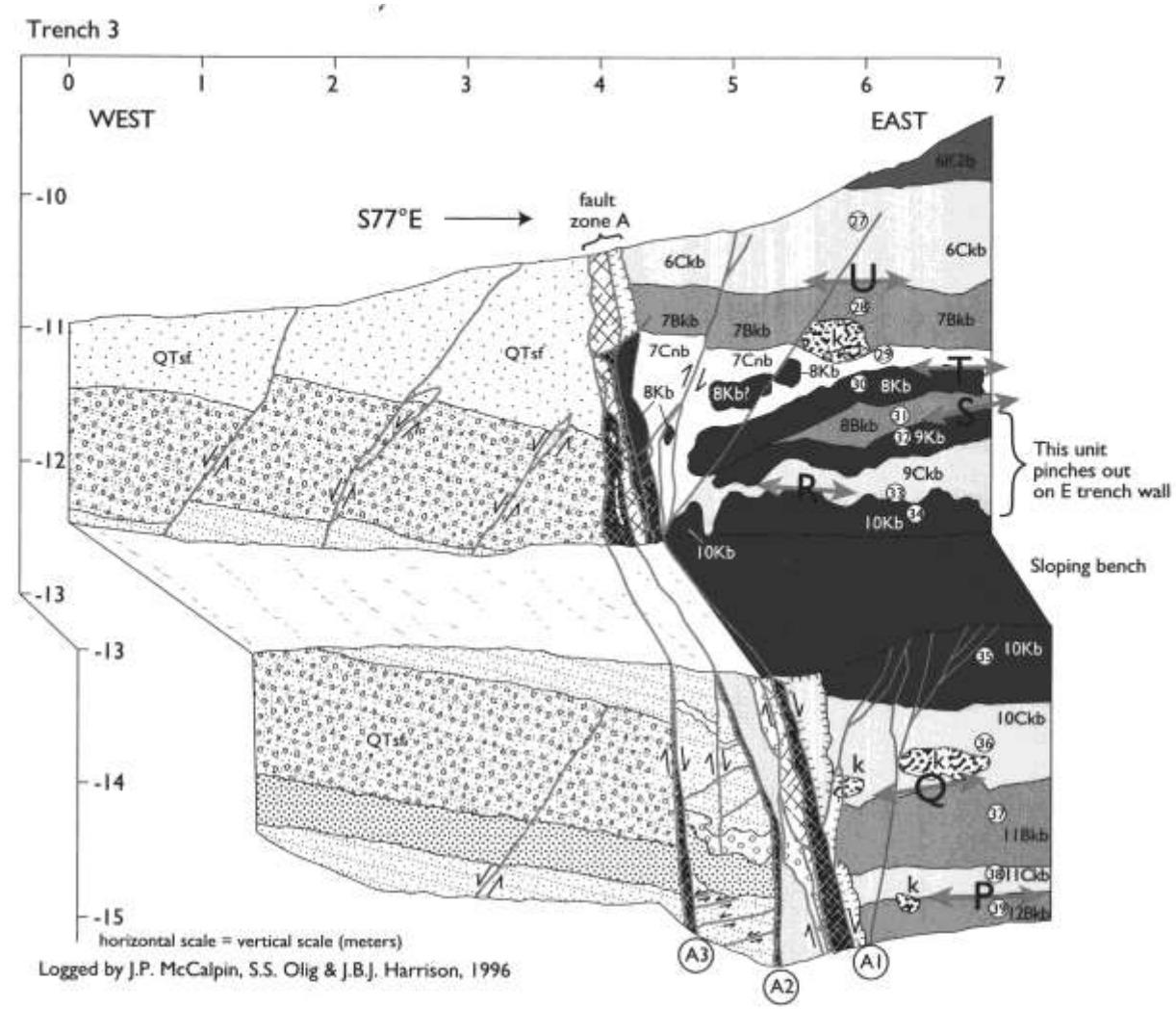

Units on upthrown block

- QTsf — Lithologies in the Santa Fe Group (Plio-Pleistocene)-Ceja Gravel Member
- Massive, unstratified medium-coarse-grained sand
- Laminated medium-grained sand
- Massive, poorly stratified sand and gravel
- Well stratified gravelly sand
- Small pebble (pea) gravel
- Large pebble gravel

Units in fault zone

- Fault
- Crack (no vertical displacement)
- A — Fault strand
- Intensely sheared sand and gravel, fabric parallel to fault dip
- Massive sheared sand and gravel, no fabric
- Sheared and cemented sand
- Massive carbonate cemented sand or gravel, cementation from fault-related ground water (not pedogenic)

Units on downthrown block

- Massive silty sand, mainly of eolian origin (Pleistocene)
- Krotovina
- ① Location of soil samples

Soil horizons (b = buried soil)

- K, K2 — Horizon containing stage III-IV calcium carbonate (as defined by Gile et al. 1966)
- Bk — Horizon of calcium carbonate and/or clay accumulation
- Ck — Horizon of minor calcium carbonate accumulation
- Cn — Horizon of unaltered parent material

Y — Event horizon, dashed where possible

FIGURE 11—Log of trench 3, north wall. The vertical scale at left shows depth below the surface of the Llano de Albuquerque.

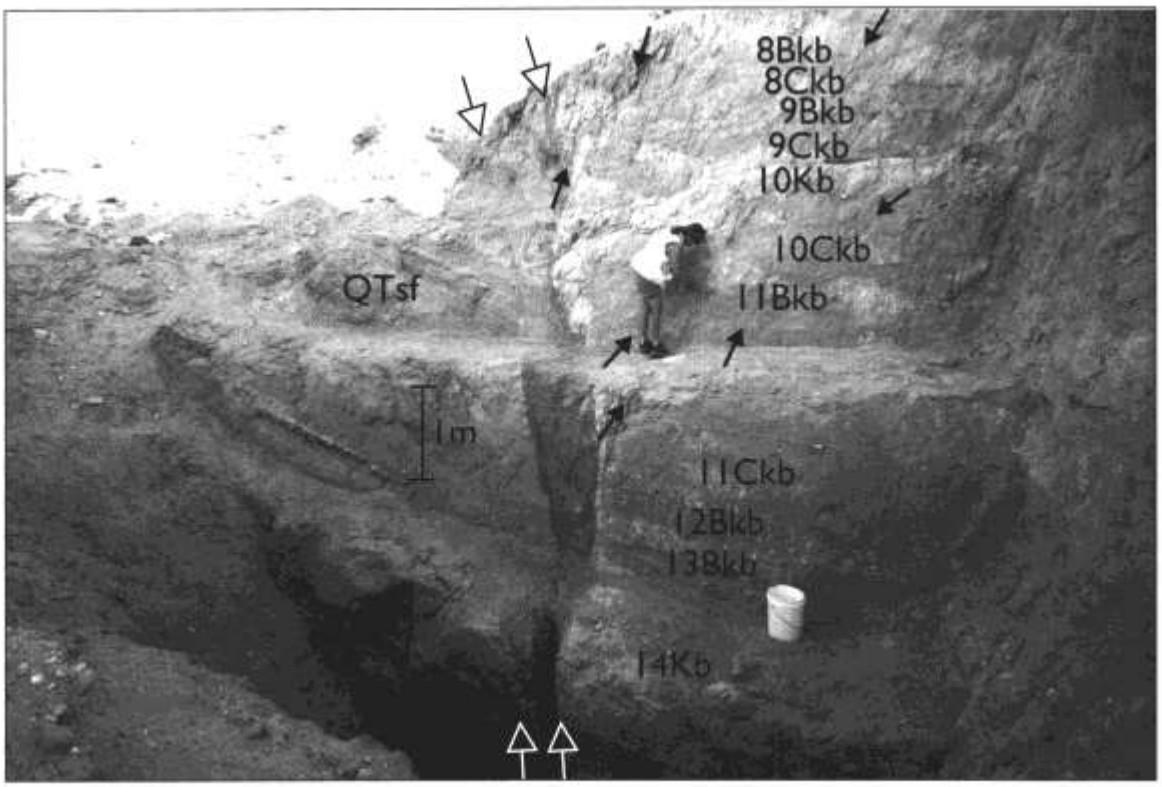

FIGURE 12—Photograph of trench 4. The three upper walls are visible, but the lowest wall is in shadow at bottom. Fault zone A is at left center, marked by open arrows at top and bottom of photo. Arrows with solid heads show small reverse faults in the hanging wall. This photo is taken approximately parallel to fault strike, rather than perpendicular to the trench walls.

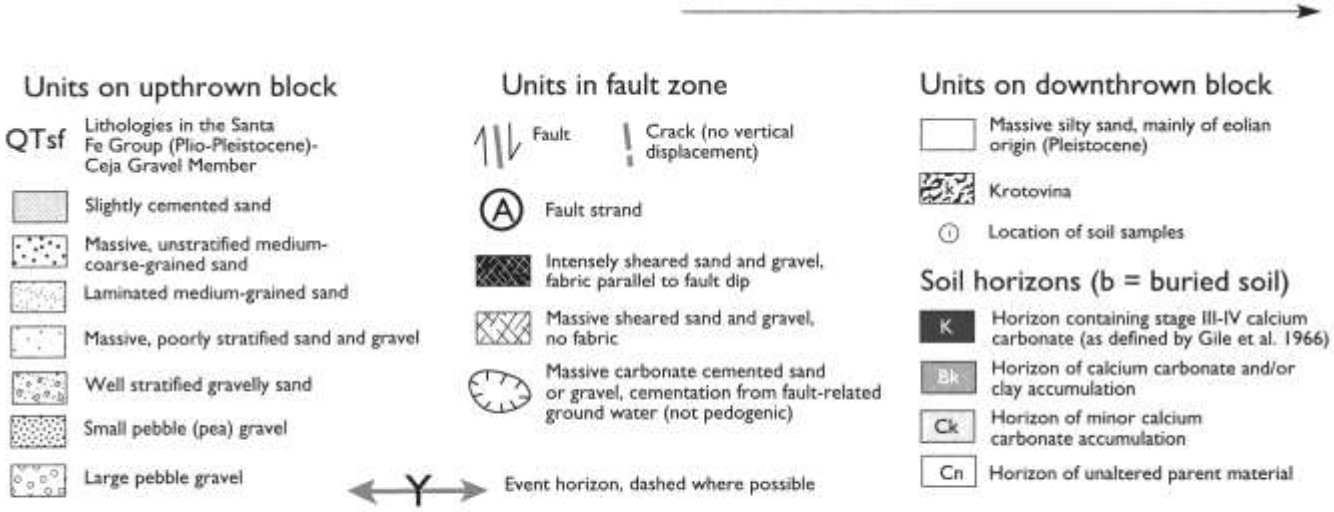

FIGURE 13—Log of trench 4, north wall. Fault zone A trends approximately north-south, whereas the trench walls trend S75°E, so the fault trace steps westward on each successively higher trench wall. Dashed box shown on the uppermost trench wall shows the location of the retrodeformation sequence of Figure 23. The vertical scale at left shows depth below the surface of the Llano de Albuquerque.

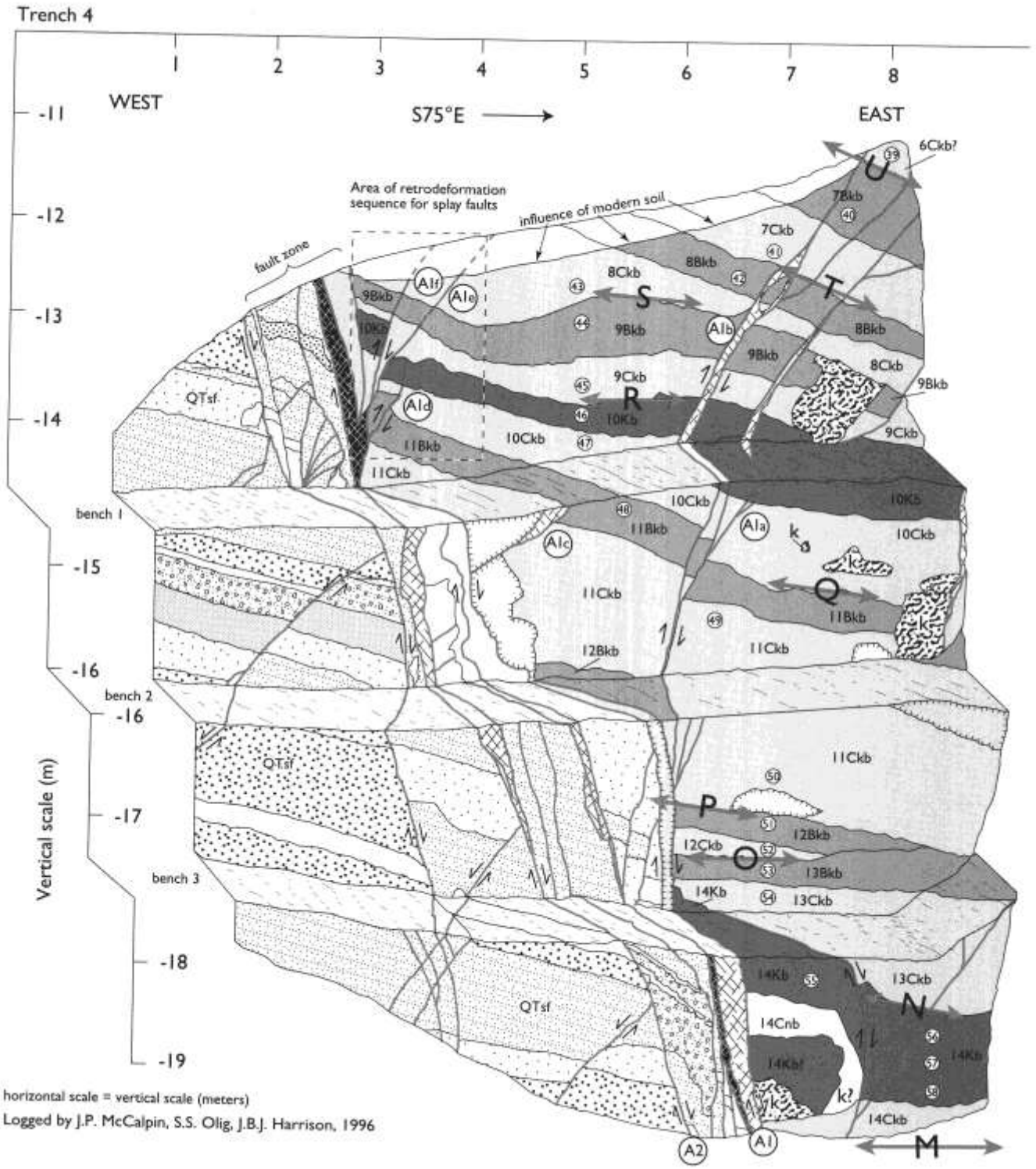
Trench 4
WEST
S75°E
EAST
1
2
3
4
5
6
7
8
-11
-12
-13
-14
-15
-16
-17
-18
-19
Vertical scale (m)
Area of retrodeformation sequence for splay faults
influence of modern soil
fault zone
bench 1
bench 2
bench 3
QTsf
A1f
A1e
A1d
A1c
A1b
A1a
A2
A1
U
T
S
R
Q
P
O
N
M
6Ckb?
7Bkb
7Ckb
8Bkb
8Ckb
9Bkb
9Ckb
10Kb
10Ckb
11Bkb
11Ckb
12Bkb
12Ckb
13Bkb
13Ckb
14Kb
14Cnb
14Kbf
14Ckb
k?
horizontal scale = vertical scale (meters)
Logged by J.P. McCalpin, S.S. Olig, J.B.J. Harrison, 1996

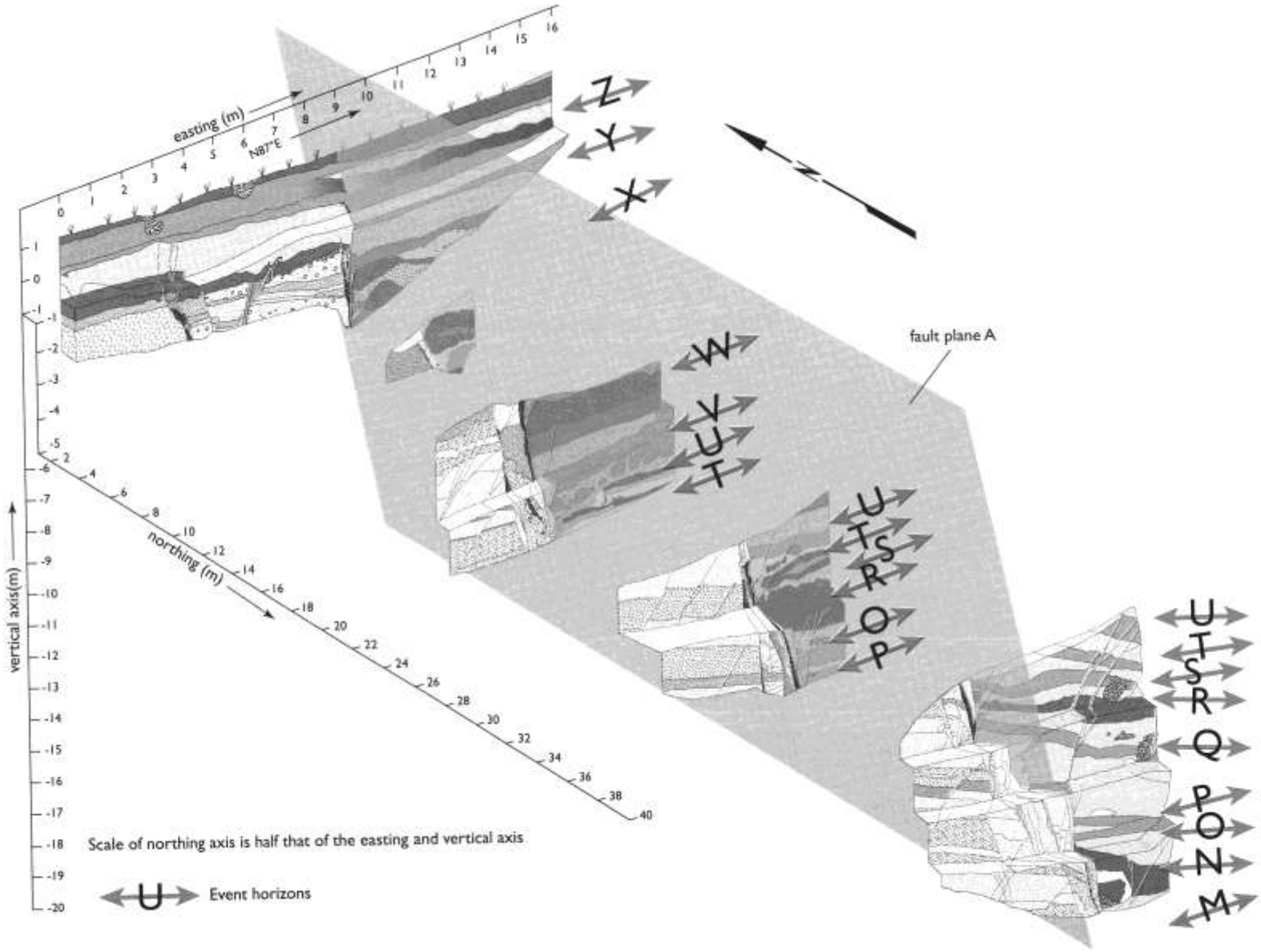

FIGURE 14—Perspective drawing of trenches 1–4, north is to upper left. Double-headed arrows at right show the location of the 14 event horizons (tops of buried soils). Fault plane A is defined as a planar, east-dipping normal fault that can be traced through five trenches.

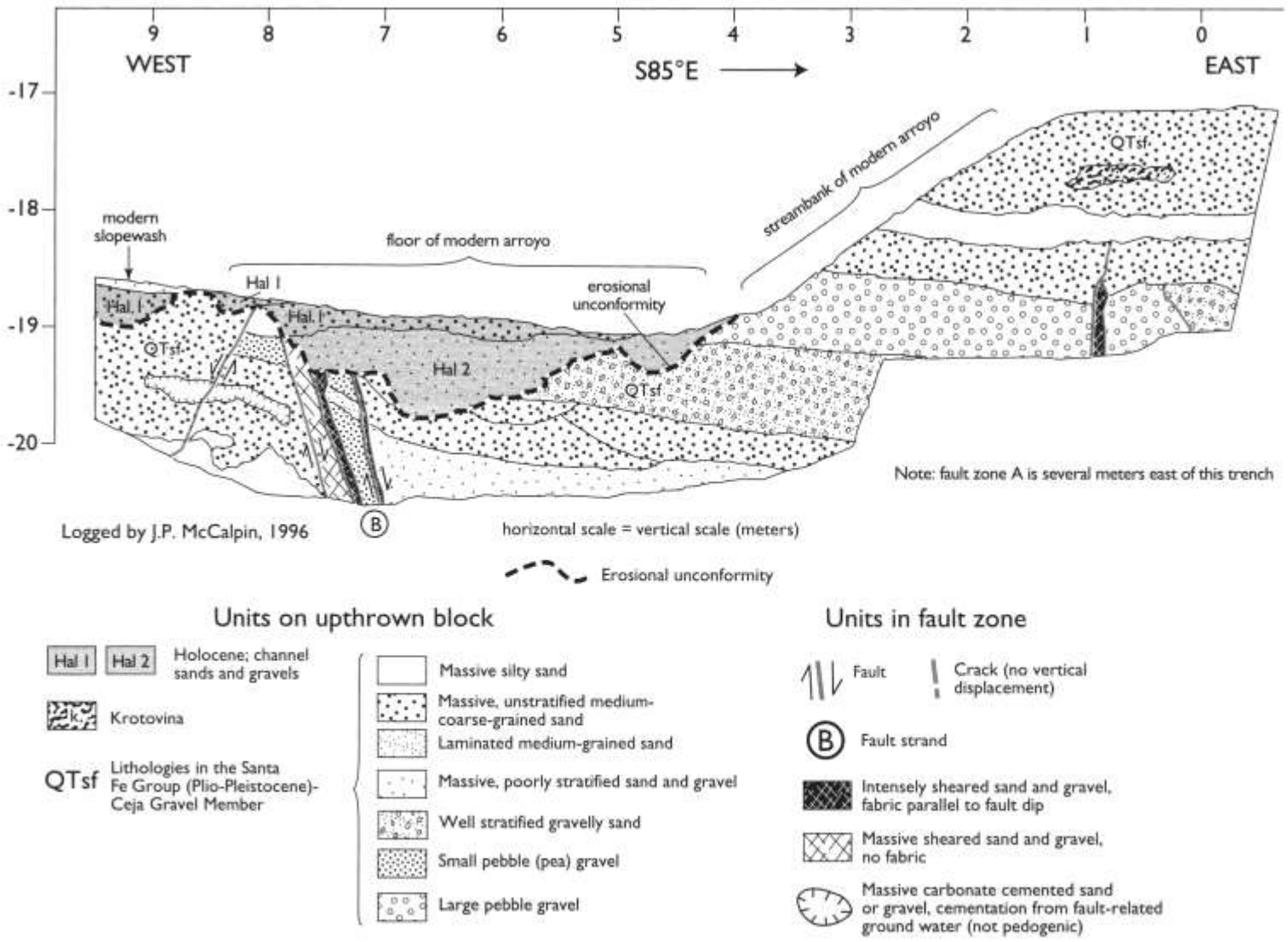

FIGURE 15—Log of trench 5, north wall. This trench exposed only the Ceja Member of the footwall, overlain by Holocene alluvium of the modern arroyo. Fault A is inferred to be several meters east of this trench. The vertical scale at left shows depth below the surface of the Llano de Albuquerque.

TABLE 2—Particle size, bulk density, and carbonate content of soil samples from trenches 1–4 and exposure 1 in the syntectonic depositional wedge. Soil horizons in a trench were sampled in multiple locations if horizon properties appeared to vary vertically or laterally.

Trench	Soil horizon	Thickness (cm)	% sand	% silt	% clay	Bulk density (g/cm^3)	Weight % $CaCO_3$
1	1Bk	17	78	10	12	1.75	5.5
1	1Bk	13	58	28	14	1.56	15.7
1	1Bk	21	58	28	14	1.46	11.4
1	1Ck1	21	82	8	10	1.69	4.0
1	1Ck1	36	84	7	9	1.71	2.6
1	2Bk	23	84	2	14	1.72	3.1
1	2Bk	23	84	2	14	1.73	3.1
1	2Ck	34	90	2	8	1.70	3.1
1	2Ck1	34	91	5	4	1.67	4.7
1	2Ck2	81	94	3	3	1.63	4.8
1	3Bkb	17	79	12	9	1.57	10.5
1	3Bkb	17	83	8	9	1.79	4.5
1	3Bkb	23	86	3	11	1.66	10.9
1	3Ck1b	60	92	4	4	1.67	2.0
1	3Ck2b	90	91	4	5	1.53	2.3
1	3Cnb	25	90	5	5	1.59	2.8
E1[1]	3Kb	15	84	8	8	1.65	6.5
E1[1]	3Bk1b	25	75	7	18	1.70	5.2
E1[1]	3Bk2b	22	76	12	12	1.94	8.1
E1[1]	3Ck1b	60	81	10	9	1.86	11.6
E1[1]	3Ck2b	90	82	4	14	1.67	6.7
E1[1]	3Cnb	25	90	6	4	1.62	4.1
E1[1]	4Bkb	13	95	2	3	N/A	1.4
2	4Bkb	80	89	5	6	1.65	13.6
2	4Kb	61	87	5	8	1.78	10.8
2	4K2b	32	89	4	7	1.66	9.9
2	5K1b	85	78	9	6	1.63	52.1
2	5K2b	64	87	5	13	1.55	33.2
2	5Ckb	74	92	2	8	1.73	7.7
2	6Bkb	62	86	4	10	1.73	10.5
2	7Kb	23	84	5	11	1.64	20.4
3	6Bkb	70	90	3	7	1.64	8.4
3	7Kb	46	86	6	8	1.88	8.5
3	7Ck2b	17	87	7	6	1.76	5.6
3	8Kb	23	87	6	7	1.76	8.7
3	8Bkb	20	85	7	8	1.71	9.4
3	9Kb	17	88	5	7	1.72	9.4
3	9Ckb	20	88	6	6	1.59	3.9
3	10Kb	37	86	6	8	1.56	10.4
3	10Kb	57	86	5	9	1.64	7.9
3	10Ckb	51	85	7	8	1.65	5.1
3	11Bkb	63	88	4	8	1.64	7.4
3	11Ckb	20	88	5	7	1.66	8.4
3	12Bkb	23	89	4	7	1.63	5.3
4	6Ckb?	37	91	3	6	1.68	9.1
4	7Bkb	70	90	4	6	1.63	6.4
4	7Ckb	56	92	3	5	1.61	5.4
4	8Kb	37	90	4	6	1.62	7.2
4	8Bkb	44	89	8	3	1.58	5.4
4	9Kb	48	87	6	7	1.69	6.1
4	9Ckb	41	91	4	5	1.67	5.3
4	10Kb	30	87	7	6	1.64	8.7
4	10Ckb	26	89	6	5	1.68	4.0
4	11Bkb	41	86	7	7	1.76	12.7
4	11Ckb	83	87	7	6	1.69	3.8
4	11Ckb	80	86	7	7	1.68	3.7
4	12Bkb	26	81	9	10	1.78	5.8
4	12Ckb	17	81	10	9	1.84	3.1
4	13Bkb	22	86	7	7	1.67	5.0
4	13Ckb	30	86	7	7	1.69	3.5
4	14Kb	44	81	10	9	1.65	10.8
4	14Kb	30	81	8	11	1.88	9.9
4	14Kb	30	82	9	9	1.89	7.1
4	14Kb	26	85	7	8	1.69	7.6

[1]Exposure 1, 5 m northeast of trench 2.

TABLE 3—Soil carbonate percents and weights from soil horizons in a composite soil column for the syntectonic depositional wedge. If a given soil horizon was sampled in multiple trenches or multiple locations in a single trench (Table 2), values listed here are averages of values listed in Table 2.

Sample no. (see trench logs)	Soil horizon	Thickness (cm)	Depth below Llano de Albuquerque (m)	Current weight % $CaCO_3$ (grams)	Current bulk density (g/cm^3)	Current total weight of $CaCO_3$ (grams)	Original weight % $CaCO_3$ (grams)	Original bulk density (g/cm^3)	Original weight of $CaCO_3$ (grams)	Cumulative original weight of $CaCO_3$ (grams)	Weight of secondary $CaCO_3$ (grams)	Cumulative weight of secondary $CaCO_3$ (grams)	TL/IRSL age estimate (ka)	Age (ka) assuming accumulation rate of 0.26 g/ka
1	1Bk	17	0.17	5.49	1.75	1.63	3	1.55	0.79	74.99	0.84	0.84		3
2	1Bk	13	0.3	15.71	1.56	3.19	3	1.55	0.60	74.20	2.58	3.42		13
3	1Bk	21	0.51	11.41	1.46	3.50	3	1.55	0.98	73.59	2.52	5.94		23
4	1Ck1	21	0.72	4.01	1.69	1.42	3	1.55	0.98	72.62	0.45	6.39		25
5	1Ck1	36	1.08	2.59	1.71	1.59	3	1.55	1.67	71.64	-0.08	6.31	27.7	24
6	2Bkb	23	1.31	3.05	1.72	1.21	3	1.55	1.07	69.97	0.14	6.45		25
7	2Bkb	23	1.54	3.07	1.73	1.22	3	1.55	1.07	68.90	0.15	6.60		25
8	2Ckb	34	1.88	3.05	1.7	1.76	3	1.55	1.58	67.83	0.18	6.78	38.3	26
9	2Ck1b	34	2.22	4.7	1.67	2.67	3	1.55	1.58	66.25	1.09	7.87		30
10	2Ck2b	81	3.03	4.76	1.63	6.28	3	1.55	3.77	64.67	2.52	10.39	41.2	40
11	3Bkb	40	3.43	10.48	1.57	6.58	2	1.55	1.24	60.90	5.34	15.73		61
13	3Bkb	20	3.63	10.89	1.66	3.62	2	1.55	0.62	59.66	3.00	18.72		72
14	3Ck1b	60	4.23	1.99	1.67	1.99	2	1.55	1.86	59.04	0.13	18.86		73
15	3Ck2b	90	5.13	2.32	1.53	3.19	2	1.55	2.79	57.18	0.40	19.26		74
16	3Cnb	25	5.38	2.78	1.59	1.11	2	1.55	0.78	54.39	0.33	19.59	82	75
17	4Bkb	14	5.52	13.63	1.65	3.15	3	1.55	0.65	53.61	2.50	22.09		85
18	4Kb	61	6.13	10.79	1.78	11.72	3	1.55	2.84	52.96	8.88	30.97		119
19	4K2b	32	6.45	9.94	1.66	5.28	3	1.55	1.49	50.13	3.79	34.76		134
22	5K1b	85	7.3	52.1	1.63	72.18	3	1.55	3.95	48.64	68.23	102.99		397
23	5K2b	64	7.94	33.18	1.55	32.91	3	1.55	2.98	44.69	29.94	132.93		512
24	5Ckb	74	8.68	7.68	1.73	9.83	3	1.55	3.44	41.71	6.39	139.32	>293	536
25,27	6Bkb	66	9.34	9.44	1.69	10.53	3	1.55	3.07	38.27	7.46	146.78		565
26,28	7Kb	35	9.69	14.46	1.76	8.91	3	1.55	1.63	35.20	7.28	154.06		593
27	7Ck1b	70	10.39	8.41	1.64	9.65	3	1.55	3.26	33.57	6.40	160.46		618
28,29	7Ck2b	32	10.71	7.06	1.82	4.11	3	1.55	1.49	30.32	2.62	163.09		628
30,42	8Kb	30	11.01	7.93	1.69	4.02	3	1.55	1.40	28.83	2.63	165.71		638
31,43	8Bkb	32	11.33	7.42	1.65	3.92	3	1.55	1.49	27.44	2.43	168.14		647
32,44	9Kb	33	11.66	7.74	1.71	4.37	3	1.55	1.53	25.95	2.83	170.98		658
33,45	9Ckb	31	11.97	4.62	1.63	2.33	3	1.55	1.44	24.41	0.89	171.87		662
34,46	10Kb	34	12.31	9.54	1.6	5.19	3	1.55	1.58	22.97	3.61	175.48		676
35	10Kb	57	12.88	7.94	1.64	7.42	3	1.55	2.65	21.39	4.77	180.25		694
36,47	10Ckb	39	13.27	4.53	1.67	2.95	3	1.55	1.81	18.74	1.14	181.39		698
37,48	11Bkb	52	13.79	10.52	1.7	9.30	3	1.55	2.42	16.93	6.88	188.27		725
38,49	11Ckb	52	14.31	6.11	1.68	5.34	3	1.55	2.42	14.51	2.92	191.19		736
50	11Ckb	80	15.11	3.7	1.68	4.97	3	1.55	3.72	12.09	1.25	192.44		741
39,51	12Bkb	25	15.36	5.55	1.71	2.37	3	1.55	1.16	8.37	1.21	193.65		746
52	12Ckb	17	15.53	3.12	1.84	0.98	3	1.55	0.79	7.21	0.19	193.84		746
53	13Bkb	22	15.75	5.01	1.67	1.84	3	1.55	1.02	6.42	0.82	194.65		749
54	13Ckb	30	16.05	3.48	1.69	1.76	3	1.55	1.40	5.39	0.37	195.02		751
55	14Kb	44	16.49	10.75	1.65	7.80	3	1.55	2.05	4.65	5.76	200.78		773
56	14Kb	30	16.79	9.86	1.88	5.56	3	1.55	1.40	4.00	4.17	204.95		789
57	14Kb	30	17.09	7.11	1.89	4.03	3	1.55	1.40	2.60	2.64	207.58		799
58	14Kb	26	17.35	7.55	1.69	3.32	3	1.55	1.21	1.21	2.11	209.69		807

Note: the stratigraphic thicknesses listed in Table 3 do not exactly match the depths below surface of horizon tops, as shown on the trench logs, because soils in trenches 2–4 have a small component of southward dip. Thus soils 6–14 become slightly deeper below the surface when traced from trench 2 to trench 4.

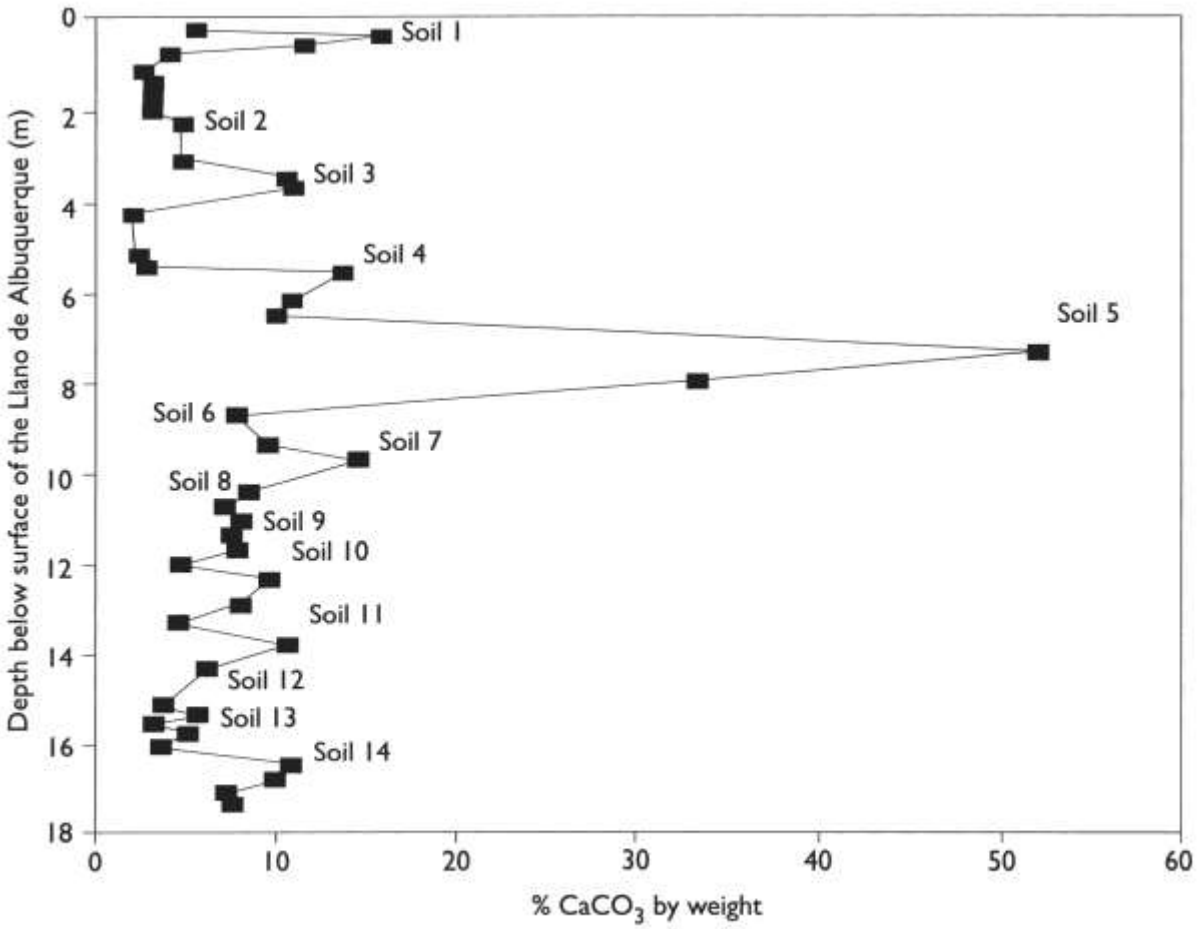

FIGURE 16—Current weight % calcium carbonate in the syntectonic depositional wedge, as a function of depth below the Llano de Albuquerque. Most values above 10% are from K horizons (stage III), with strongest development in soil 5 (horizon 5K1b, 52% $CaCO_3$; horizon 5K2b, 33% $CaCO_3$). Bk and Ck horizons range from 4–8% $CaCO_3$. The lowest values come from Cn horizons such as 3Cnb (2–3% $CaCO_3$).

lated them with nine luminescence dates (thermo- and infrared stimulated luminescence) from selected horizons.

Quantitative soil parameters

We measured gravel:sand:silt:clay contents, total calcium carbonate, and bulk density for each of the soil horizons in the 14 soils of the syntectonic wedge (Table 2). Our overall aim was to compute the weight of secondary (pedogenic) calcium carbonate in each of the soils (Table 3) and use those weights to estimate the duration of soil formation, as done by Machette (1978). Several assumptions must be made to calculate weights of secondary soil carbonate, and ours differ from Machette's (1978) in several respects. First, we assume that the massive sand deposits in the wedge (eolian and reworked eolian?) originally contained 3% carbonate by weight, that being the lowest value we find in horizons with the least degree of soil development (Cn horizons). In contrast, the coarser gravels and sands of inferred fluvial origin (unit 3) that are unaffected by soil formation (horizon 3Cn) contain 2.78% carbonate, with other soil horizons of unit 3 containing as little as 1.99% carbonate. We thus assume the original carbonate content of fluvial deposits was 2%, or a bit less than the eolian material. In contrast, Machette (1978) assumed original (primary) carbonate content of wedge sediments ranging from 0.5% for Ceja Member deposits, to 3% for fluvial units, to 4-10% for sandy (eolian) deposits. We prefer to use a single, consistent estimate of primary carbonate content for eolian and fluvial sediments, rather than use highly variable values based on the lowest measured value in each soil, because we believe those variable values are affected by secondary carbonate.

We assume an original bulk density of sand-rich deposits of 1.55 g/cm^3, based on the lowest current densities of wedge deposits. Machette (1978) assumed densities of 1.6-1.7 g/cm^3, based on his lowest values for modern bulk density. We prefer a lower density value because our analysis of the scarp profile ("County Dump fault, Geomorphology," p. 5) suggests much of the syntectonic wedge may be airfall eolian sand and silt, which would have a lower initial density than water-laid or colluvial sediments.

To calculate the weight of secondary carbonate in a 1 cm^2 vertical column in each horizon (Tables 2, 3), we calculated the weight of total carbonate (horizon thickness x % carbonate x bulk density) and the weight of (inferred) original carbonate (horizon thickness x original % carbonate x original bulk density). The difference between these two weights is assumed to represent secondary (pedogenic) carbonate. Where the same soil horizon was sampled in two trenches, we averaged the % CaCO3 and bulk density values (e.g., horizons 6Bkb through 12Bkb).

In the 33 soil horizons sampled (over 17.3 m of stratigraphic thickness), weight percent of carbonate ranges from a minimum of 1.99% (alluvium of unit 3) to 52.1% (horizon 5K1b; Fig. 16). In general, the 16 Ck horizons have 2.0-8.4% carbonate (mean = 4.51 ± 1.86%), the 13 Bk horizons have 3.0-15.7% carbonate (mean = 8.58 ± 3.83%), and the 12 K horizons have 7.1-52.1% carbonate (mean = 14.8 ± 13.2%). The mean carbonate contents of the 16 Ck horizons (4.51 ±

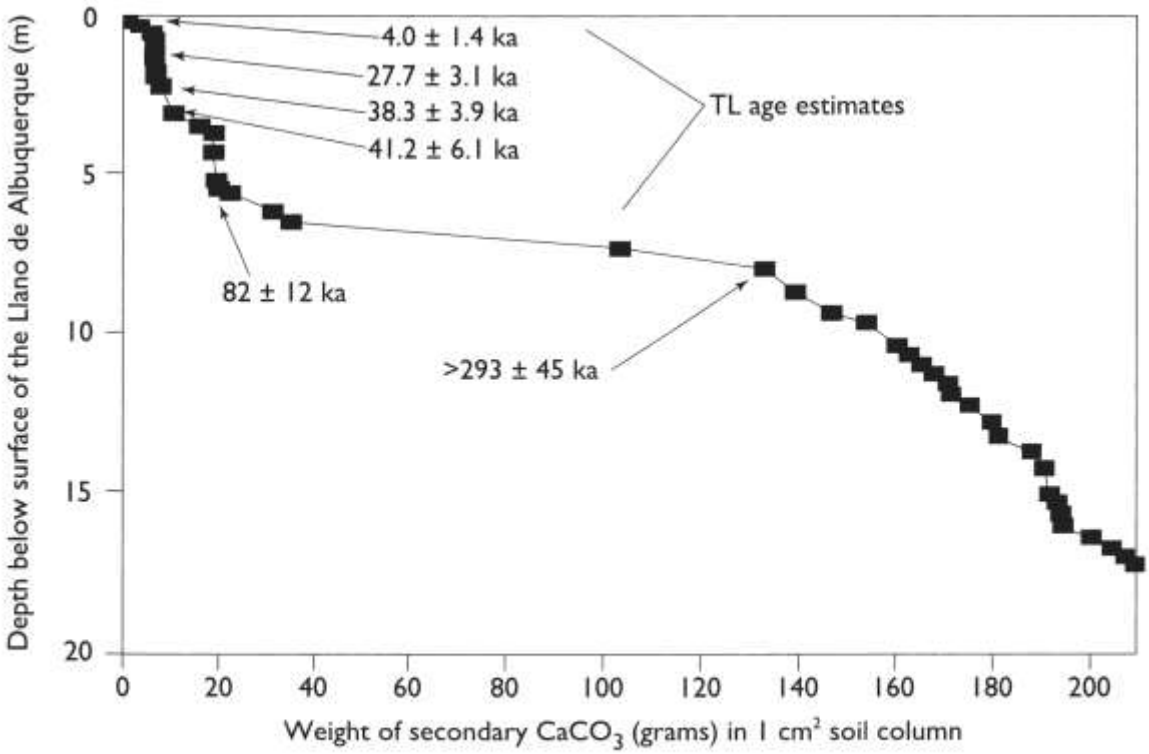

FIGURE 17—Cumulative weight of secondary $CaCO_3$ in the syntectonic depositional wedge, as a function of depth below the Llano de Albuquerque. TL age estimates are from Table 5. Nearly half of the total carbonate comes from soils 4 and 5, dated between 82 ka and greater than 293 ka.

1.86%) and the 13 Bk horizons (8.58 ± 3.83%) can be compared via the Z statistic of Sheppard (1975), where Z = (mean$_s$ — mean2)/(sq rt (sigma$_1^2$ + sigma$_2^2$)). This test indicates that there is only a 35% chance that these two groups of carbonate contents could have been drawn from a single normal distribution. Thus, our field definition of Ck and Bk horizons based on macroscopic properties seems supported by statistically significant differences in carbonate content between the groups.

In contrast, our Bk and K horizons have very similar average carbonate contents. The mean carbonate of the 13 Bk horizons (8.58 ± 3.83%) and the 12 K horizons (14.8 ± 13.2%) have a 63% chance of being drawn from the same Gaussian population. If the anomalously high carbonate values from the two soil 5 K horizons are excluded from this comparison, the mean carbonate values (8.58 ± 3.83% for Bk horizons, 9.28 ± 2.1% for K horizons) have a 95% chance of being derived from a single normal distribution. Thus, our field assignment of horizon designations for the upper horizons of soils 6-14 as either Bk or K, based on the presence of stage **III** carbonate, is not well reflected by differences in bulk carbonate contents.

Bulk densities range from 1.46 to 1.89 g/cm^3 with the more carbonate-rich horizons generally having the lower densities. Total carbonate in a 1 cm^2 column through the entire 17-m-thick colluvial soil section is 282 g, with 76 g inferred to be original (primary) carbonate. Therefore total secondary carbonate is estimated as 206 g (Fig. 17). This value is about 17% larger than Machette's (1978) estimate of 176 g, made from a 19-m-thick composite soil section in the syntectonic wedge. Secondary carbonate increases with depth in a relatively linear pattern through soils 6-14 but increases much more rapidly in the strong K horizons of soil 5. The rate of increase in soil 4 is similar to that in soils 6-14, but the rate decreases in soils 1-3 because of their overall low carbonate contents.

Our secondary carbonate value is 17% greater than Machette's (1978) for several reasons. First, we assume that the primary carbonate content of wedge sediments is lower than did Machette (as described above), and this tends to proportionally increase our estimate of secondary carbonate relative to his estimate. Second, we assume a lower original bulk density (1.55 g/cm^3) compared to Machette's 1.7 g/cm^3, and this also reduces our primary carbonate estimate.

Luminescence dating

Luminescence dating determines the elapsed time since the last exposure of detrital minerals to daylight. We used the thermoluminescence (TL) and infrared stimulated luminescence (IRSL) methods on the 4-11 micron (fine silt) fraction of soil horizons in the syntectonic wedge stratigraphic section. One sample was taken from the modern (Holocene) eolian sand blanket that mantles the scarp face, which we assume is a modern analog to eolian-derived deposits in the syntectonic wedge. The remaining eight samples were taken from soil horizons 1Ck2, 2Ck1b, 2Ck2b, 3Cn2b, and 5Ckb. The last sample (from 5Ckb) was collected at a depth of 8.38 m below the surface of the Llano de Albuquerque, or about halfway down the syntectonic wedge.

The modern eolian sand blanket yielded a TL age of 4.0± 1.4 ka (Table 4) at a depth of 20-25 cm. The "plateau" plot for this sample (Fig. 18) indicates a very young age (low DE values), as expected. The dose response curves are supralinear, typical of very young or "modern" sediments (Berger 1988, 1990). The TL age represents an insignificant "Zero-point" error for samples older than ca. 40 ka. Indeed, because sample He was from a depth of 20-25 cm, its burial age is not zero but somewhere between 1 and 4 ka. Furthermore, this youthful result indicates that during the accumulation of surface sediment by a combination of eolian, slopewash, pedoturbation, and other unknown processes, sufficient zeroing of light-sensitive TL takes place at this site to lend

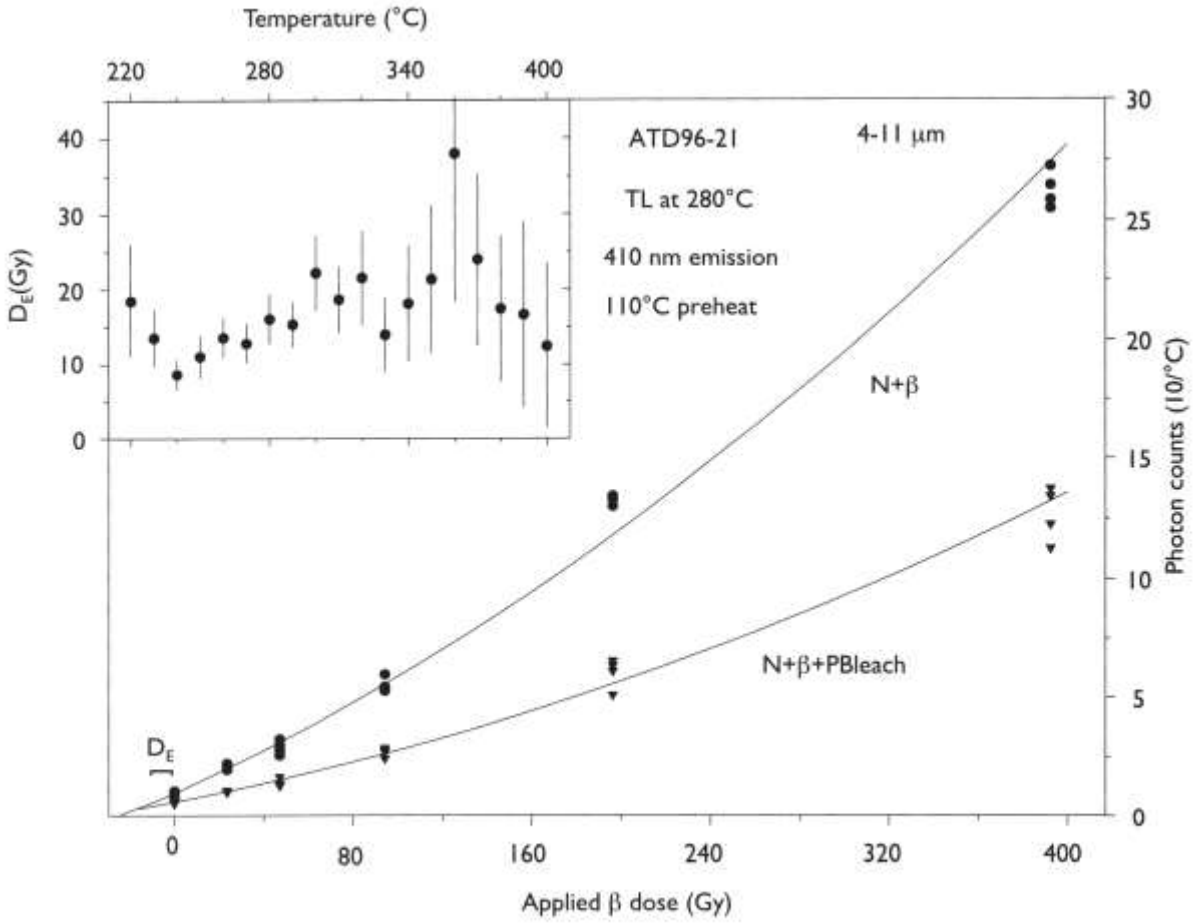

FIGURE 18—Thermoluminescence data from sample ATD96-21, in the surface blanket of Holocene eolian sand. N+β, natural sample plus laboratory beta dose; N+β+PBleach, natural sample plus laboratory beta dose, minus the effect of partially bleaching the sample.

TABLE 4—Thermoluminescence (TL) and infrared stimulated luminescence (IRSL) data and age estimates.[1]

Soil horizon	Sample number	Preheat[2]	Bleach[3]	D_E (Gy)[4]	Temp. (°C)[5]	Age estimate (ka)
He	ATD96-21	110 °C/3 days	PB/560 (8 hrs)	13.5 ± 4.7	210–350	4.0 ± 1.4
1Ck2b	ATD96-1	130 °C/3 days	TB/400 (3 days)	92.3 ± 9.0	290–410	27.7 ± 3.1
2Ck1b	ATD96-7	145 °C/3 days	TB/400 (3 days)	133 ± 11	280–390	38.3 ± 3.9
2Ck2b	ATD96-4	145 °C/3 days	TB/400 (3 days)	133 ± 18	260–390	41.2 ± 6.1
2Ck2b	IRSL[5]	160 °C/3 days	TB/780 (6 hrs)	211 ± 38	5–15 sec	65 ± 12
3Cnb	ATD96-17	145 °C/3 days	TB/560 (3 days)	333 ± 43	250–380	82 ± 12
3Cnb	IRSL[5]	160 °C/3 days	TB/780 (6 hrs)	531 ± 79	5–80 sec	130 ± 21
3Cn2b	ATD96-10	147 °C/3 days	TB/400 (3 days)	515 ± 56	300–400	160 ± 20
5Ckb	ATD96-14	147 °C/3 days	TB/400 (3 days)	1010 ± 140	310–370	293 ± 45

[1]TL and IRSL recorded near 410 nm wavelength emissions (e.g., Lang and Wagner 1997; Krbetschek et al. 1997). For TL analyses, the heating rate was 5 °C/sec. The polymineral 4–11 micron size fraction was used for all luminescence measurements.

[2]The chosen pre-readout annealing (see Berger and Anderson 1994; Berger 1994, for rationale).

[3]The value in parentheses specifies the laboratory optical bleaching time. PB = "partial bleach" method; TB = "total bleach" method. TB and PB specify use of different optical-filter passbands for bleaching, as follows: 560 = 560–800 nm at 90% transmission; 400 = 390–740 nm at 95% transmission; 780 = pass sunlight > 780 nm (near infrared). These choices largely follow the practice of Berger (1994), but the 780 nm bleaching is a modification suggested by Huntley and Clague (1996).

[4]Weighted mean equivalent dose plus average error over temperature interval in next column (or IRSL stimulation interval). A weighted = saturating-exponential regression model (Berger et al. 1987) was employed for all samples except ATD96-21, for which a weighted quadratic (Berger et al. 1987) was employed.

[5]This row presents data from IRSL experiments. The "Temp." column specifies diode-on time interval.

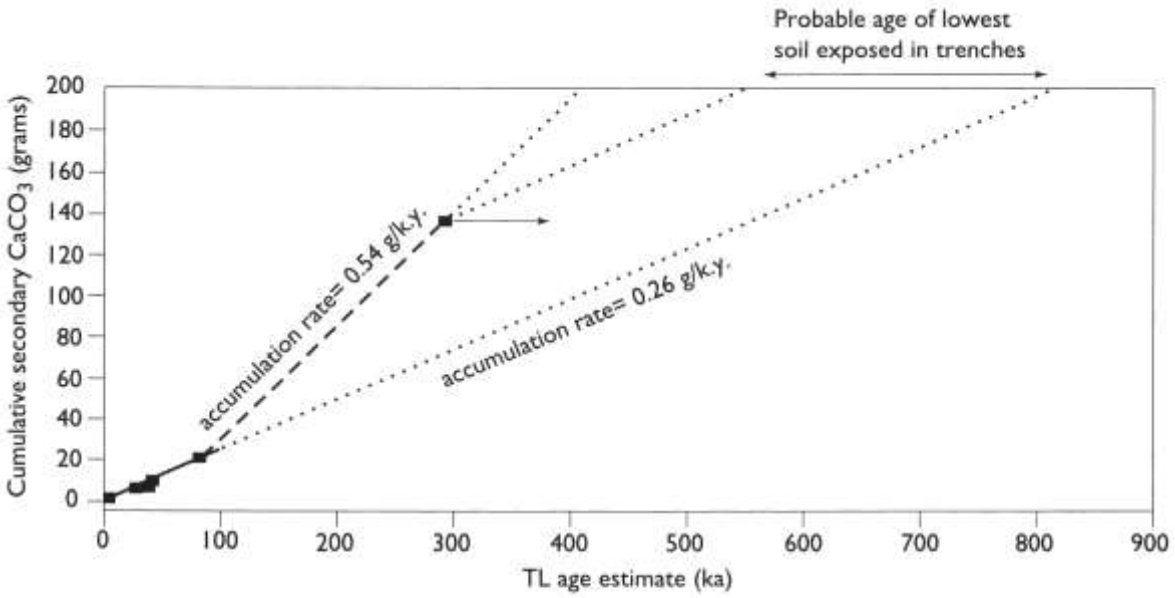

FIGURE 19—Cumulative secondary $CaCO_3$ in the syntectonic wedge, as a function of TL age. The five black boxes at lower left show five of our six TL ages from 4 ka to 82 ka. The black box with the arrow is the minimum TL age estimate of 293 ± 45 ka from horizon 5Ckb. Two dotted lines are extended upward from the 293 ka date, the left one at a slope of 0.54 g/k.y., the right one at a slope of 0.26 g/k.y. These two intercepts at the top of the graph define the minimum age of the lowest soil exposed in the trenches. A linear accumulation rate of 0.26 g/k.y., which assumes the 293 ka age estimate is a considerable underestimate, predicts that the lowest exposed soil is ca. 807 ka.

confidence that the zeroing assumption has been satisfied for all older, similar sediments at this site and in this region.

TL samples from horizons 1Ck2, 2Ck1b, and 2Ck2b yield a stratigraphically consistent series of ages between 27.7 ka and 41.2 ka. Because the parent material of these horizons was poorly stratified sand with a small silt component, similar to the modern eolian sand blanket, we assume that the initial TL, signal level was zero and that the TL ages are accurate.

Sample ATD96-10 was collected from poorly stratified, pebbly sandy alluvium of unit 3 and yielded a TL, age of 160 ± 20 ka. The TL behavior of this sample is consistent, and there is no internal reason to doubt the accuracy of the TL age. However, the sampled deposit overlies and underlies exotic blocks of calcic soils from unit 5 (horizon 5K1b) that fell into the fault zone. Thus, the sampled deposit is probably not in situ and may have been derived from strata once on the upthrown block. For this reason the initial (predepositional) TL signal may not have been zero in all grains at final deposition, and the TL age may be too old.

The sample taken from unit 3 in exposure 1, 5 m east of the fault zone and presumably unaffected by scarp-derived colluviation, yielded a younger age of 82 ± 12 ka (Table 4). The sampled parent material was a massive silty sand of probable eolian-colluvial origin, so its provenance is more conducive to accurate TL dating than the sample dated at 160 ± 20 ka from sediments of unknown provenance in the fault zone. In addition, its position on the depth plot (Fig. 19) of secondary carbonate is more consistent with dated samples above and below it, than is the stratigraphically higher date of 160 ka. The IRSL age of unit 3 is 130 ± 21 ka, or about 60% older than the TL age. This age discordance is not understood, because the opposite trend is expected if the TL signal includes a relict (pre-depositional) component. Additional annealing and other experiments are required to help understand this discordance. Without such understanding, it is prudent to exclude these IRSL results from our interpretation of the chronology. Since this project was completed, Berger (2003) also observed some discordant IRSL and TL results and interpreted the TL results as accurate.

The stratigraphically lowest sample (ATD96-14, from horizon 5Ckb) yielded the oldest TL age estimate of 293 ± 45 ka. The D_E—T plot (Fig. 20) is interpreted to indicate that the **DE** value of 1,010 ± 140 Gy is a minimum, and that the true depositional age of this sample could be older. Use of a hotter annealing would still leave sufficient TL for good measurements, and the present dose-response (Fig. 20) is not near saturation, so extraction of an older signal is possible, but such an experiment was beyond the scope of this project.

These TL ages from the upper half of the colluvial wedge section can be used to extrapolate to the age of the bottom of the syntectonic wedge. The bottom of the wedge, in turn, should have been deposited in response to the initial formation of the fault-angle depression. Therefore, the age of the bottom of the syntectonic wedge should approximate the inception of post-Llano de Albuquerque displacement on the County Dump fault. The inception of faulting, however, is not necessarily contemporaneous with the abandonment of the Llano de Albuquerque as a depositional surface ca. 1 Ma, as discussed later.

Two TL age trends were plotted. First, we plotted TL age as a function of depth below the Llano de Albuquerque surface (Fig. 21). This age-depth curve has variable slopes, ranging from very steep in alluvial unit 3 to very gentle in strong soils, such as units 4 and 5. Clearly, the stratigraphic section containing soils 1-5 includes some rapidly deposited parent materials, such as unit 2, and soil horizons that represent stable geomorphic surfaces that lasted hundreds of thousands of years (soil 5). Because of this highly variable sedimentation rate, we cannot use a simple age-depth trend to extrapolate the ages of soils 6-14.

Our second plot (cited previously) is cumulative secondary carbonate as a function of TL age (Fig. 19). If carbonate accumulation rates have been constant through time, and no significant dissolution or reprecipitation has occurred, the age versus secondary carbonate trend should provide a better basis for extrapolating the ages of soils 6-14. The age-car-

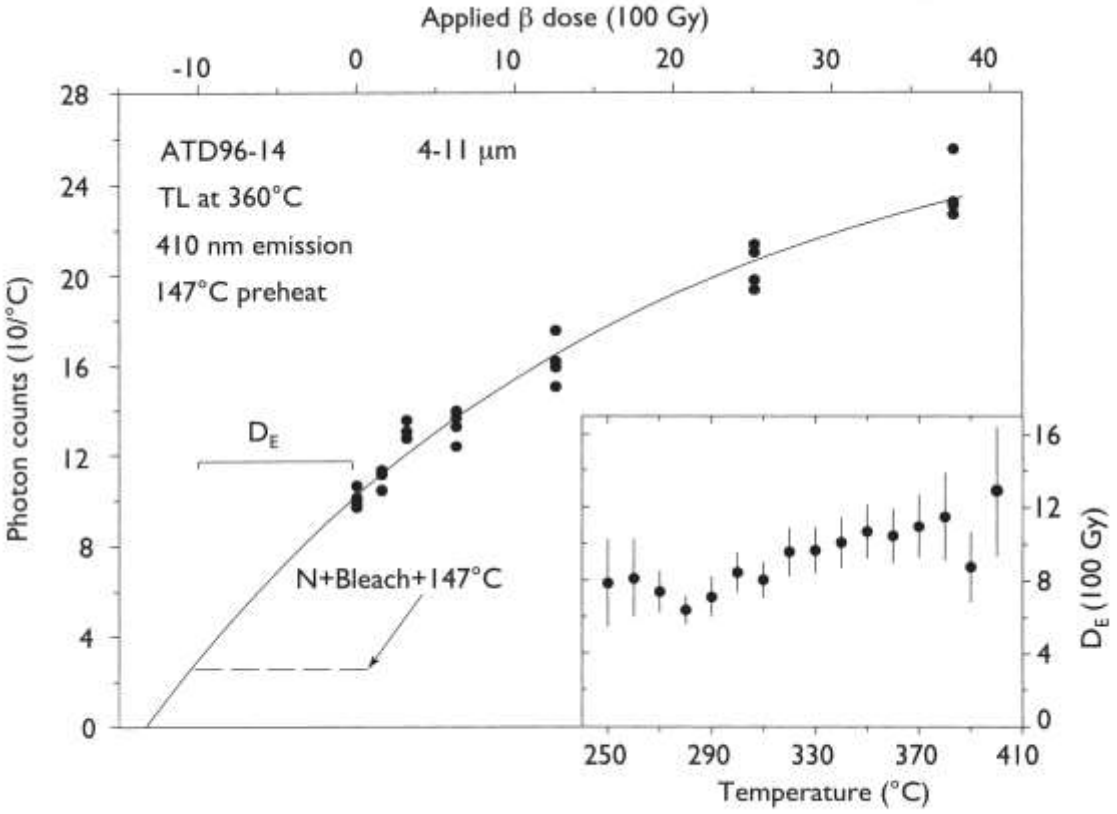

FIGURE 20—Thermoluminescence data from sample ATD96-14, from soil horizon 5Ckb. This sample was the stratigraphically lowest sample dated, although additional samples were collected at deeper levels.

bonate curve also contains segments of different slopes, with the four TL ages from soils 1-4 defining a carbonate accumulation rate of 0.26 g/k.y. over the time period 4-82 ka, and the two TL ages from soils 4 and 5 (from 82 to > 293 ka) yielding a maximum accumulation rate of 0.54 g/k.y. These rates can be compared with those determined elsewhere in the southwestern U.S. (Machette 1985) and fall closest to cited rates from Las Cruces, New Mexico, of 0.25 g/k.y. for pluvial climates in the Pleistocene and 0.5 g/k.y. for interpluvial climates. We note, however, that if the TL age for the deepest sample is only a minimum, then the carbonate accumulation rate for soils 4 and 5 would be lower, perhaps much lower, than 0.54 g/k.y.

One possible explanation for the more rapid accumulation of carbonate between 82 and 293 ka, as opposed to 4-82 ka, is different climate. The period 82-293 ka covers marine oxygen-isotope stages 4, 5, 6, 7, and 8, of which stages 5 and 7 were extended, warm, interpluvial periods. In contrast, the period 4-82 ka includes stages 1, 2, 3, and 4, and a higher percentage of that period was characterized by cold, pluvial climates. During pluvial climates the higher available moisture may have flushed the eolian influx carbonate to lower positions in the profile, or transported it entirely through the profile.

An alternative scenario is that the base of unit 5 is considerably older than the minimum TL age estimate of 293 ka, and that the carbonate accumulation rate at this site has averaged 0.26 g/k.y. over all of post-Llano de Albuquerque time. In that case, soil 5 by itself would require about 520 k.y. to form, and the extrapolated age of the base of the syntectonic wedge would be ca. 807 ka. Such an age is permissible with current age estimates of the abandonment of the Llano de Albuquerque as ca. 1 Ma.

Finally, the fact that Machette's (1978) soil Z is developed on the Ceja Member beneath the syntectonic wedge requires that soil Z formed after the abandonment of the Llano de Albuquerque but before the development of the syntectonic wedge. In other words, there was a period of soil formation and tectonic quiescence after abandonment of the Llano de Albuquerque ca. 1 Ma and before the inception of faulting on the County Dump fault. Soil Z contains 35 g of secondary carbonate (Machette 1978, table 1). At an accumulation rate of 0.26 g/k.y. soil Z would require 135 k.y. to form. Thus, a maximum-age scenario is that the syntectonic wedge began to form ca. 807 ka, following a 135 k.y. period of soil formation that began with abandonment of the Llano de Albuquerque. This would date Llano de Albuquerque abandonment at ca. 942 ka, which is roughly consistent with age estimates of ca. 1-1.6 Ma for the Llano de Albuquerque cited in "Regional setting," p. 4.

Interpretation

Origin of sediments and soils in the syntectonic depositional wedge

The 19-m-thick syntectonic depositional wedge appears at first glance to be similar in shape (if not dimensions) to a scarp-derived colluvial wedge, such as the colluvial wedges of smaller fault scarps in the western U.S. (McCalpin 1996a). However, the sedimentology of the syntectonic wedge (massive, unstratified silty sand) indicates that it is not merely reworked gravels derived from upper Santa Fe Group beds on the upthrown block. Instead, the wedge deposit is similar to deposits of eolian sand (units He, 1 and 2) that presently overlie the fault plane and blanket the scarp face. This similarity suggests that, during a typical faulting event on this fault, the free face created is smaller than the thickness of

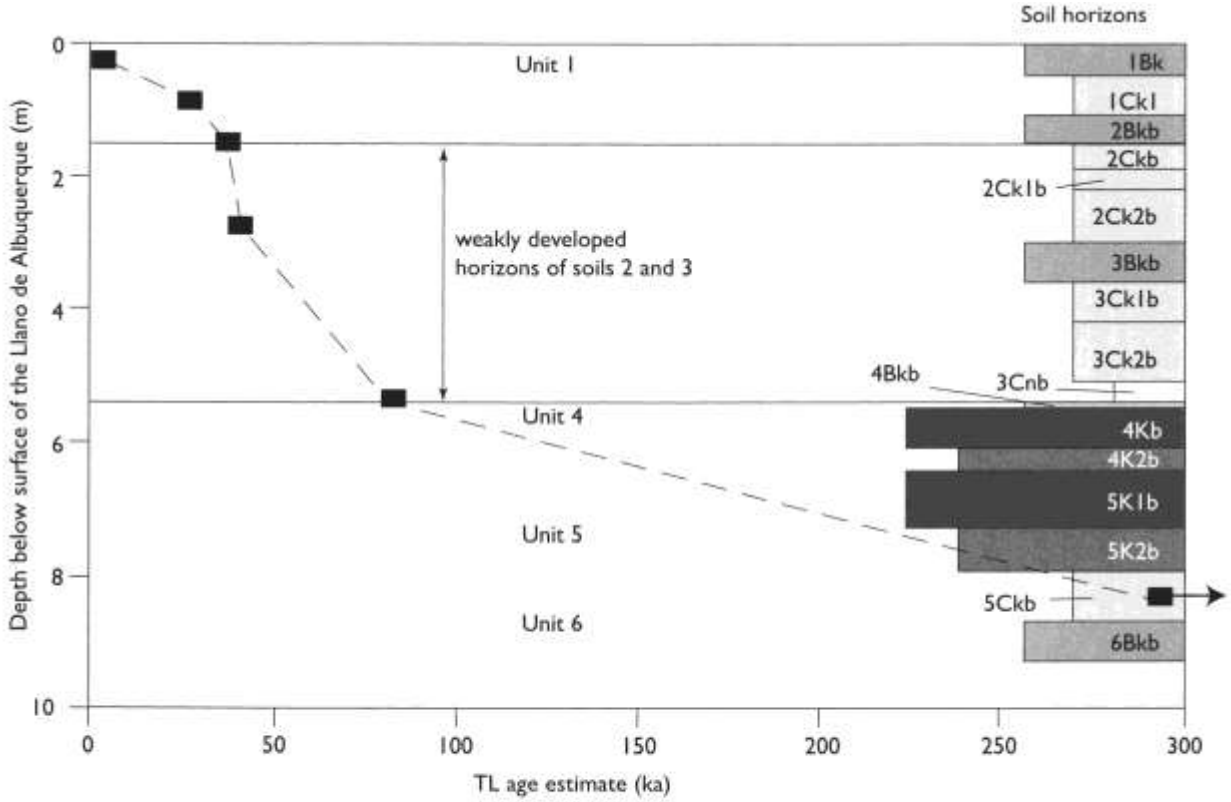

FIGURE 21—Thermoluminescence age as a function of depth below the Llano de Albuquerque. Black boxes show the six TL age estimates; IRSL age estimates are not shown. Soil horizons are shown at right, with darker shade and wider boxes indicating stronger soil development. Note that the apparent "sedimentation rate" is greatest in weakly developed soil horizons of units 2 and 3 and smallest in the most strongly developed soils (4 and 5). These latter soils represent long times of soil formation and local landscape stability.

eolian deposits on the scarp face, and thus no beds of the gravelly Santa Fe Group are exposed in the free face. In this scenario, post-faulting erosion would progress upslope into the upthrown block by eroding part of the eolian blanket and redepositing it as sheets of reworked sand on the down-thrown block.

A second observation is the general scarcity of carbonate soil chunks and blocks in the colluvium adjacent to the fault plane. If a strong petrocalcic soil (Bk or K horizons) existed at the ground surface when faulting occurred, one would expect the displacement to have shattered the brittle carbonate, and for blocks of soil horizons to fall from the free face and become deposited in the proximal colluvium near the fault plane. However, this is present at only one stratigraphic level (trench 1) where blocks of soils 4 and 5 fell into unit 3 as it was being deposited. In all other cases the sediments in the colluvial sequence do not contain exotic blocks of soils and do not visibly vary in grain size or bedding when traced laterally up to the fault plane. One possible explanation for the scarcity of soil blocks in the colluvium is that, at the time of faulting, the eolian blanket on the scarp face did not possess a strong soil, as is true of the Holocene sand blanket at present. If the sand blanket was relatively uncemented when faulted, post-faulting sheetwash could transport the loose sand from the upthrown block to the downthrown block, where it would be deposited atop the loose sand that predated faulting. This resulting depositional contact of loose, retransported post-faulting sand atop loose prefaulting sand on the downthrown block might be very difficult to detect.

The sequence of faulting, deposition on the downthrown block, and soil formation can be reconstructed in detail in only two locations in our trenches, because, below the level of unit 3: (1) there are no correlative beds on both sides of the fault, and (2) unambiguous scarp-derived colluvial wedges do not exist.

Reconstruction of trench 1—We constructed a schematic retrodeformation sequence of trench 1 by progressively removing post-faulting deposits and reversing displacements on the main fault zone (Fig. 22). The retrodeformation sequence honors the laws of superposition, original horizontality, and cross-cutting relationships, but is otherwise simplified by: (1) deleting minor faults B, C, and D, and (2) accounting for the deposition of the upper part of unit 3 and the subsequent formation of its Bk horizon in a single step. Otherwise, the deposition of units (2L, 2U, 1L, 1U, where L = lower and U = upper) is represented as a separate step from subsequent soil development. In addition, the amount of vertical displacement to "reverse" in each fault movement cannot be known precisely. The minimum displacement in an event is that necessary to expose stratigraphic units in the free face, blocks of which were subsequently deposited in the post-faulting colluvial wedge. The maximum displacement is assumed to just fall short of exposing beds on the upthrown block (Ceja gravels) that evidently did not contribute to colluvial sedimentation. Generally, application of the latter rule prohibits displacements large enough to expose Ceja gravels in the free face.

The retrodeformation sequence (Fig. 22) begins with units 4 and 5, with their soils, covering the fault plane. This geometry is necessary because blocks of soils 4 and 5, some upside-down, are found interbedded in unit 3. For these blocks to have fallen into unit 3, soils 4 and 5 had to have existed somewhere at an elevation higher than unit 3 near

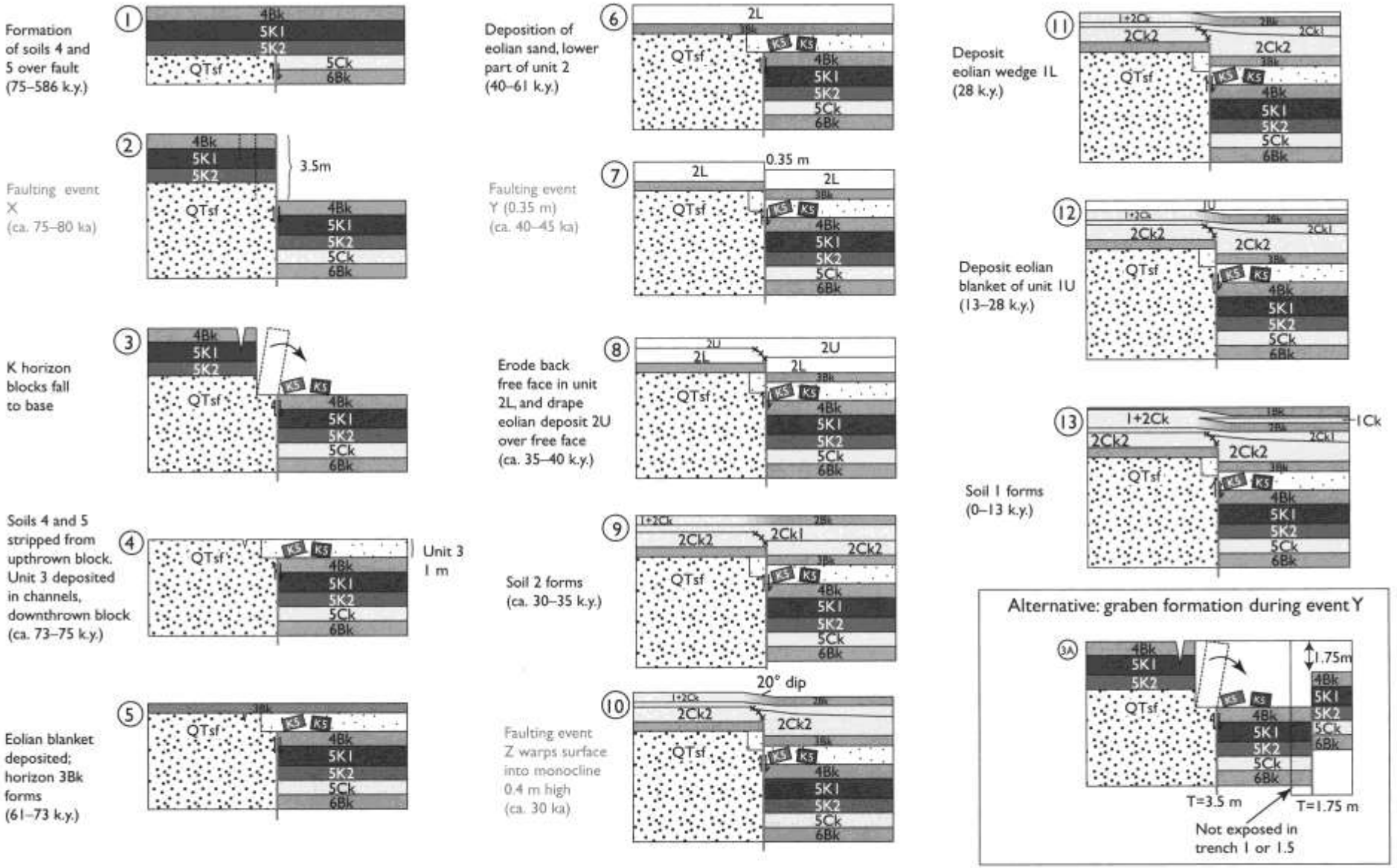

FIGURE 22—Schematic retrodeformation sequence for fault zone A in trench 1. Stage 1 (upper left) is the oldest stage, stage 13 (lower right) is the present trench geometry. Age ranges are estimated from a combination of soil carbonate (Table 3) and luminescence (Table 4) age estimates. This sequence of diagrams was simplified by depicting fault zone A as a single vertical fault. The diagrams were produced by starting with stage 13, and then successively removing deposits and reversing the effects of faulting, one stage at a time. Vertical displacements in faulting events Z and Y are based on measured displacements of units 2 and 3. Vertical displacement in event X is that necessary to expose the base of unit 5 in the fault free face, and thus to explain how overturned blocks of unit 5 were incorporated into unit 3. The graben-formation alternative at lower right would explain the overturned blocks without requiring 3.5 m vertical displacement, but trenches 2–4 did not show evidence for such a graben east of fault zone A.

the fault plane. Because soils 4 and 5 underlie unit 3 on the downthrown block, the only way they could have existed higher than unit 3 near the fault plane is if they were exposed in the fault free face. This geometry then requires the soils to have existed on both the upthrown and downthrown blocks before faulting (just as soils 1 and 2 presently cover the fault plane).

The vertical displacement (3.5 m) inferred for the earliest event here (event X, or the 3rd-to-latest event in the overall chronology) is required to: (1) expose soil 5 in the free face, and (2) uplift the upthrown block sufficiently so that all of soil 5 would be eroded from the upthrown block before deposition of the upper (eolian blanket) part of unit 3. Strictly speaking, our retrodeformation sequence only requires 3.5 m of vertical displacement on fault A, and the net vertical displacement across the entire deformation zone could be smaller if there are antithetic faults east of trench 1 (Fig. 22, Alternative). However, none of our other trenches exposed such antithetic faults.

Soil 3Bkb is vertically displaced 0.75 m, and it is ambiguous whether this displacement represents one or two small faulting events. Our preferred interpretation is two events (Y and Z), but the existence of the latter displacement event depends on the interpretation of parent material unit 1L (Fig. 22, stage 10) and the underlying flexure in the top of soil 2Bkb. The 1Ck2 /2Bkb (Fig. 4) contact is generally parallel to the ground surface (slopes east at about 2.5-3°) away from the fault, but steepens over the fault to a dip of as much as 20° east. This dip is significantly steeper than any part of the present ground surface on the fault scarp (see Fig. 3). Our preferred interpretation is that the top of soil 2Bkb once comprised the ground surface of the scarp face, which sloped about 3° east. Subsequent to its formation, soil 2Bkb was monoclinally warped to 20° east by a small faulting event. Soon thereafter, the eolian sand of parent material 1L was deposited in the swale at the base of the monoclinal warp. The amplitude of the flexure, ca. 0.4 m, is inferred as the vertical displacement in this event (event Z).

Given a displacement of approximately 0.4 m in event Z and a cumulative vertical displacement of 0.75 m in events Y and Z, we infer a displacement of approximately 0.35 min event Y. This value is similar to the difference in stratigraphic thickness between parent material unit 2U on either side of fault A, which is reasonable because unit 2U on the downthrown block contains a component of scarp-derived colluvial sand.

The retrodeformation sequence suggests that, through much of the evolution of the fault scarp, eolian deposits and their soils existed as blankets across the scarp face that covered the fault zone. Subsequent uplift led to erosion of the deposits and soils on the upthrown block, while burying and preserving them on the downthrown block. Thus, the 19 m of sandy sediments and soils that comprise the syntectonic wedge are primarily downfaulted and preserved remnants of eolian blankets that once mantled the scarp, rather than being colluvium derived from erosion of footwall gravels exposed in high free faces, as has been described on normal fault scarps elsewhere (e.g., Nelson 1992).

Reconstruction of trench 4—The second area where a local deformation sequence can be reconstructed is in the uppermost wall of trench 4. **In** this 1.5 m x 2.5 m area of the trench wall, several west-dipping splay faults displace soils 8, 9, and 10 by different amounts. The easternmost of the three splay faults in this area (fault A1d in Figs. 13, 23) displaces horizons 11Ckb, 11Bkb, and Ckb and can be traced to the top of unit 10Kb as a fracture but is overlain by horizon 9Ckb. A western splay fault (fault Alf) displaces horizon 9Ckb and can be traced through 9BkB and 8Ckb as a fracture, indicating younger movement than on fault A1d.

The retrodeformation sequence (Fig. 23) attempts to reproduce the unique geometry of soils 9-11 as they cross faults Aid and Alf. Across fault A1d: (1) horizon 11Bkb maintains constant thickness, (2) 10Ckb is thinner on the upthrown than on the downthrown block, (3) horizon 10Kb is not vertically displaced, but the fault can be traced through the horizon, and (4) horizon 9Ckb apparently is not faulted. A similar suite of relations exists across fault Alf, but the respective affected units are one unit younger than across fault A1d. The key to the retrodeformation sequence is realizing that the deposition of eolian sand can be a rapid process, but the development of soil horizons can take from 10^4 to 10^5 yrs. We assume that the upward displacement decrease or truncation of faults is not simply the result of upward die out (Bonilla and Lienkaemper 1991).

As explained earlier, the scarcity of exotic blocks of Bk and K horizons in the proximal colluvial deposits suggests that these horizons were not at the surface, nor exposed in the free face, at the time of faulting. A second assumption is that eolian deposition across the scarp face produced a blanket, the top of which sloped smoothly eastward across the fault plane, as does soil 1 today, rather than laying down a blanket of uniform thickness that is draped over a topographic step and retains a steep (>> 3°) depositional surface in the draped area. We see no evidence in today's landscape, nor in trench 1, that eolian blankets drape steeply over buried fault free faces.

Only one sequence of events will reproduce the unique geometry of soil horizons across faults A1d and Alf (Fig. 23). The sequence requires that a soil (in stage 1, 11Bkb) developed across the fault zone be buried by a blanket of eolian sand (stage 2, unit 10). Subsequent faulting (stage 3) creates a small free face entirely developed in the loose sand. This scarp is rapidly destroyed by erosion, which thins the parent material on the upthrown block (stage 4). After scarp stabilization, soil horizons then develop from the stabilized ground surface downward (stage 5), creating upper soil horizons of maximum development that generally maintain constant thickness. The underlying weaker soil horizons, however, have different thicknesses across the fault due to the post-faulting difference in parent material thickness. The A1d fault plane can be traced with some difficulty through horizon 10Kb because the deposit was faulted before most (all?) of the carbonate in horizon 10Kb accumulated. The sharp truncation of fault A1d by unit 9 (stage 6) shows that soil formation was followed by deposition of a sand blanket (unit 9). The sequence of events across fault Alf follows the same pattern. No other sequence of deposition-vs-faultingvs-soil formation will result in the geometries exposed in trench 4.

Given our proposed sequence model of past faulting, deposition, and soil formation, we must then ask, Where is the event horizon that formed the ground surface at the time of faulting? According to Fig. 23, stages 4 and 8, the event horizon is at the top of each parent material (depositional) unit. Because each unit subsequently developed a soil, the event horizon is also at the top of each soil. Thus, if we apply the above model developed from the subsidiary faults to the main fault zone at a larger scale, the 13 buried soils in the syntectonic wedge become evidence for 14 event horizons (Z through N), one at the top of each of the buried soils, and one (M) beneath the lowest soil (soil 14), because unit 14 was deposited atop the downfaulted Llano de Albuquerque surface on the hanging wall.

The key question now becomes, Do each of these event horizons record an individual paleoearthquake? Obviously, the preservation of the entire syntectonic wedge was made possible by 24 m of cumulative vertical fault displacement over the past 0.8-1.5 m.y. However, that observation does

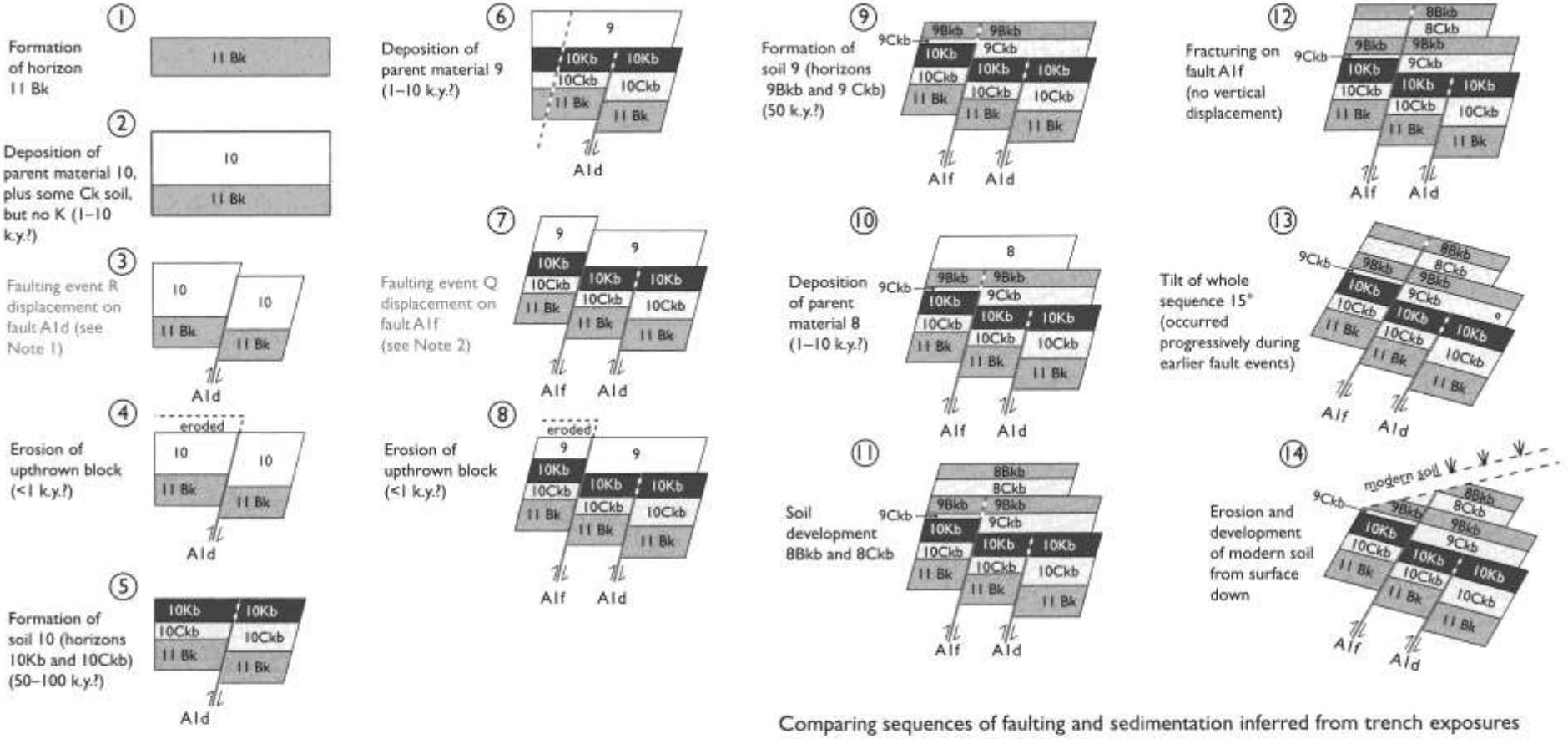

Note 1: the truncation of fault A1d at the top of parent material 10 requires that all of parent material 10 had accumulated before faulting event R

Note 2: because fault A1f is not truncated at the top of parent material 9, not all of parent material 9 needs to have been present before faulting event Q

Comparing sequences of faulting and sedimentation inferred from trench exposures

	Sequence for large, infrequent events	VS.	Sequence for small, frequent events with rapid eolian deposition
EARTHQUAKE DEFORMATION CYCLE	1) FAULTING		1) Deposition on upthrown and downthrown blocks
	2) Creation of accommodation space		2) FAULTING
	3) Erosion of upthrown block		3) Creation of accommodation space
	4) Deposition on downthrown block		4) Erosional stripping of upthrown block
	5) Soil formation		5) Soil formation
	6) FAULTING		6) Deposition on upthrown and downthrown blocks
	7) etc.		7) FAULTING

not require that each buried soil records a separate paleoearthquake. For example, the stacked soils may have been buried by scarp-blanketing eolian sand remobilized by climate changes and then later downfaulted and preserved on the hanging wall while being eroded away on the footwall.

The arguments that each event horizon records a paleoearthquake are mainly indirect. First, some type of geomorphic disturbance to the scarp caused burial of 13 soils adjacent to the fault over the past 0.8-1.5 m.y. The main possible causes are climate changes and surface rupture. Let us assume, for the sake of argument, that the 13 soils were buried as a result of climate changes. We must then ask, Where are the results of the repeated surface ruptures that we know must have occurred to create the 24 m of vertical displacement? There is no other indication of rapid readjustment of the scarp except for the buried soils, yet we know that, on other normal fault scarps, surface rupture has always triggered a sedimentologic response (McCalpin 1996a). Second, we know that at least one faulting event (event X, Fig. 22) triggered deposition on the scarp in the form of blocks of petrocalcic soil. In addition, the channel alluvium (unit 3) into which these blocks are mixed was probably deposited by a stream that was deflected up against the fault by hanging wall tilting shortly after faulting. Third, the reconstruction of soil and fault geometry in trench 4 indicates that movement on two subsidiary faults was temporally related to local deposition and soil formation in the same way. Such a consistent temporal relation would be coincidental if soil burial on the scarp was driven by climate changes, but expected if soil burial was related to faulting.

Paleoearthquake chronology and recurrence

As explained above, the 13 buried soils in the syntectonic wedge are inferred to be the result of successive earthquakes, and thus the time of soil development for each soil (neglecting time required for deposition) equates to the time between successive earthquakes. Soil development times are estimated directly from TL dates for soils 1-5, and lower in the section, indirectly from the increase of TL age with increasing cumulative secondary carbonate (Fig. 19). For soils 6-14, age is estimated as 293 ka (age of lower soil 5) plus 3.85 ka/g of secondary carbonate (Table 3).

Soil development (recurrence) times range from 4 to 202 k.y., with a mean of 40.8 k.y. The longest (202 k.y., time required to develop soil 5) and shortest (4 k.y., time required to develop soil 12) intervals are anomalous with respect to the other 11 intervals. Without these two extreme values, the other 11 intervals have a mean of 29.5 k.y., sigma of 11 k.y., and COV of 0.37.

One possible explanation of the irregularity of recurrence at this site could be that the 202-k.y. span represented by soil 5 includes more than one seismic cycle, and that the 4-k.y. span of soil 12 does not represent a seismic cycle, but rather a nontectonic episode of deposition and soil formation induced by climatic changes. We assign a low probability to the first explanation, because any additional faulting events that broke the strong carbonate horizons of soil 5 should have created obvious scarp-derived soil blocks that would be difficult to overlook in the trench exposures. Admittedly, the vertical gap between trenches 1 and 2 span just this critical boundary zone, and it is possible (although not likely) that the exotic soil blocks in trenches 1 and 1.5 represent different faulting events. However, the very strength and thickness of soil 4 and 5 horizons argue for a long period of landscape stability at this site between about 82 and 293 ka.

The 4-k.y. span represented by soil 12 may not record a seismic cycle, but because that soil was defined on the same basis as the other 12 buried soils, we cannot disassociate soil 12 from faulting without simultaneously weakening the case for a seismic origin of the other 12 buried soils.

Short-term recurrence can be assessed most confidently by observing that the most recent event (Z) occurred at about 30 ka (0.4 m displacement), event Y at about 40 ± 5 ka (-0.35 m displacement), and event X at 85 ± 10 ka (-3.5 m displacement; Table 5). The two recurrence intervals defined by this series are 5-15 k.y. and 30-60 k.y. These recurrence values come from strata that are dated by TL, and so are not affected by the ambiguity in extrapolated ages that affect soils 6-14.

Paleoearthquake slip rate and magnitude

The long-term (post-abandonment of the Llano) vertical slip rate of the County Dump fault can be estimated from the 24 m of far-field surface offset and the estimated 0.8-1.5 Ma age of the Llano de Albuquerque, yielding 0.016-0.03 mm/yr. The latest three paleoearthquakes occurred subsequent to 82 ka and resulted in as much as 4.25 m of vertical displacement, according to the retrodeformation analysis of trench 1, yielding a maximum slip rate of 0.052 mm/yr. However, that 4.25-m estimate includes an estimated 3.5 m from a single event (event X), which is by far the largest displacement inferred for any faulting event (see following paragraphs) and is 50% greater than the thickest soil (soil X) in the colluvial wedge. Perhaps a more representative short-term slip rate can be computed from the 0.75-m cumulative offset of soil 2Ck2, dated by TL at 41.2 ka. This displacement was accomplished by one or two events (Y, 35 cm; Z, 40 cm) with

TABLE 5—Estimated soil ages, earthquake recurrence intervals, and vertical displacements (soil thicknesses) of paleoearthquakes at the County Dump site.

Unit	Age of soil top (ka)[1]	Recurrence interval (k.y.)[2]	Soil thickness or reconstructed displacement (m)
1			1.08
2	30 (Z)		0.40
3	40 ± 5 (Y)	5–15	0.35
4	85 ± 10 (X)	30–60	3.50
5	134	402	2.23
6	536	29	0.66
7	565	63	1.37
8	628	19	0.62
9	647	15	0.64
10	662	36	1.30
11	698	43	1.84
12	741	5	0.42
13	746	5	0.52
14	751	N/A	>1.30
mean		60	1.22
sigma		104	0.69

[1]Age of dated paleoearthquake (for X, Y, or Z) or age of soil top (= event horizon) from last column in Table 3, inferred from carbonate weight and accumulation rate. This age also equals the age of the bottom of the overlying soil.

[2]For soil 5 and below, estimated as the difference between the ages of soil tops. Above soil 5 recurrence interval and displacements of lettered paleoearthquakes Z, Y, and X are estimated from luminescence dates and the retrodeformation sequence.

FIGURE 23—Retrodeformation sequence for splay faults in upper trench 4. Stage 1 (upper left) is the oldest stage, stage 14 (lower right) is the present trench geometry. This sequence of diagrams was simplified by depicting fault A1d and A1f as planar reverse faults. The diagrams were produced by starting with stage 14, and then successively removing deposits and reversing the effects of faulting, one stage at a time. The thinning of soil horizons on the hanging wall cannot be accomplished by simple upward die out of faults, but requires inter-faulting erosion and multiple faulting events.

displacements closer to the mean thickness of colluvial soils (Table 5). The resulting slip rate is 0.019 mm/ yr, which is close to the long-term slip rate estimate if one assumes the age of the Llano de Albuquerque is 0.8-1.5 Ma.

The magnitude of paleoearthquakes on the County Dump fault can be estimated from either fault length or displacement per event, but both methods rely on untestable assumptions for the County Dump fault. For fault length, it is critical to know whether the fault is only 10 km long (the length of fault scarps south of the Albuquerque volcanoes), or whether it continues an additional 20-25 km to the northern rim of the Llano de Albuquerque, as inferred by Machette et al. (1998) and Personius et al. (1999). No fault scarps can be traced continuously between our trench site and the prominent east-facing scarps west of the town of Rio Rancho, which Personius et al. (1999) map as the northern part of the County Dump fault. Possible fault lengths thus range from approximately 10 to 35 km. If Quaternary surface ruptures spanned the 35-km fault length of Personius et al. (1999), this implies earthquakes of moment magnitude (Mw) 6.9 (Wells and Coppersmith 1994, data for normal faults).

The thickness of soils in the colluvial sequence (Table 5) is assumed to be a rough proxy for vertical displacement in individual faulting events. Based on this assumption, mean vertical displacement in the past 14 events at the County Dump site is 1.2 ± 0.6 m. We do not know if the displacements at our site were closer to the average or to the maximum displacement for each faulting event. If we assume they were the maximum displacement, it implies Mw = 6.5-6.8; if we assume displacements were nearer the average, it implies Mw = 6.5-6.9 (Wells and Coppersmith 1994, data for normal faults).

When converted to paleoearthquake magnitude, the displacement values indicate magnitudes similar to those suggested by maximum rupture length. If each buried soil in the syntectonic wedge were downfaulted and preserved by faulting, then this similarity between per-event displacement and fault (rupture) length is understandable. In contrast, if soils were buried due to climate changes and then later passively downdropped by the fault, any correspondence between unit thickness and fault length would have to be coincidental.

Conclusions

Our major finding is that the five relatively thick buried soils in the syntectonic depositional wedge, described by Machette (1978), can be subdivided into 14 thinner units, each carrying a distinct buried soil, within 5-10 m of the fault plane. These thinner units have a mean thickness of 1.2 m and a standard deviation of 0.6 m. Based on this number of buried soils, and the assumption that each paleoearthquake is followed by soil burial on the hanging wall, we infer that past faulting events have been smaller (1.2 ± 0.6 m vertical displacement) but more frequent than estimated by Machette (1978). The latest two paleoearthquakes have reconstructed displacements across the fault plane of 0.4 m and 0.35 m with the next earlier event having a much larger displacement (< 3.5 m).

The long-term frequency of paleoearthquake faulting is difficult to determine because: (1) the estimated age of the faulted Llano de Albuquerque surface varies from 0.8 to 1.5 Ma, and (2) we were able to obtain TL age estimates from only the upper 8.3 m of the 19.4-m-thick colluvial wedge sequence. Over the short term, the latest three faulting events include a probable event at ca. 30 ka (event Z, 0.4 m vertical displacement), a definite event at ca. 40 ± 5 ka (event Y, 0.35 m vertical displacement), and a definite event at ca. 85 ± 10 ka (event X, < 3.5 m vertical displacement); all events are constrained by bracketing TL dates. Thus, the latest two seismic cycles have recurrence intervals of ca. 5-15 k.y. and 30-60 k.y. Those times are similar to the mean development time of the 14 colluvial soils (29.5 ± 11 k.y.) if the anomalous longest and shortest values are omitted.

Overall, the pattern of displacements observed in our trenches suggests that faulting occurs at intervals of ca. 30-25 k.y. and results in displacements of approximately 1 m or less on the County Dump fault. These values are significantly smaller than the mean estimates of ca. 125 k.y. for recurrence and 4.25 m for paleoearthquake displacement made by Machette (1978), and correlate better with the displacements expected on a fault that is 10-35 km long.

A second major finding is that only a small proportion of the sediments in the large syntectonic depositional wedge was derived from direct erosion of the fault scarp crest, and the larger proportion is probably remnants of tabular blankets of eolian sand that once mantled the scarp face. This conclusion is similar to that of other studies of intrabasin faults in the Albuquerque region (Personius and Mahan 2003; Olig et al. in press). Geometric relationships between faults, colluvial parent materials, and soil horizons suggest that these sand blankets were deposited between faulting events, and were later preserved by downfaulting on the hanging wall, rather than being scarp-derived colluvial wedges. Therefore, the thickness of individual units in the syntectonic wedge may be determined more by depositional factors, than by the vertical displacement of the faulting event that led to its burial and preservation on the downthrown block. This hypothesis, if true, implies there is only an indirect correlation between the thickness of buried soil units and the vertical displacements of past faulting events on the County Dump fault.

Acknowledgments

This study was made possible by landowner permission from Westland Development Company, as represented by Mr. Leroy Chavez, Vice President of Development. Local geology experts John Hawley, Mike Machette, Steve Personius, Sean Connell, and Florian Maldonado gave valuable advice. Thanks go to our logging assistants Dennis McMahon, Marsha Fronterhouse, and Karen Holmes. We thank Sean Connell, Jamie Gardner, and Keith Kelson for their detailed reviews of this paper. This study was supported by USGS-NEHRP contract 1434-HQ-96-GR-02751, awarded to GEO-HAZ Consulting, Inc. and the New Mexico Bureau of Geology and Mineral Resources. This publication is supported by Grant # 2005-GE-T5-0012 awarded by the Office of Domestic Preparedness (ODP). This publication does not necessarily reflect ODP's views.

References

Aitken, M. J., 1985, Thermoluminescence dating: Academic Press, London, 359 pp.

Aitken, M. J., 1998, An introduction to optical dating: Oxford University Press, New York, 256 pp.

Berger, G. W., 1988, Dating Quaternary events by luminescence; *in* Easterbrook, D. J. (ed.), Dating Quaternary sediments: Geological Society of America, Special Paper 227, pp. 13-50.

Berger, G. W., 1990, Effectiveness of natural zeroing of the thermoluminescence in sediments: Journal of Geophysical Research, v. 95, no. B8, pp. 12,375-12,397.

Berger, G. W., 1994, Thermoluminescence dating of sediments older than 100 ka: Quaternary Science Reviews, v. 13, no. 5-7, pp. 445-455.

Berger, G. W., 2003, Luminescence chronology of late Pleistocene loess-paleosol and tephra sequences near Fairbanks, Alaska: Quaternary Research, v. 60, pp. 70-83.

Berger, G. W., and Anderson, P. M., 1994, Thermoluminescence dating of an Arctic lake core from Alaska: Quaternary Science Reviews, v. 13, pp. 497-501.

Berger, G. W., Lockhart, R. A., and Kuo, J., 1987, Regression and error analysis applied to the dose response curves in thermoluminescence dating: Nuclear Tracks and Radiation Measurements, v. 13, no. 4, pp. 177-184.

Birkeland, P. W., 1984, Soils and geomorphology: Oxford University Press, 372 pp.

Bonilla, M. G., and Lienkaemper, J. J., 1991, Factors affecting the recognition of faults exposed in exploratory trenches: U.S. Geological Survey, Bulletin 1947,54 pp.

Bryan, K., and McCann, F. T., 1937, The Ceja del Rio Puerco-a border feature of the Basin and Range province in New Mexico, Part 1, stratigraphy and structure: Journal of Geology, v. 45, no. 8, pp. 801-828.

Chapin, C. E., and Cather, S. M., 1994, Tectonic setting of the axial basins of the northern and central Rio Grande rift; *in* Keller, G. R., and Cather, S. M. (eds.), Basins of the Rio Grande rift-structure, stratigraphy, and tectonic setting: Geological Society of America, Special Paper 291, pp. 5-25.

Connell, S. D., 1997, Geology of the Alameda 7.5-minute quadrangle, Bernalillo County, New Mexico: New Mexico Bureau of Geology and Mineral Resources, Open-file Digital Geologic Map OF-DM 10, scale 1:24,000.

Connell, S. D., and Wells, S. G., 1999, Pliocene and Quaternary stratigraphy, soils, and tectonic geomorphology of the northern flank of the Sandia Mountains, New Mexico-implications for the tectonic evolution of the Albuquerque Basin; *in* Pazzaglia, F., and Lucas, S. G. (eds.), Albuquerque geology: New Mexico Geological Society Guidebook 50, pp. 379-391.

Connell, S. D., Allen, B. D., and Hawley, J. W., 1998, Subsurface stratigraphy of the Santa Fe Group from borehole geophysical logs, Albuquerque area, New Mexico: New Mexico Geology, v. 20, no. 1, pp. 2-7.

Connell, S. D., Koning, D. J., and Cather, S. M., 1999, Revisions to the stratigraphic nomenclature of the Santa Fe Group, northwestern Albuquerque Basin, New Mexico; *in* Pazzaglia, F., and Lucas, S. G. (eds.), Albuquerque geology: New Mexico Geological Society, Guidebook 50, pp. 337-353.

Connell, S. D., Love, D. W. , Sorrell, J. D., and Harrison, J. B. J., 2001, Plio-Pleistocene stratigraphy and geomorphology of the central part of the Albuquerque Basin; *in* 45th Field Conference of the Rocky Mountain Cell of the Friends of the Pleistocene: New Mexico Bureau of Geology and Mineral Resources, Open-file Report 454C and D, variously paginated.

Connell, S. D., Cather, S. M., Karlstrom, K., Read, A., Ilg, **B.,** Menne, B., Picha, M., Andronicus, C., Bauer, P., and Anderson, **0.,** 1995, Geology of the Placitas 7.5-min quadrangle, Sandoval County, New Mexico: New Mexico Bureau of Geology and Mineral Resources, Open-file Geologic Map OF-GM 2, scale 1:12,000. With discussion of the Cenozoic geology by S. D. Connell and S. M. Cather.

Forman, S. L., Pierson, **J.,** and Lepper, K., 1998, Luminescence geochronology; *in* Sowers, J. M., Noller, J. S., and Lettis, W. R. (eds.), Dating and earthquakes-review of Quaternary geochronology and its application to paleoseismology: U.S. Nuclear Regulatory Commission, Report NUREG-5562, pp. 2-259-2-288.

Gardner, J. N., Reneau, S. L., Lavine, A., Lewis, C. J., Katzman, D., McDonald, E. V., Lepper, K. E., Kelson, K. I., and Wilson, C. J., 2003, Paleoseismic trenching in the Guaje Mountain fault zone, Pajarito fault system, Rio Grande rift, New Mexico: Los Alamos National Laboratory, Report LA-14087-MS, 68 pp., 5 plates.

Gile, L. H., Peterson, F. F., and Grossman, R. B., 1966, Morphological and genetic sequences of carbonate accumulation in desert soils: Soil Science, v. 101, no. 5, pp. 347-360.

Hawley, J. W. (ed.), 1978, Guidebook to the Rio Grande rift in New Mexico and Colorado: New Mexico Bureau of Mines and Mineral Resources, Circular 163,241 pp.

Hawley, **J.** W, Bachman, G. **0.,** and Manley, K., 1976, Quaternary stratigraphy in the Basin and Range and Great Plains provinces, New Mexico and western Texas; *in* Mahaney, W. C. (ed.), Quaternary stratigraphy of North America: Dowden, Hutchison and Ross, Inc., Stroudsburg, Pennsylvania, pp. 235-274.

Hawley, J. W., Haase, C. S., and Lozinsky, R. P., 1995, An underground view of the Albuquerque Basin, New Mexico; *in* Ortega-Klett, C. T. (ed.), Proceedings of the 39th Annual New Mexico Water Conference, The Water Future of Albuquerque and Middle Rio Grande Basin: New Mexico Water Resources Research Institute, Report 290, pp. 37-55.

Huntley, D. J., and Clague, J. **J.,** 1996, Optical dating of tsunami-laid sands: Quaternary Research, v. 46, pp. 127-140.

Kelley, V. C., 1977, Geology of Albuquerque Basin, New Mexico: New Mexico Bureau of Mines and Mineral Resources, Memoir 33, 60 pp.

Kelson, K. I., Hitchcock, C. S., and Harrison, J. B. J., 1999, Paleoseismology of the Tijeras fault near Golden, New Mexico; *in* Pazzaglia, F. J., and Lucas, S. G. (eds.), Albuquerque geology: New Mexico Geological Society, Guidebook 50, pp. 201-210.

Kelson, K. I., Bauer, P. W., Connell, S. D., Love, D. W., Rawling G. C., and Mansell, M., 2004, Initial paleoseismic and hydrogeologic assessment of the southern Sangre de Cristo fault at the Taos Pueblo site, Taos County, New Mexico; *in* Brister, B. S., Bauer, P. W., Read, A. S., and Lueth, V. W. (eds.), Geology of the Taos region: New Mexico Geological Society, Guidebook 55, pp. 289-299. Krbetschek, M. R., Götze, J., Dietrich, A., and Trautmann, T., 1997, Spectral information from minerals relevant for luminescence dating: Radiation Measurements, **v.** 27, pp. 695-748.

Lambert, P. W., 1968, Quaternary stratigraphy of the Albuquerque area, New Mexico: Unpublished Ph.D. dissertation, University of New Mexico, 329 pp.

Lang, A. and Wagner, G. A., 1997, Infrared stimulated luminescence dating of Holocene colluvial sediments using the 410 nm emission: Quaternary Science Reviews, v. 16, pp. 393-396.

Machette, M. N., 1978, Dating Quaternary faults in the southwestern United States by using buried calcic paleosols: U.S. Geological Survey, Journal of Research, v. 6, no. 3, pp. 369-381.

Machette, M. N., 1982, Quaternary and Pliocene faults in the La Jencia and southern part of the Albuquerque-Belen Basins, New Mexico-evidence of fault history from fault scarp morphology and Quaternary geology; *in* Grambling, J. A., Wells, S. G., and Callender, J. F. (eds.), Albuquerque country II: New Mexico Geological Society, Guidebook 33, pp. 161-169.

Machette, M. N., 1985, Calcic soils of the American Southwest; *in* Weide, D. L., and Faber, M. L. (eds.), Soils and Quaternary geomorphology of the American Southwest: Geological Society of America, Special Paper 203, pp. 1-21.

Machette, M. N., Long, T., Bachman, G. **0.,** and Timbel, N. R., 1997, Laboratory data for calcic soils in central New Mexico: Background information for mapping Quaternary deposits in the Albuquerque Basin: New Mexico Bureau of Mines and Mineral Resources, Circular 205,63 pp.

Machette, **M.** N., Personius, S. F., Kelson, K. I., Haller, K. M., and Dart, R. L., 1998, Map and data for Quaternary faults and folds in New Mexico: U.S. Geological Survey, Open-file Report 98-521,443 pp.

Maldonado, , Connell, S. D., Love, D. W., Grauch, V. **J.** S., Slate, J. L., McIntosh, W. C., Jackson, P. B., and Byers, F. M., Jr., 1999, Neogene geology of the Isleta Reservation and vicinity, Albuquerque Basin, New Mexico; *in* Pazzaglia, , and Lucas, S. G. (eds.), Albuquerque geology: New Mexico Geological Society, Guidebook 50, pp. 175-188.

May, R **J.,** and Machette, M. N., 1984, Thermoluminescence dating of soil carbonate: U.S. Geological Survey, Open-file Report 84- 0083,25 pp.

May, S. **J.,** and Russell, L. R., 1994, Thickness of the syn-rift Santa Fe Group in the Albuquerque Basin and its relation to structural style; *in* Keller, G. R., and Cather, S. M. (eds.), Basins of the Rio Grande rift-structure, stratigraphy, and tectonic setting: Geological Society of America, Special Paper 291, pp. 113-123.

McCalpin, J. P. (ed.), 1996a, Paleoseismology: Academic Press, New York, 588 pp.

McCalpin, J. P., 1996b, Field techniques in paleoseismology, Chapter 2; *in* McCalpin, J. P. (ed.), Paleoseismology: Academic Press, pp. 33-84.

McCalpin, **J.** P., 1997, Paleoseismicity of Quaternary faults near Albuquerque, New Mexico: Unpublished final technical report submitted to U.S. Geological Survey by GEO-HAZ Consulting, Inc., Contract 1434-HQ-96-GR-02751, October 6,1997,18 pp.

McCalpin, J. P., 2005, Late Quaternary activity of the Pajarito fault, Rio Grande rift of northern New Mexico, USA: Tectonophysics, v. 408, no. 1-4, pp. 213-236.

McCalpin, J. P., and Berry, M. E., 1996, Soil catenas to estimate ages of movements on normal fault scarps, with an example from the Wasatch fault zone, Utah, USA: Catena, v. 27, no. 3-4, pp. 265-286.

McCalpin, J. P., and Harrison, J. B. J., 2000, Paleoseismicity of Quaternary faults near Albuquerque, New Mexico: Unpublished final technical report submitted to U.S. Geological Survey by GEOHAZ Consulting, Inc., Contract 49-HQ-GR-0056, June 3, 2000, 35 pp.

McCalpin, J. P., and Harrison, J. B. J., 2001, Paleoseismicity of Quaternary faults near Albuquerque, New Mexico: Unpublished final technical report submitted to U.S. Geological Survey by GEOHAZ Consulting, Contract 99-HQ-GR-0056, August 4, 2001. McCalpin, J. P., Harrison, J. B. J. and Berger, G. W., in press, Quaternary faulting on the Calabacillas fault near Albuquerque, New Mexico, USA; *in* Michetti, A. M., Audemard., F. A., and McCalpin, J. P. (eds.), Paleoseismology in the 21st century: Geological Society of America, Special Paper.

Mercier, J. -L., Carey-Gailhardis, E., Mouyaris, N., Simeakis, K., Roundoyannis, T., and Anghelidhis, C., 1983, Structural analysis of recent and active faults and regional state of stress in the epicentral area of the 1978 Thessaloniki earthquakes (northern Greece): Tectonics, v. 2, no. 6, pp. 577-600.

Morgan, G. S., and Lucas, S. G., 1999, Pliocene (Blancan) vertebrates from the Albuquerque Basin, north-central New Mexico; *in* Pazzaglia, F., and Lucas, S. G. (eds.), Albuquerque geology: New Mexico Geological Society, Guidebook 50, pp. 363-370.

Nelson, A. R., 1992, Lithofacies analysis of colluvial sediments-an aid in interpreting the recent history of Quaternary normal faults in the Basin and Range Province, western United States: Journal of Sedimentary Petrology, v. 63, pp. 607-621.

Olig, S. S., Eppes, M. C., Forman, S. L., Love, D. W., and Allen, B. D., in press, Late Quaternary earthquakes on the central Hubbell Spring fault, New Mexico, USA; evidence for coseismic, non-characteristic ruptures of intrabasin faults in the Rio Grande rift; *in* Michetti, A. M., Audemard., F. A., and McCalpin, J. P. (eds.), Paleoseismology in the 21st century: Geological Society of America, Special Paper.

01lerhead, J., Huntley, D. J., and Berger, G. W., 1994, Luminescence dating of the Buctouche Spit, New Brunswick: Canadian Journal of Earth Sciences, v. 31, no. 3, pp. 523-531.

Pazzaglia, F. J., and Lucas, S. G. (eds.), 1999, Albuquerque geology: New Mexico Geological Society, Guidebook 50, 448 pp.

Peate, D. W., Chen, J. H., Wasserburg, G. J., Papanastassiou, D. A., and Geissman, J., 1996, ^{238}U-^{230}Th dating of a geomagnetic excursion in Quaternary basalts of the Albuquerque volcanoes field, New Mexico (USA): Geophysical Research Letters, v. 23, no. 17, pp. 2271-2274.

Personius, S. F., and Mahan, S. A., 2000, Paleoearthquake recurrence on the East Paradise fault zone, metropolitan Albuquerque, New Mexico: Seismological Society of America, Bulletin, v. 90, no. 2, pp. 357-369.

Personius, S. F., and Mahan, S. A., 2003, Paleoearthquakes and eolian-dominated fault sedimentation along the Hubble Springs fault zone near Albuquerque, New Mexico: Seismological Society of America, Bulletin, v. 93, no. 3, pp. 1355-1369.

Personius, S. F., Eppes, M. C., Mahan, S. A., Love, D. W., Mitchell, D. K., and Murphy, A., 2000, Log and data from a trench across the Hubbell Spring fault zone, Bernalillo County, New Mexico: U.S. Geological Survey, Miscellaneous Field Studies Map MF-2348, available at http://greenwood.cr.usgs.gov/pub/mf-maps/mf2348, accessed April 12, 2004.

Personius, S. F., Machette, M. N., and Kelson, K. I., 1999, Quaternary faults in the Albuquerque area-an update; *in* Pazzaglia, F. J., and Lucas, S. G. (eds.), Albuquerque geology: New Mexico Geological Society, Guidebook 50, pp. 189-200.

Russell, L. R., and Snelson, S., 1994a, Structural style and tectonic evolution of the Albuquerque Basin segment of the Rio Grande rift, New Mexico, USA; *in* Landon, S. M. (ed.), Interior rift basins: American Association of Petroleum Geologists, Memoir 59, pp. 205-258.

Russell, L. R., and Snelson, S., 1994b, Structure and tectonics of the Albuquerque Basin segment of the Rio Grande rift-insights from reflection seismic data; *in* Keller, G. R., and Cather, S. M. (eds.), Basins of the Rio Grande rift-structure, stratigraphy, and tectonic setting: Geological Society of America, Special Paper 291, pp. 83-112.

Sanford, A. R., Jaksha, L. H., and Cash, D. J., 1991, Seismicity of the Rio Grande rift in New Mexico; *in* Slemmons, D. B., Engdahl, E. R., Zoback, M. D., and Blackwell, D. D. (eds.), Neotectonics of North America: Geological Society of America, Decade Map, v. 1, pp. 229-244.

Sheppard, J. C., 1975, A radiocarbon dating primer: Eastern Washington State University, College of Engineering, Bulletin 338, 77 pp.

Soil Survey Staff, 1975, Soil taxonomy: U.S. Department of Agriculture, Soil Conservation Service, Agricultural Handbook No. 436, 754 pp.

Soil Conservation Service, 1994, Key to soil taxonomy: U.S.
Department of Agriculture, Soil Conservation Service, 6th ed., 306
pp. Von Hake, C. A., 1975, Earthquake history of New Mexico:
U.S. Geological Survey, Earthquake Information Bulletin, v. 7, no. 3, pp. 23-26.

Wells, D. L., and Coppersmith, K. J., 1994, New empirical relationships among magnitude, rupture length, rupture width, rupture area, and surface displacement: Seismological Society of America, Bulletin, v. 84, no. 4, pp. 974-1002.

Wintle, A. G., and Huntley, D. J., 1980, Thermoluminescence dating of ocean sediments: Canadian Journal of Earth Sciences, v. 17, no. 3, pp. 348-360.

Selected conversion factors*

TO CONVERT	MULTIPLY BY	TO OBTAIN
Length		
inches, in	2.540	centimeters, cm
feet, ft	3.048×10^{-1}	meters, m
yards, yds	9.144×10^{-1}	m
statute miles, mi	1.609	kilometers, km
fathoms	1.829	m
angstroms, Å	1.0×10^{-8}	cm
Å	1.0×10^{-4}	micrometers, µm
Area		
in^2	6.452	cm^2
ft^2	9.29×10^{-2}	m^2
yds^2	8.361×10^{-1}	m^2
mi^2	2.590	km^2
acres	4.047×10^{3}	m^2
acres	4.047×10^{-1}	hectares, ha
Volume (wet and dry)		
in^3	1.639×10^{-1}	cm^3
ft^3	2.832×10^{-2}	m^3
yds^3	7.646×10^{-1}	m^3
fluid ounces	2.957×10^{-2}	liters, l *or* L
quarts	9.463×10^{-1}	l
U.S. gallons, gal	3.785	l
U.S. gal	3.785×10^{-3}	m^3
acre-ft	1.234×10^{-3}	m^3
barrels (oil), bbl	1.589×10^{-1}	m^3
Weight, mass		
ounces avoirdupois, avdp	2.8349×10^{1}	grams, gr
troy ounces, oz	3.1103×10^{1}	gr
pounds, lb	4.536×10^{-1}	kilograms, kg
long tons	1.016	metric tons, mt
short tons	9.078×10^{-1}	mt
oz mt^1	3.43×10^{1}	parts per million, ppm
Velocity		
ft sec^{-1} (= ft/sec)	3.048×10^{-1}	m sec^{-1} (= m/sec)
mi hr^{-1}	1.6093	km hr^{-1}
mi hr^{-1}	4.470×10^{-1}	m sec^{-1}

TO CONVERT	MULTIPLY BY	TO OBTAIN
Pressure, stress		
lb in^{-2} (=lb/in^2), psi	7.03×10^{-2}	kg cm^{-2} (kg/cm^2)
lb in^{-2}	6.804×10^{-2}	atmospheres, atm
lb in^{-2}	6.895×10^{3}	newtons (N)/m^2, N m^{-2}
atm	1.0333	kg cm^{-2}
atm	7.6×10^{2}	mm of Hg (at 0°C)
inches of Hg (at 0°C)	3.453×10^{-2}	kg cm^{-2}
bars, b	1.020	kg cm^{-2}
b	1.0×10^{6}	dynes cm^{-2}
b	9.869×10^{-1}	atm
b	1.0×10^{-1}	megapascals, MPa
Density		
lb in^{-3} (= lb/in^3)	2.768×10^{1}	gr cm^{-3} (= gr/cm^3)
Viscosity		
poises	1.0	gr cm^{-1} sec^{-1} *or* dynes cm^{-2}
Discharge		
U.S. gal min^{-1}, gpm	6.308×10^{-2}	l sec^{-1}
gpm	6.308×10^{-5}	m^3 sec^{-1}
ft^3 sec^{-1}	2.832×10^{-2}	m^3 sec^{-1}
Hydraulic conductivity		
U.S. gal day^{-1} ft^2	4.720×10^{-7}	m sec^{-1}
Permeability		
darcies	9.870×10^{-13}	m^2
Transmissivity		
U.S. gal day^{-1} ft^{-1}	1.438×10^{-7}	$m^2 sec^{-1}$
U.S. gal min^{-1} ft^{-1}	2.072×10^{-1}	l sec^{-1} m^{-1}
Magnetic field intensity		
gausses	1.0×10^{5}	gammas
Energy, heat		
British thermal units BTU	2.52×10^{-1}	calories, cal
BTU	1.0758×10^{2}	kilogram-meters, kgm
BTU lb^{-1}	5.56×10^{-1}	cal kg^{-1}
Temperature		
°C + 273	1.0	°K (Kelvin)
°C + 17.78	1.8	°F (Fahrenheit)
°F - 32	5/9	°C (Celsius)

Divide by the factor number to reverse conversions.
Exponents: for example 4.047×10^{3} (see acres) = 4,047; 9.29×10^{-2} (see ft^2) = 0.0929

Colophon

Typeface: Palatino
Presswork: Starline Printing
Binding: Saddle stitch with softbound cover
Paper: Cover on Kivar®4-12 Linenweave. Text on 70-lb white matte.
Ink: Cover—PMS 320, four color process. Text—Black, PMS 485
Print run: 1,000


New Mexico Bureau of Geology and Mineral Resources
New Mexico Tech
Earth Science for the 21st Century

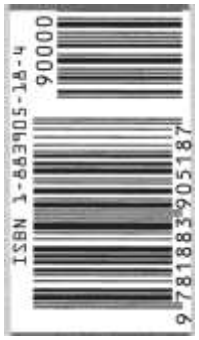
ISBN 1-883905-18-4
90000
9781883905187